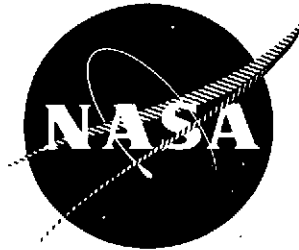


**CR-134734**

**W-05196**



# **DEVELOPMENT OF A 200 W CW HIGH EFFICIENCY TRAVELING-WAVE TUBE AT 12 GHz**

by

**J. A. Christensen and Dr. I. Tammaru**

**HUGHES AIRCRAFT COMPANY  
ELECTRON DYNAMICS DIVISION**

prepared for

**NATIONAL AERONAUTICS AND SPACE ADMINISTRATION**

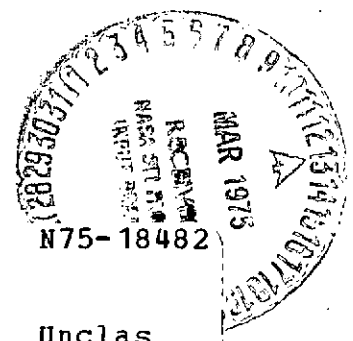
**NASA Lewis Research Center**

**Contract NAS 3-15831**

(NASA-CR-134734) DEVELOPMENT OF A 200 W CW  
HIGH EFFICIENCY TRAVELING WAVE TUBE AT 12  
GHz Final Report (Hughes Aircraft Co.)  
128 p HC \$5.75

CSSL 09E

G3/33



Unclas  
11087

# DOCUMENT RELEASE AUTHORIZATION

NASA Scientific and Technical Information Facility P.O. Box 33, College Park, Maryland 20740		Control No. _____ Date: _____									
D E S C R I P T I O N	TITLE: Development of a 200 W CW High Efficiency Traveling Wave Tube at 12 GHz										
	AUTHOR(S): J.A. Christensen & Dr. I. Tammaru										
	ORIGINATING ORGANIZATION: Hughes Aircraft Co., Torrance, California		COGNIZANT NASA CENTER Lewis Research Center 21000 Brookpark Road Cleveland, OH 44135								
	CONTRACT NO: NAS 3-15831										
	SECURITY CLASSIFICATION:										
	TITLE: <u>unclassified</u> DOCUMENT: <u>unclassified</u>										
	REPORT NO: <u>W-05196</u>										
	DATE: <u>October, 1974</u>										
	NASA CR NO: <u>134734</u>	WORK UNIT NO: _____	NASA TECHNICAL MONITOR G.J. Chomos	OFFICE CODE: 3301							
	NASA TMX NO: _____										
THE FOLLOWING TO BE COMPLETED BY THE RESPONSIBLE NASA PROGRAM OFFICER OR HIS DESIGNEE											
<p>(Further information is available in SP-7034 entitled R &amp; D Reporting Guidance for Technical Monitoring of NASA Contracts)</p> <p>I. Document may be processed into the NASA Information System as follows:</p> <p><input checked="" type="checkbox"/> May be announced in STAR (or CSTAR if a limited availability is checked below)</p> <p><input type="checkbox"/> May not be announced (The attached letter may be consulted for information pertaining to the NASA non-announcement series)</p> <p><input type="checkbox"/> May not be entered into the System because _____</p> <p>(Provide a brief statement to be quoted in answering requests for the referenced document)</p>											
<p>II. Document may be made available as checked below:</p> <table style="width: 100%;"> <tr> <td><input checked="" type="checkbox"/> Publicly Available</td> <td><input type="checkbox"/> U.S. Government Agencies, NASA and NASA Contractors Only</td> </tr> <tr> <td><input type="checkbox"/> Classified but Unlimited to Security Qualified Requesters</td> <td><input type="checkbox"/> NASA and NASA Contractors Only</td> </tr> <tr> <td><input type="checkbox"/> U.S. Government Agencies and Contractors Only</td> <td><input type="checkbox"/> NASA Headquarters and Centers Only</td> </tr> <tr> <td><input type="checkbox"/> U.S. Government Agencies Only</td> <td><input type="checkbox"/> Other Limitations (Specify) _____</td> </tr> </table>				<input checked="" type="checkbox"/> Publicly Available	<input type="checkbox"/> U.S. Government Agencies, NASA and NASA Contractors Only	<input type="checkbox"/> Classified but Unlimited to Security Qualified Requesters	<input type="checkbox"/> NASA and NASA Contractors Only	<input type="checkbox"/> U.S. Government Agencies and Contractors Only	<input type="checkbox"/> NASA Headquarters and Centers Only	<input type="checkbox"/> U.S. Government Agencies Only	<input type="checkbox"/> Other Limitations (Specify) _____
<input checked="" type="checkbox"/> Publicly Available	<input type="checkbox"/> U.S. Government Agencies, NASA and NASA Contractors Only										
<input type="checkbox"/> Classified but Unlimited to Security Qualified Requesters	<input type="checkbox"/> NASA and NASA Contractors Only										
<input type="checkbox"/> U.S. Government Agencies and Contractors Only	<input type="checkbox"/> NASA Headquarters and Centers Only										
<input type="checkbox"/> U.S. Government Agencies Only	<input type="checkbox"/> Other Limitations (Specify) _____										
Signature (Program Officer or Designee): 		Office Code: <u>3301</u> Telephone No: <u>216-433-4000 x747</u>	Date Signed: <u>11/19/74</u>								
<b>MAILING LABEL</b> Use open window envelope or Clip out and paste		<b>TO:</b>  NASA Scientific and Technical Information Facility Attn: Acquisitions Branch P.O. Box 33 College Park, Maryland 20740									

1. Report No. NASA CR 134734		2. Government Accession No.		3. Recipient's Catalog No.	
4. Title and Subtitle DEVELOPMENT OF A 200W CW HIGH EFFICIENCY TRAVELING WAVE TUBE AT 12 GHZ				5. Report Date October, 1974	
				6. Performing Organization Code	
7. Author(s) J.A. Christensen and Dr. I. Tammaru				8. Performing Organization Report No. W-05196	
9. Performing Organization Name and Address Hughes Aircraft Company Electron Dynamics Div. 3100 W. Lomita Blvd. Torrance, California 90509				10. Work Unit No.	
				11. Contract or Grant No. NAS 3-15831	
				13. Type of Report and Period Covered Contractor Report	
12. Sponsoring Agency Name and Address National Aeronautics and Space Administration Washington, DC 20546				14. Sponsoring Agency Code	
15. Supplementary Notes Project Manager, G.J.Chomos, Spacecraft Technology Division NASA-Lewis Research Center 21000 Brookpark Road Cleveland, Ohio 44135					
16. Abstract  This final report presents the design, development, and test results of an experimental PPM focused, traveling-wave tube that produces 235 watts of CW RF power over 85 MHz centered at 12.080 GHz. The tube uses a coupled cavity RF circuit with a velocity taper for greater than 30 percent basic efficiency. Overall efficiency of 51 percent is achieved by means of a nine stage depressed collector designed at NASA Lewis Research Center. This collector is cooled by direct radiation to deep space.					
17. Key Words (Suggested by Author(s)) Traveling Wave Tube Coupled Cavity Slow Wave Circuit Velocity Resynchronization Multistage Depressed Collector				18. Distribution Statement Unclassified-Unlimited	
19. Security Classif. (of this report) Unclassified		20. Security Classif. (of this page) Unclassified		21. No. of Pages 128	
				22. Price* \$3.00	

\* For sale by the National Technical Information Service, Springfield, Virginia 22151

NASA-C-168 (Rev. 6-71)

**ORIGINAL PAGE IS  
OF POOR QUALITY**

## FOREWORD

The work described herein was done by Hughes Aircraft Company, Electron Dynamics Division, under NASA Contract NAS 3-15831 with Mr. G. J. Chomos, NASA-Lewis Research Center, N/S 54-5, as Project Manager.

Hughes also wishes to acknowledge the assistance of Dr. H. G. Kosmahl and Mr. A. N. Curren during this program.

# ABSTRACT

This final report presents the design, development, and test results of an experimental PPM focused, traveling-wave tube that produces 235 watts of CW RF power over 85 MHz centered at 12.080 GHz. The tube uses a coupled cavity RF circuit with a velocity taper for greater than 30 percent basic efficiency. Overall efficiency of 51 percent is achieved by means of a nine stage depressed collector designed at NASA Lewis Research Center. This collector is cooled by direct radiation to deep space.

**PRECEDING PAGE BLANK NOT FILMED**

## SUMMARY

This final report describes the development of an experimental PPM focused, traveling-wave tube that produces between 235 and 250 watts of CW RF output power over an 85 MHz frequency band centered at 12.080 GHz. This tube was developed for use in the CTS Communications Satellite. The tube incorporates a coupled-cavity RF circuit with a velocity taper to provide greater than 30 percent basic efficiency. An overall efficiency is achieved through the use of a multiple stage collector with nine depressed elements. This collector is cooled entirely by radiation. To obtain the maximum depressed collector efficiency, a magnetic spent beam refocusing section is utilized between the output of the RF circuit and the collector. The refocusing section allows reduction of the transverse electron velocities and dilution of the space charge at the entrance to the collector.

During the development described herein, five traveling-wave tubes, Hughes Model 284H, were fabricated and tested. The first device, serial number E-1, incorporated the basic RF circuit design (without the velocity taper), a modulating anode electron gun, periodic permanent magnetic focusing, refocusing solenoid and an undepressed bucket type collector. The tube provided necessary interaction and focusing data used to calibrate the large signal analysis computer program. The remaining four devices utilized a two step velocity (period) taper and multi-stage collector for high efficiency. OST's serial numbers P-1, P-2 and ETM-1 did not achieve specified performance due to high circuit RF losses and a  $TM_{020}$  mode instability. The final tube 284H serial number ETM-2 achieved full specification RF performance at saturation, producing 235 watts minimum output power with basic and overall efficiencies of 30 and 51 percent respectively.

**PRECEDING PAGE BLANK NOT FILMED**

## TABLE OF CONTENTS

<u>Section</u>	<u>Page</u>
1.0 INTRODUCTION	1
2.0 284H OST DESIGN APPROACH	3
2.1 RF Circuit	3
2.2 Electron Gun	25
2.3 PPM Focusing Design	28
2.4 Refocusing Solenoid	31
2.5 RF Couplers and Windows	36
2.6 Multi-stage Depressed Collector (MDC)	40
2.7 OST Package Design	55
2.8 Fabrication Techniques	62
3.0 OST DESIGN STUDY	65
4.0 284H OST DEVELOPMENT RESULTS AND DISCUSSION OF RESULTS	85
4.1 Summary	85
4.2 284H Serial Number E-1	86
4.3 284H Serial Number P-1	90
4.4 284H Serial Number P-2	101
4.5 284H Serial Number ETM-1	104
4.6 284H Serial Number ETM-2	109
5.0 CONCLUSION	133

**PRECEDING PAGE BLANK NOT FILMED**

# LIST OF ILLUSTRATIONS

<u>Figure</u>	<u>Page</u>
2-1 General cavity configuration	7
2-2 $\omega$ - $\beta$ characteristics for 284H S/N E-1	10
2-3 Impedance and loss characteristics for 284H S/N E-1	11
2-4 $\omega$ - $\beta$ and dispersion characteristics of 284H velocity taper tubes	12
2-5 Phase velocity characteristics of 284H final design	14
2-6 Impedance characteristics of 284H final design	15
2-7 Velocity parameter b of 284H final design	16
2-8 Cavity loss characteristics of 284H final design	17
2-9 284H S/N E-1 performance, calculated versus measured	19
2-10 284H S/N E-1 corrected circuit voltage and impedance	20
2-11 284H calculated performance for optimum taper design	23
2-12 284H ETM-2 calculated versus measured basic efficiency	24
2-13 284H electron gun	26
2-14 Double PPM focusing structure and axial magnetic field	30
2-15 Computer analysis of focused electron beam for the 284H	32
2-16 Refocusing section designs	34
2-17 284H refocusing section	35
2-18 284H OST power sensor	37
2-19 284H OST voltage sensor outputs	39
2-20 284H multistage depressed collector equipotentials	41
2-21 284H radiation cooled depressed collector	43
2-22 284H mass model	47

PRECEDING PAGE BLANK NOT FILMED



<u>Figure</u>	<u>Page</u>
2-23 284H mass model resonance tests	49
2-24 284H MDC vacuum envelope with thermal choke	52
2-25 Computed MDC steady-state temperature profiles	53
2-26 Computed MDC steady-state temperature profiles	54
2-27 MDC to TWT heat transfer analysis	56
2-28 Photo of 284H with cover removed	57
2-29 284H OST resonance deflections	61
3-1 Definitions of axes	81
3-2 Voltage sensor outputs	82
3-3 Pressure sensor	83
4-1 284H E-1 on test	87
4-2 284H E-1 output section	88
4-3 284H E-1 saturated output power	91
4-4 284H E-1 basic saturated efficiency	92
4-5 284H E-1 Computer calibration	93
4-6 Final 284H P-1 output match and transmission loss	95
4-7 284H S/N P-1 saturated output power	97
4-8 284H S/N P-1 basic saturated efficiency	98
4-9 284H S/N P-1 output power with constant drive	100
4-10 284H S/N P-1 small signal gain	102
4-11 284H S/N P-2 output section match and transmission loss	103
4-12 284H S/N ETM-1 output section match and transmission loss	106
4-13 Saturated output power for 284H S/N ETM-1	107

<u>Figure</u>	<u>Page</u>
4-14 284H S/N ETM-1 saturated efficiencies	108
4-15 284H ETM-1 swept power output for constant power	114
4-16 Output power of 284H ETM-1 at 10 dB below optimum drive	115
4-17 Power out versus power in for 284H S/N ETM-1	116
4-18 Phase linearity at optimum drive for 284H ETM-1	117
4-19 Phase linearity at 10 dB below optimum drive for 284H ETM-1	118
4-20 Output RF circuit match	120
4-21 284H S/N ETM-2 saturated power output	121
4-22 284H S/N ETM-2 saturated efficiencies	124
4-23 284H ETM-2 swept power output	125
4-24 284H S/N ETM-2 swept $P_{out}$ over 150 MHz bandwidth	126
4-25 284H ETM-2 power out versus power in	130
4-26 Phase linearity at saturation	131

## 1.0 INTRODUCTION

The purpose of the contract effort described in this report was to design, develop, and produce traveling-wave tubes with greater than 200 watts RF output power at 12 GHz and overall efficiencies of 50 percent. Flight model tubes of the resulting final design were to be used in the high power experiment of the Communications Technology Satellite, a joint effort of Canada and the United States.

The tube developed by Hughes Aircraft Company, Electron Dynamics Division, incorporated several design features that had not previously been used in space applications: (1) an electron gun using a barium impregnated tungsten cathode; (2) a high power coupled-cavity RF circuit with a velocity taper for high basic efficiency; (3) a nine stage depressed collector with a beam refocusing section for high overall efficiency; and (4) radiation cooling of the collector to minimize the heat load on the satellite. The electrical design of the collector was done by NASA, Lewis Research Center.

The development program consisted of the design, fabrication, and test of five tubes. The first of these did not incorporate the velocity taper or multi-stage collector and was used to obtain interaction and focusing data. The remaining four tubes were built with both the velocity taper and the nine stage depressed collector.

## 2.0 284H OST DESIGN APPROACH

### 2.1 RF CIRCUIT

#### 2.1.1 General Description

The RF circuit for this traveling-wave tube was the coupled-cavity slow-wave structure, selected for its excellent thermal capability and rugged construction. A significant feature was the inclusion of an RF wave phase velocity taper at the circuit output. The taper was implemented by reducing the cavity period in two discrete steps, and was the chief factor in achieving a high interaction efficiency. The RF circuit was made up of two internally terminated sections to achieve stable operation with a minimum of 36 dB saturated gain. Weakly coupled lossy ceramics, designed to resonate in a region above 20 GHz, were included to suppress oscillation in higher order circuit modes. The coupled cavity structure formed part of a double period PPM focusing array.

#### 2.1.2 Evolution of Design

The RF circuit design of the 284H TWT evolved through a combined theoretical and experimental effort, which is summarized as follows.

Preliminary large signal computer analysis indicated that for high electronic efficiency a low beam voltage was desired. The computer evaluation assumed constant beam power and an interaction impedance proportional to the square root of the voltage. Both single and double step velocity taper circuits were investigated. A beam voltage of 8 kV was subsequently selected from focusing considerations, since at lower voltages the pole pieces tended to saturate. Using prior experience with narrow band tubes the circuit was designed for operation at a relatively low value of phase shift per cavity (about  $1.30 \pi$ ) for high interaction impedance. The beam hole was chosen to give a radial propagation parameter  $\gamma_a$  of 0.85 consistent with a high efficiency design.

An experimental tube (E-1) without velocity taper was built to establish the effective hot interaction parameters (and also to verify the gun and focusing designs).

Measurements of transmission loss in the RF circuit of this tube yielded a value of 0.12 dB per cavity at a phase shift of  $1.30 \pi$ . In the initial computer design work on the first taper tube a loss of 0.1 dB per cavity in the standard circuit had been used; the loss per unit length in the two-step phase velocity taper had been assumed to be constant. It became evident that the loss would play an important role in the design and performance of this TWT, particularly since the cavity loss in the tapers was expected to be significantly larger. Both experimental and theoretical efforts were therefore initiated to reduce the RF dissipation.

In the meantime, the first taper tube (P-1) was built according to the original design except that the number of cavities in the first and second tapers was decreased from 8 and 6 respectively, to 7 and 5. The phase velocity reductions in the tapers were 15 and 30 percent. This was achieved by decreasing the cavity period correspondingly. The measured transmission loss was 0.17 dB per cavity in the first taper and 0.25 dB per cavity in the second taper (at a phase shift of  $1.30 \pi$ ), resulting in considerable RF dissipation. Because of this, and the difficulty in obtaining a good RF match in the output section in this first taper tube, the basic efficiency was only about 18 percent, or comparable to the maximum basic efficiency of the experimental tube E-1.

Experimental work in reducing the RF dissipation was carried out in several directions. Since the resistivity of a braze alloy is considerably higher than that of copper (typically by a factor of 5) the brazing technique was modified to minimize the flow of braze material onto the cavity walls. Experiments were made to verify that the thickness of the copper plating (nominally 1/4 mil) was adequate. Special attention was given

to the design of the last cavity (the coupler or match cavity), in particular to the size of the last coupling aperture and the position of the backwall in relation to this aperture. Thus it was found that matching schemes which required the backwall to be close to the ferrule, leaving only a narrow coupling hole, resulted in large RF dissipation (as much as 0.5 dB in the coupler alone).

Theoretically, two approaches for reducing the loss were available due to its inverse relation with the group velocity or, equivalently, the slope of the  $\omega\beta$  curve. Either the cold bandwidth could be increased or the operating point could be shifted toward the middle of the passband (larger phase shift per cavity). In both cases a reduction in interaction impedance would result.

Increasing the cold bandwidth would reduce the impedance and loss proportionately. Going to a larger phase shift per cavity appeared more advantageous. According to measurements on the circuit of the experimental tube the loss at a phase shift of  $1.40\pi$  was 13 percent lower than the value at  $1.30\pi$ , while the effective (hot) impedance decreased by 9 percent. In addition, the increased cavity period associated with a larger phase shift design would further reduce the loss by an estimated 12 percent. The remaining tubes were consequently built with a standard cavity period of 0.114 inches instead of 0.107, with the passband adjusted to a phase shift of  $1.4\pi$  at the operating midband frequency.

The result of the combined experimental and theoretical work was a reduction in the loss by one-third in the standard circuit, to 0.08 dB per cavity at midband, with a decrease of interaction impedance of less than 10 percent. The loss reduction in the tapers was even larger; at operating midband frequency the loss per cavity was 0.10 dB and 0.15 dB in the first and second tapers respectively.

The next two tubes were built with identical RF circuits using the increased cavity period. The velocity taper configuration, similar to that on P-1, was 7 and 5 cavities in the first and second tapers with phase velocity reductions of 15 and 30 percent. The first of these tubes, P-2, oscillated in the  $TM_{02}$  cavity mode at 28 GHz. The second tube, ETM-1, was stable but had low beam current, about 15 percent less than the original design value. It nevertheless delivered 175 W with a peak basic efficiency of 28 percent and an overall efficiency of 45 percent (including heater and refocusing power).

The last tube, ETM-2, was provided with a higher perveance gun to achieve a minimum of 200 W output power. Two changes were made to reduce the RF dissipation further. Computer analysis of the large signal interaction showed that a ten percent reduction in RF power dissipation in the circuit could be obtained, at the cost of one percentage point in basic efficiency, by removing the last cavity in the second taper. Part of the decrease in efficiency could be recovered by the collector since the spent beam would have more energy. Also, the step transformer in the output coupler, made of monel for mechanical stiffness, was copper plated on the inside. The tube achieved a maximum basic efficiency of 33 percent (vs. 31 percent predicted). It had excellent performance over the operating band, with a near-constant 53 percent depressed efficiency and 51 percent overall efficiency.

### 2.1.3 Circuit Characteristics

The general cavity configuration is depicted in Figure 2-1. The dimensions are summarized in Table 2-1 for both the original cavity design used in E-1, and the three sets of cavities in the final design (tubes P-2, ETM-1, and ETM-2). Not shown in the figure are the small cavities, machined into the spacers, which contain lossy dielectric "buttons", that inhibit oscillation in higher order modes. These lossy resonators,

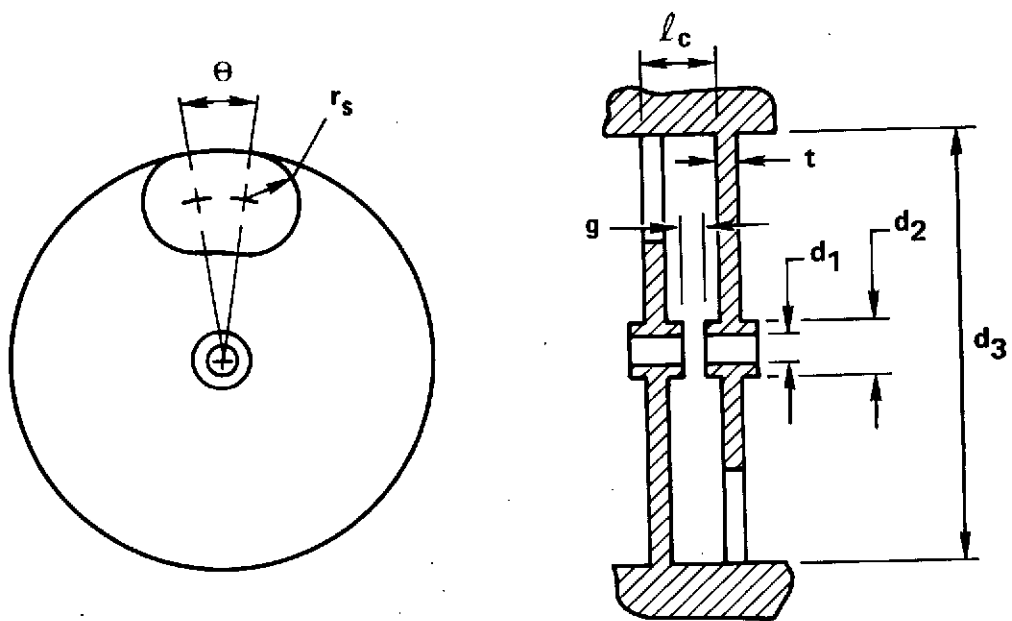



Figure 2-1 General cavity configuration



TABLE 2-1

Tube/Section	E-1	P-2, ETM-1, ETM-2		
		Std. ckt.	Taper 1	Taper 2
Beam hole diam., $d_1$ (in., cm)	.047 (.119)		Same	Same
Cavity diam., $d_3$ (in., cm)	.664 (1.687)			
Coupling hole angle, $\theta$ ( $^\circ$ , rad)	17 (.297)			
Wall thickness, $t$ (in., cm)	.032 (.081)			
Cavity period, $l_c$ (in., cm)	.107 (.272)	.114 (.290)	.097 (.246)	.080 (.203)

are located at the coupling hole symmetry line, and are tuned to a range of frequencies above 20 GHz.

Figure 2-2 exhibits the frequency versus phase shift characteristic of the experimental tube E-1. Also shown is the RF wave phase velocity expressed in terms of an equivalent voltage, called the circuit voltage,  $V_{ckt}$ .\* With a beam voltage of 8 kV, synchronous operation occurs at a phase shift of  $1.27 \pi$  (12.137 GHz); the nominal midband is around  $1.30 \pi$  (12.16 GHz) corresponding to a 4 percent overvoltage.

The measured cold interaction impedance (Pierce's impedance) and the transmission loss are plotted in Figure 2-3 as a function of phase shift per cavity. An effective beam-to-hole radius ratio of 0.6 has been assumed in evaluating the impedance. A bandwidth of 100 MHz centered at a phase shift of  $1.30 \pi$  corresponds to a phase shift range of  $1.23 \pi$  to  $1.36 \pi$  or a loss per cavity between 0.15 to 0.11 dB.

The cold interaction parameters (impedance and phase velocity) of the experimental tube E-1 were corrected by comparing predicted tube performance with measured test data. This gave the effective hot interaction parameters appropriate to the simplified interaction model assumed in the computer program. This is described further in the next subsection.

The cold RF wave properties of the standard cavity sections in the taper tubes are shown in Figure 2-4. The first taper tube, P-1, had the same basic circuit as E-1 (cavity period .107"), except the frequency was lowered by 70 MHz; this centered the design midband frequency (12.08 GHz) at  $1.30 \pi$ . The final circuit (tubes P-2, ETM-1 and ETM-2) had an increased cavity period designed to operate at approximately  $1.40 \pi$  to reduce the

---

\*)By definition, if electrons are accelerated by a voltage equal to  $V_{ckt}$ , their velocity will equal the phase velocity of the cold RF wave on the circuit. The calculation of  $V_{ckt}$  includes the effect of relativity, which amounts to about 200 volts at 8 kV. A measured increase of the cavity period that occurs at brazing has also been taken into account.

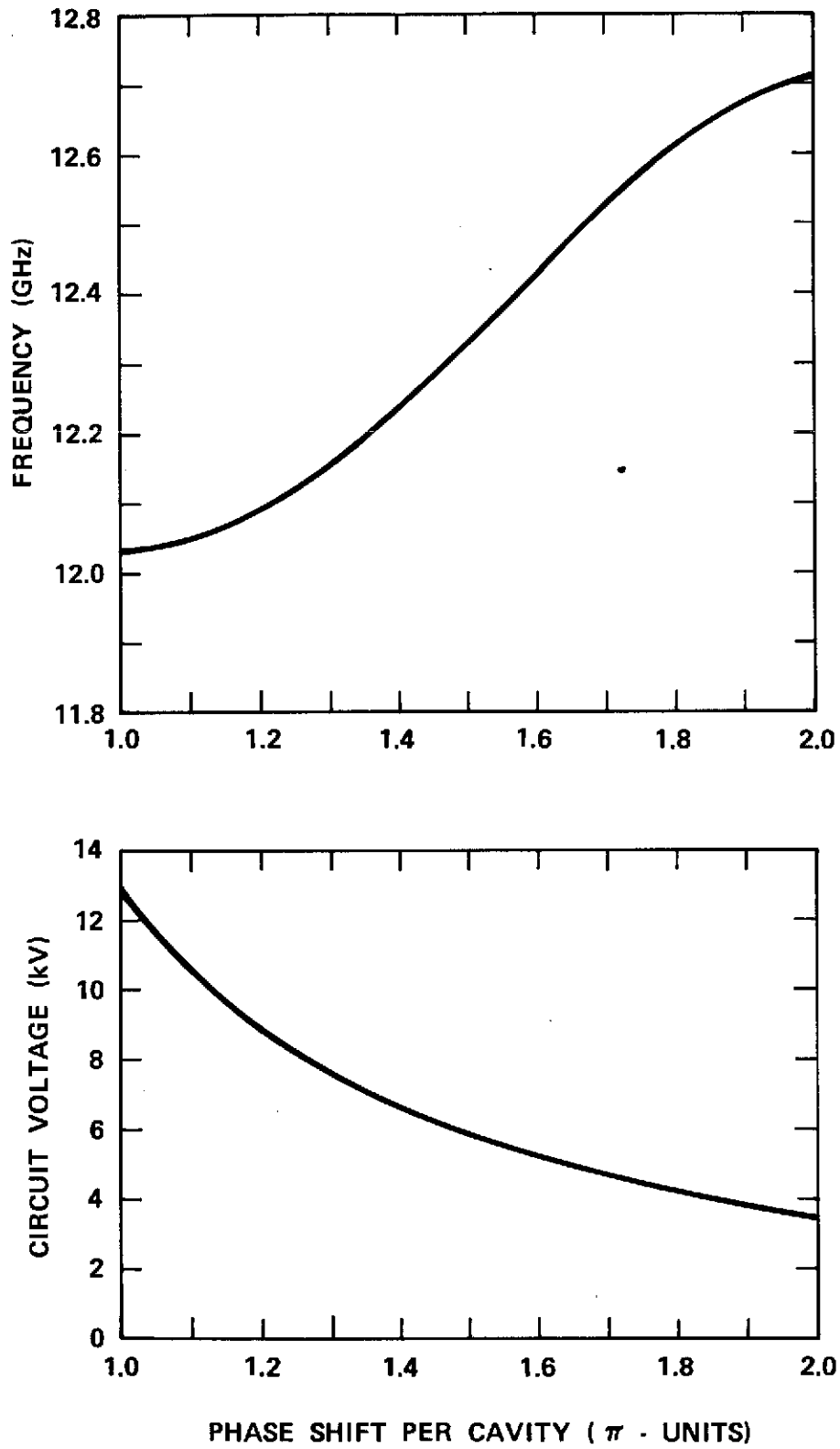


Figure 2-2  $\omega$ - $\beta$  and dispersion characteristics for 284H S/N E-1.

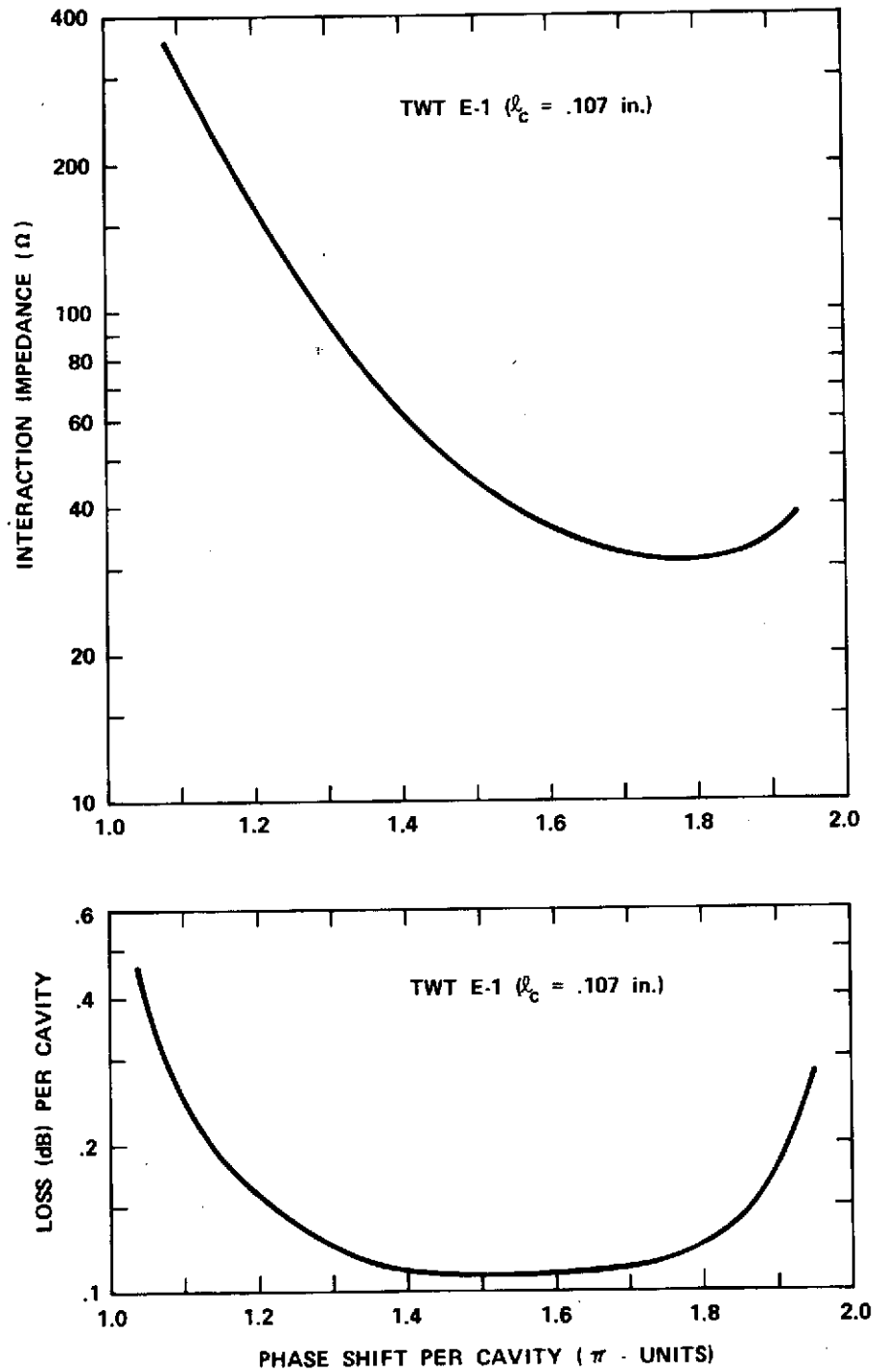


Figure 2-3 Impedance and loss characteristics for 284H S/N E-1.

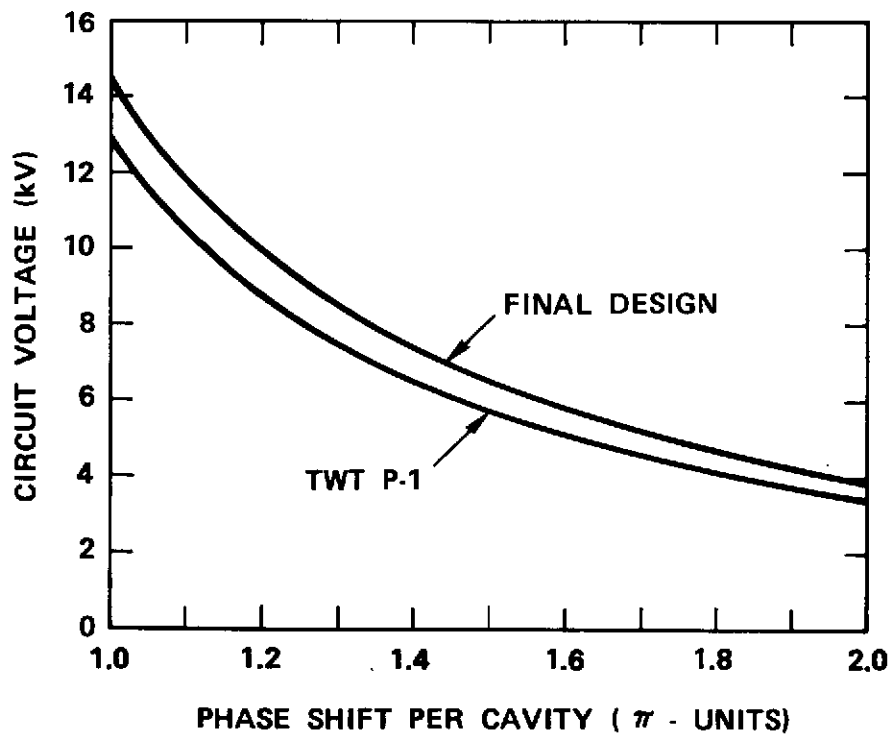
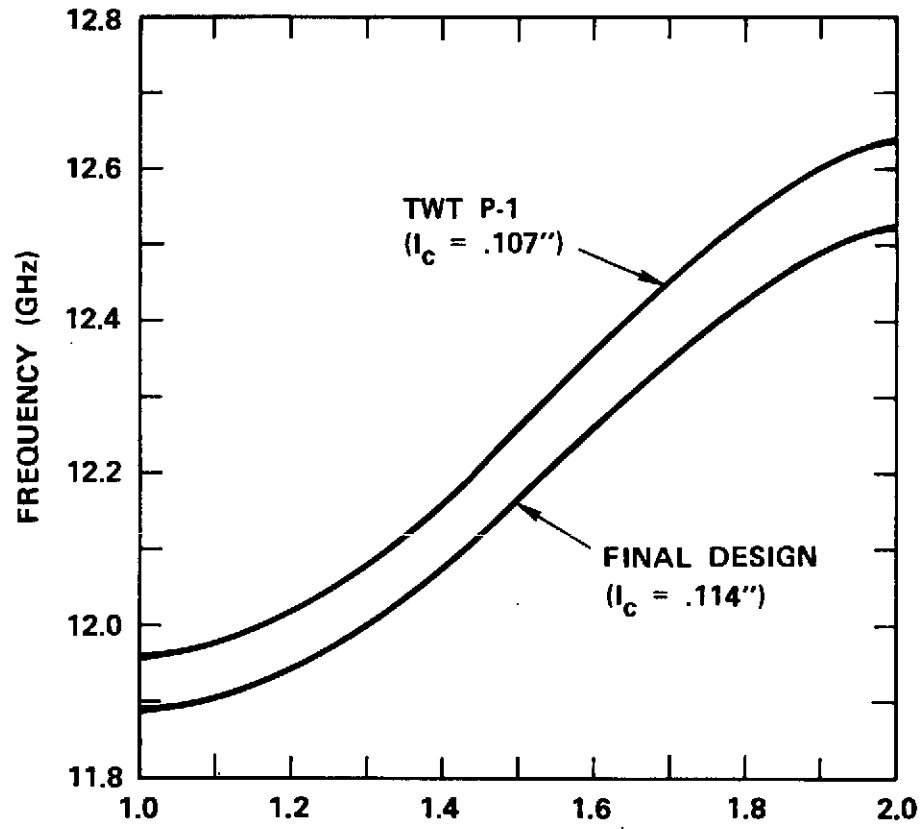


Figure 2-4  $\omega$ - $\beta$  and dispersion characteristics of 284H velocity taper tubes.

circuit loss. The cold bandwidth was 630 MHz or about six times a nominal hot bandwidth of 100 MHz. The passbands of the taper circuits were very nearly the same as that of the standard circuit with the operating midband frequency matched up with the corresponding phase shift per cavity. Because the  $\omega$ - $\beta$  characteristics of the taper circuits and the mid-band values of  $\beta l/\pi$  were the same as the standard circuit, no adjustments to the dimensions were necessary to obtain a satisfactory match over the operating band. In some of the tubes a slight change in the ferrule lengths in the transition cavities improved the VSWR.

Figure 2-5 displays the phase velocity of the three circuits in the final design versus frequency. The cold interaction impedance is shown in Figure 2-6 as a function of phase shift per cavity. An 85 MHz bandwidth about 12.08 GHz corresponds to a phase shift per cavity between  $1.35 \pi$  and  $1.45 \pi$ . Figure 2-7 presents the variation with frequency of Pierce's velocity parameter  $b$  in the final design. The parameter has been evaluated using the measured cold circuit characteristics, assuming a beam voltage of 8 kV and a beam current of 84.1 mA. The loss per cavity in the brazed circuit is plotted versus frequency in Figure 2-8, with the desired operating bandwidth indicated.

Due to the requirement for the highest possible tube interaction efficiency and the intended operation of the tube at saturation, special techniques utilized by Hughes in other communications tubes to reduce the small signal amplitude and phase variations were not incorporated. However, the good inband RF circuit matches achieved, and the skin effect losses in the output section, helped to reduce the regenerative effects which can result in large amplitude and phase variations.

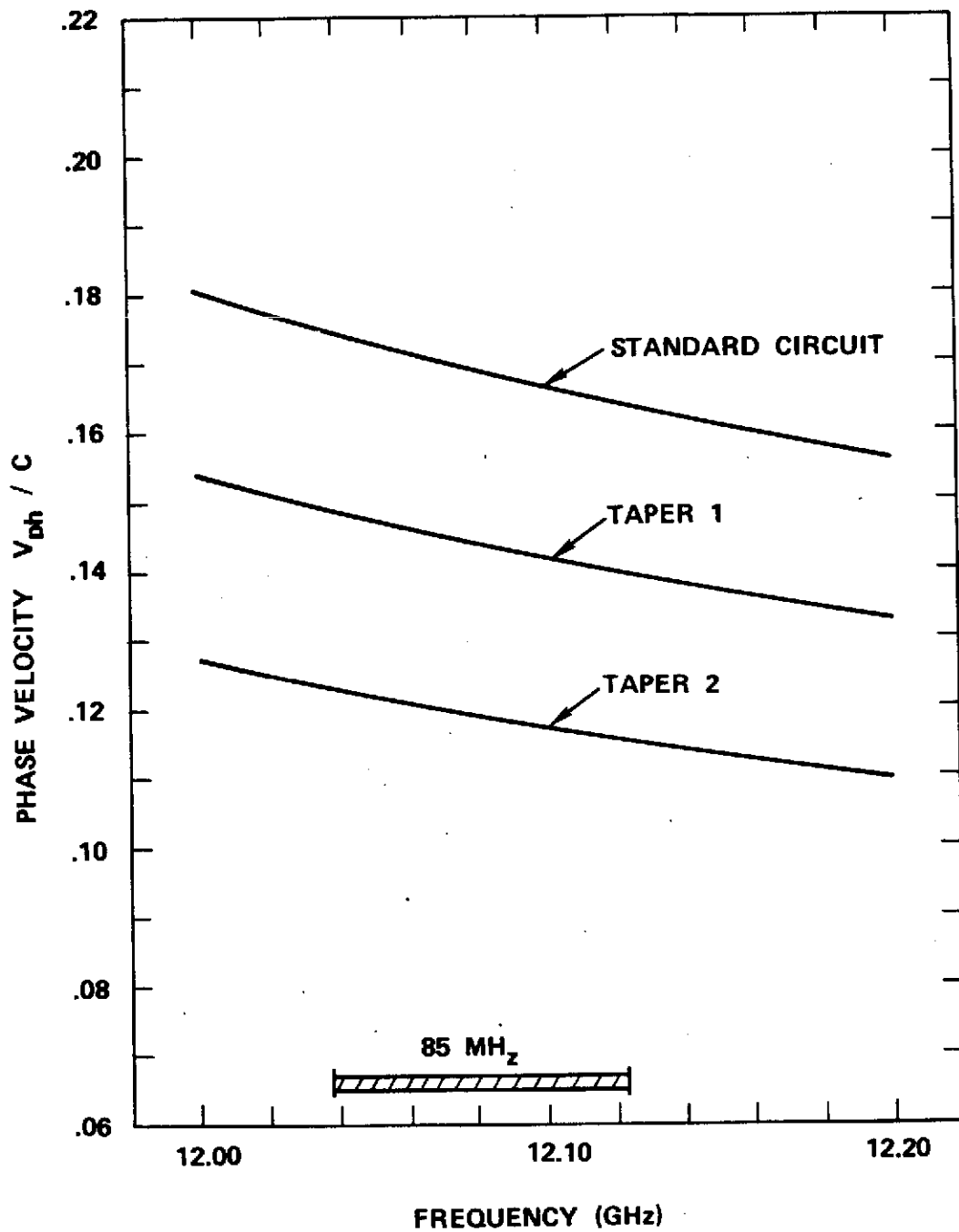


Figure 2-5 Phase velocity characteristics of 284H final design.

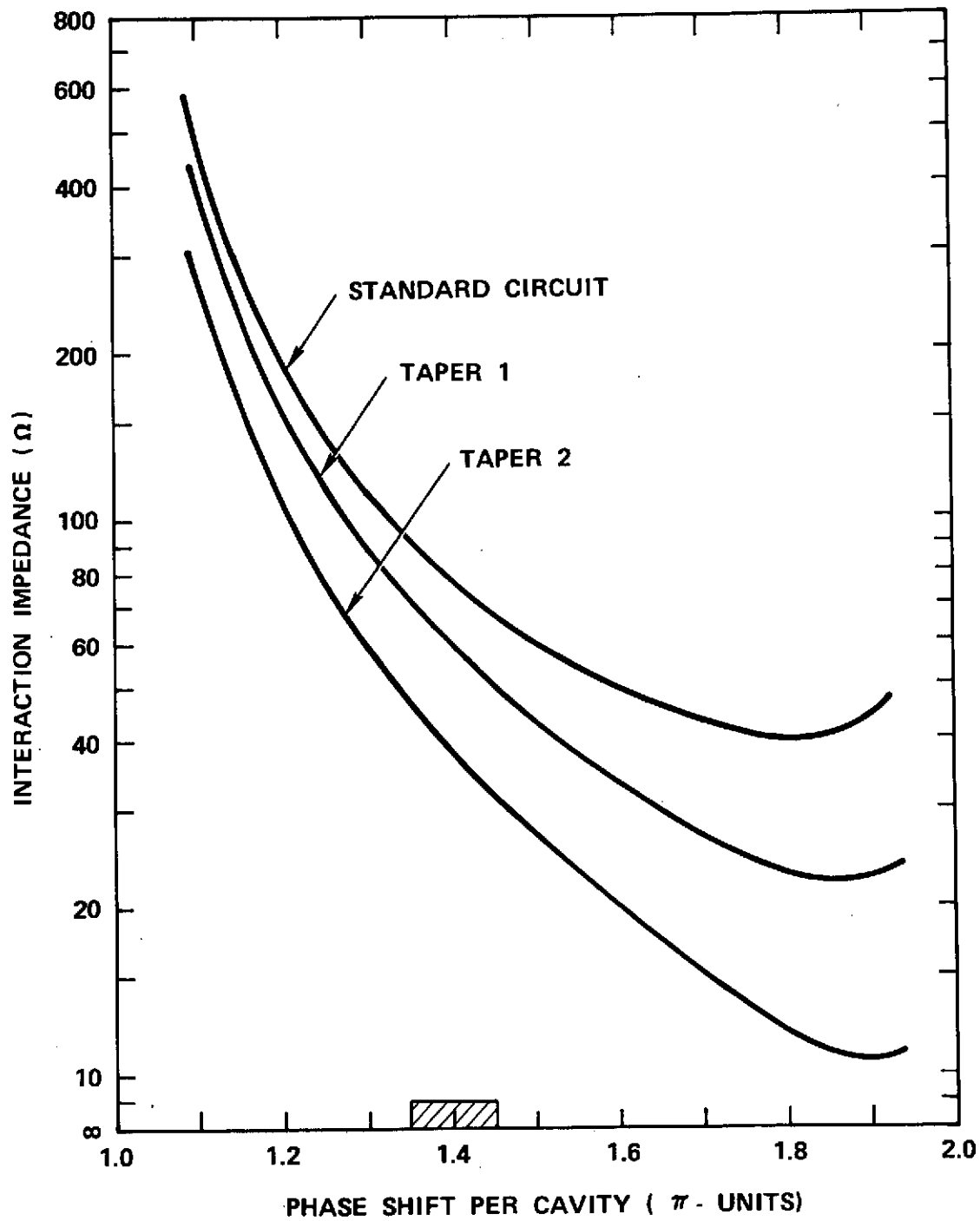


Figure 2-6 Impedance characteristics of 284H final design.



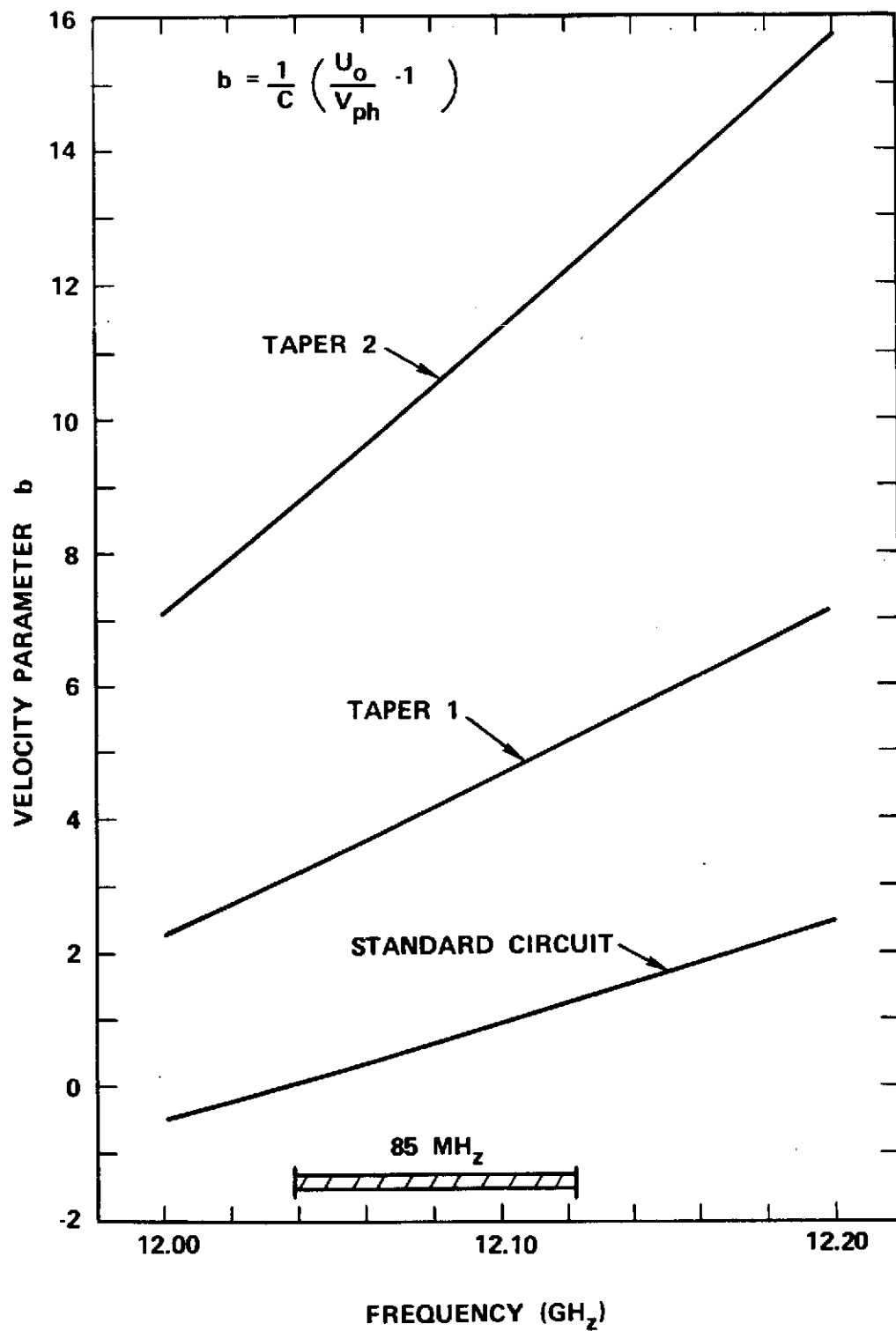


Figure 2-7 Velocity parameter  $b$  of 284H final design.

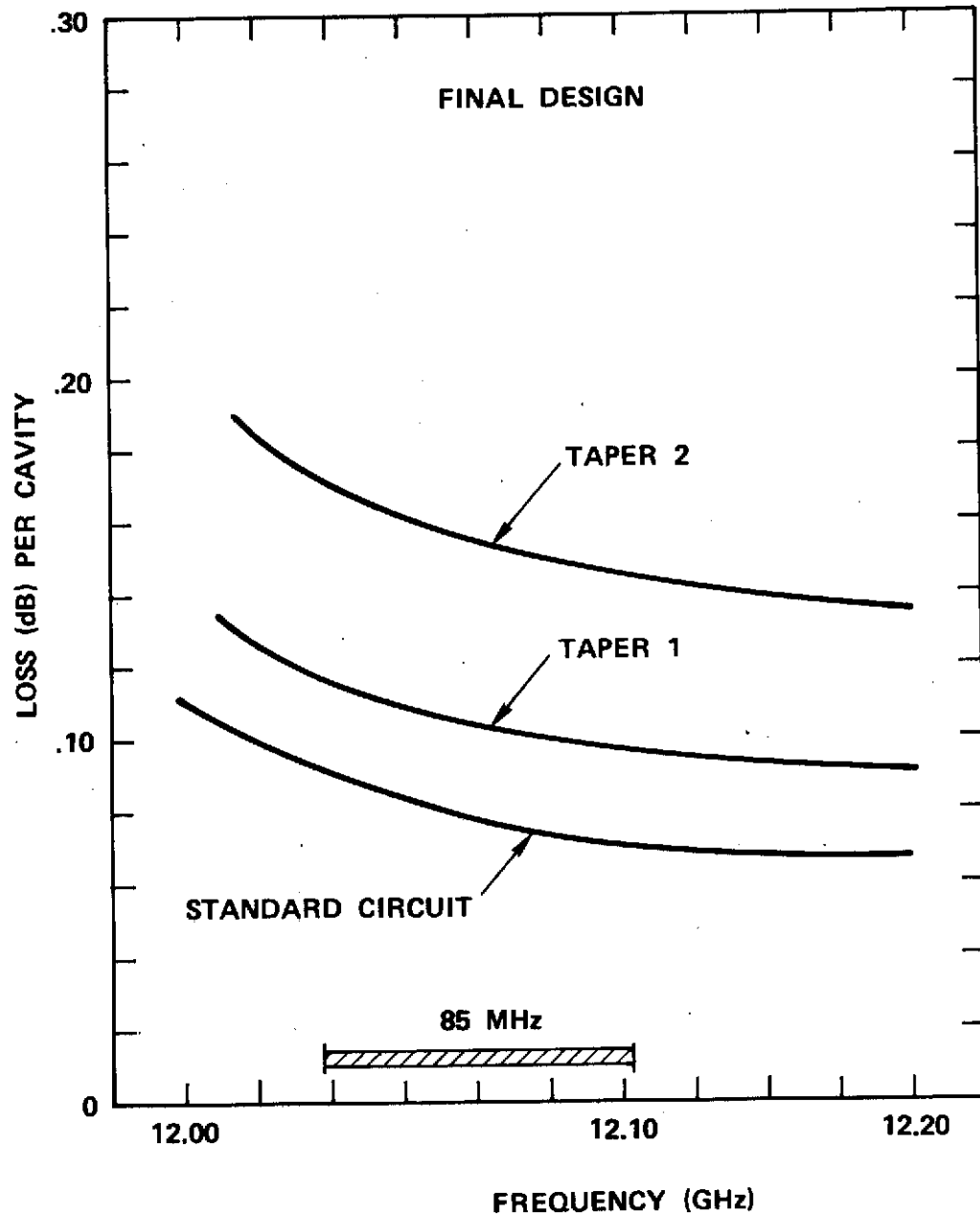


Figure 2-8 Cavity loss characteristics of 284H final design.

#### 2.1.4 Computer Design Analysis

The circuit design of the 284H relied heavily on analysis of the large signal interaction with a digital computer program. The program that was used is based on a continuous interaction between the first forward space harmonic and the electron beam, and includes the effect of space charge forces due to beam bunching. The beam is represented by disks with fixed radius. Such a one-dimensional model of the beam is expected to be quite adequate in cases where the electric RF field varies little over the beam hole area, and where the space charge forces are relatively small. Both of these criteria were satisfied in the present design because of the small radial propagation parameter  $\gamma_a$  and the low perveance beam.

The interaction model just described includes the dominant effects and is very convenient to use because of its simplicity. Other aspects of the actually more complex interaction process, such as the presence of a backward wave, may be approximately accounted for by a suitable correction of the basic parameters. In the present case, the effective interaction parameters could be found from the measured performance of the experimental tube E-1. Figure 2-9 shows the result of such a "computer calibration". The observed small signal gain, saturated gain, and saturated efficiency are closely calculated with corrected interaction impedance and phase velocity. These effective interaction parameters are displayed in Figure 2-10 as a function of phase shift per cavity. A phase shift range corresponding to 100 MHz about small signal gain maximum has been indicated. The calculation was based on the measured RF loss and a beam-to-hole radius ratio of six tenths.

The RF circuit of the taper tubes was designed by computing the performance at several frequencies over the band for a large number of different taper configurations. The interaction was calculated over the entire length of the tube (including a sever) at several drive levels. Phase velocity reductions of 12.5, 15, and 17.5 percent in the first taper, and 25, 30,

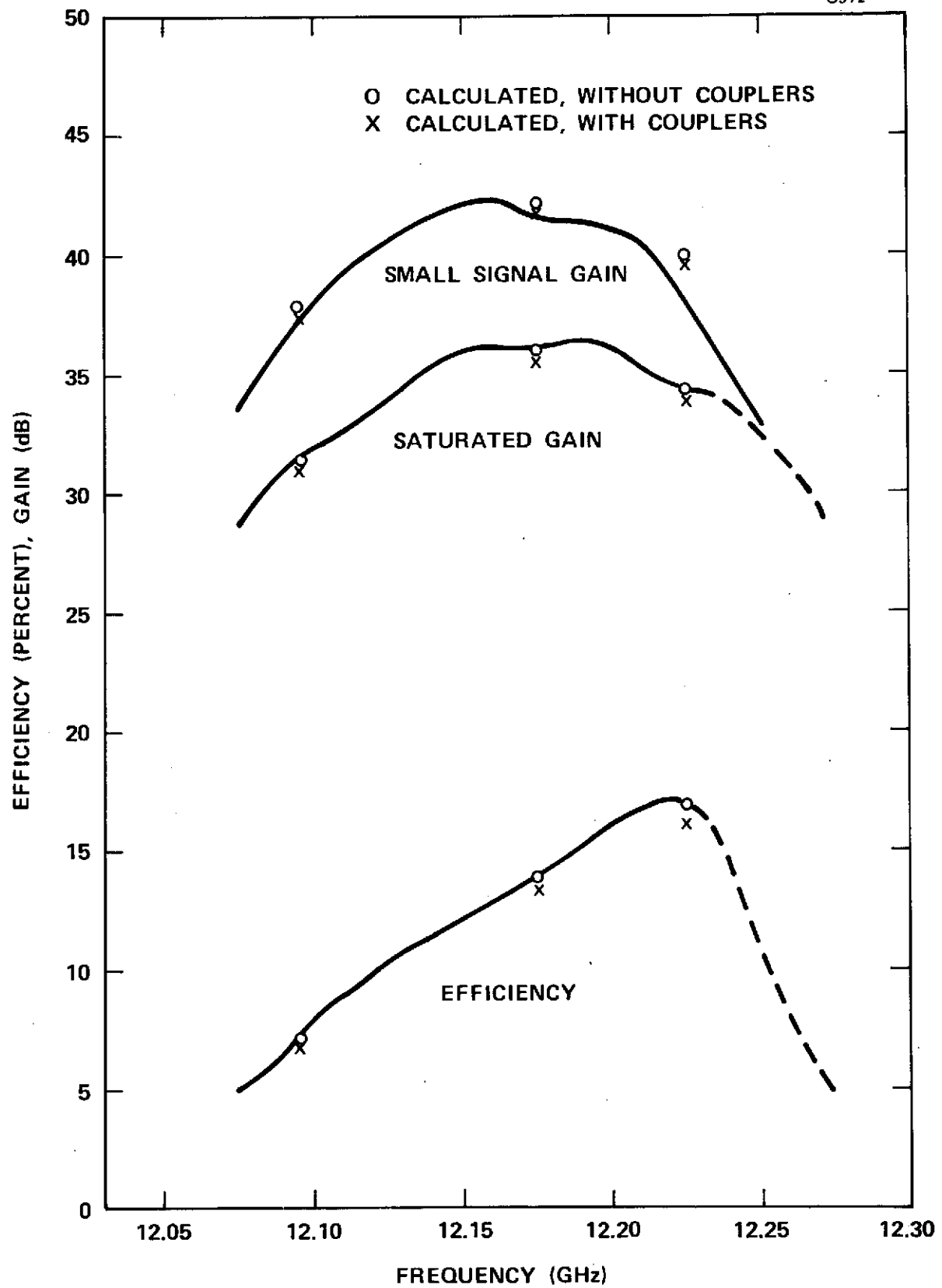


Figure 2-9 284H S/N E-1 performance, calculated versus measured.

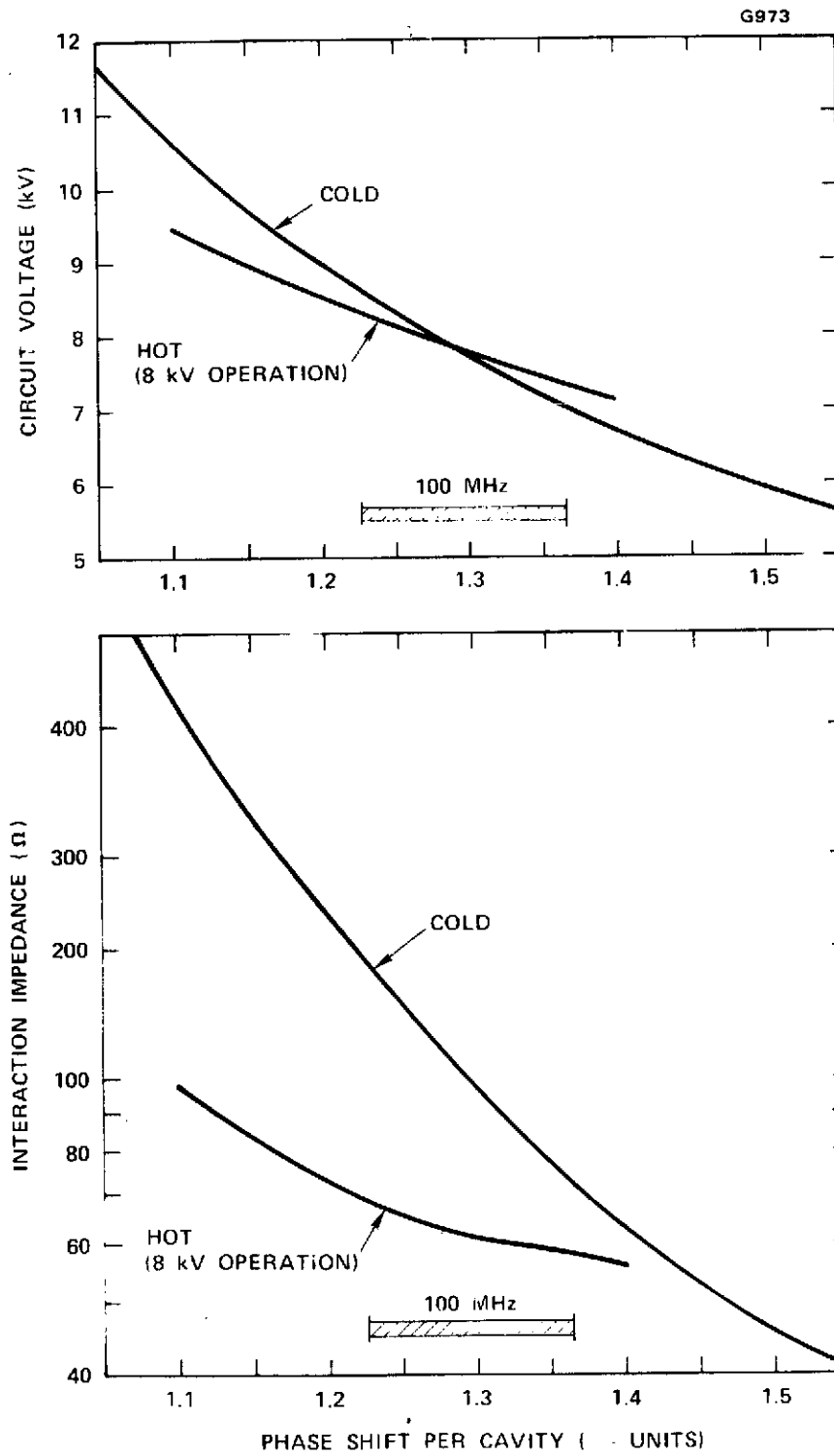


Figure 2-10 284H S/N E-1 corrected circuit voltage and impedance.

and 35 percent in the second taper were investigated in various combinations. Initially the increased loss in the tapers was not included. The combination (17.5, 35) then appeared slightly better than (15, 30). Due to the greater ease in matching and focusing a less severe taper, however, the combination (15,30) was selected. The taper lengths were varied from 6 to 9 cavities in the first taper and 3 to 7 in the second taper. In the initial analysis the optimum lengths were 8 and 6 cavities in the two tapers. For this design an efficiency of 34 percent was predicted at midfrequency.

After test results from the experimental tube E-1 became available, the design analysis was performed using the derived effective interaction parameters and the measured loss in the standard cavity sections. (The corrections to the interaction parameters for the final cavity period of 0.114 inches were estimated from those derived for the original 0.107 inch period.) The phase velocity in each taper was decreased in proportion to  $v_T/v_o$  where  $v_T$  and  $v_o$  are the cold phase velocities of the taper and standard circuits respectively. The interaction impedance was reduced by the factor  $(v_T/v_o)^2$ , which corresponded closely to the ratio of the measured cold impedances. The loss in the taper sections was increased according to the measured values.

The best taper lengths for high basic efficiency consisted of 7 cavities in the first taper and 5 cavities in the second taper. The results of a computer run for this configuration at 12.065 GHz and a drive level of 14 dbm are shown in Figure 2-11. The calculated gain, efficiency, and RF dissipation are plotted versus axial distance, expressed in terms of Pierce's dimensionless distance parameter  $y$ . Also shown is the normalized phase velocity variation. An efficiency of 31.2 percent and an RF dissipation of 9.2 percent of the beam power is calculated. The third taper tube (ETM-1), which incorporated this taper, demonstrated an efficiency of 28.3 percent at 12.070 GHz when operated at 8.2 kV despite a low beam current of 75.4 mA.

It is found from Figure 2-11 that if the second taper had one less cavity, the basic efficiency would decrease by about 0.6 percentage points, while the RF dissipation would drop from 9.2 to 8.2 percent. It was considered desirable to take advantage of this significant reduction in dissipation, even though at some higher frequencies in the band the predicted efficiency decreased by almost one percentage point with one less cavity. Thus the final tube, ETM-2, was built with four cavities in the second taper. The measured basic efficiency of the ETM-2 tube over the frequency band is compared with the calculated efficiency points in Figure 2-12. The agreement between measured and calculated efficiencies is satisfactory, considering that the higher operating voltage (8.3 vs. 8.0 kV) improves the low frequency performance, while the higher beam current (91.5 vs. 84.1 mA) increases the bandwidth and efficiency.

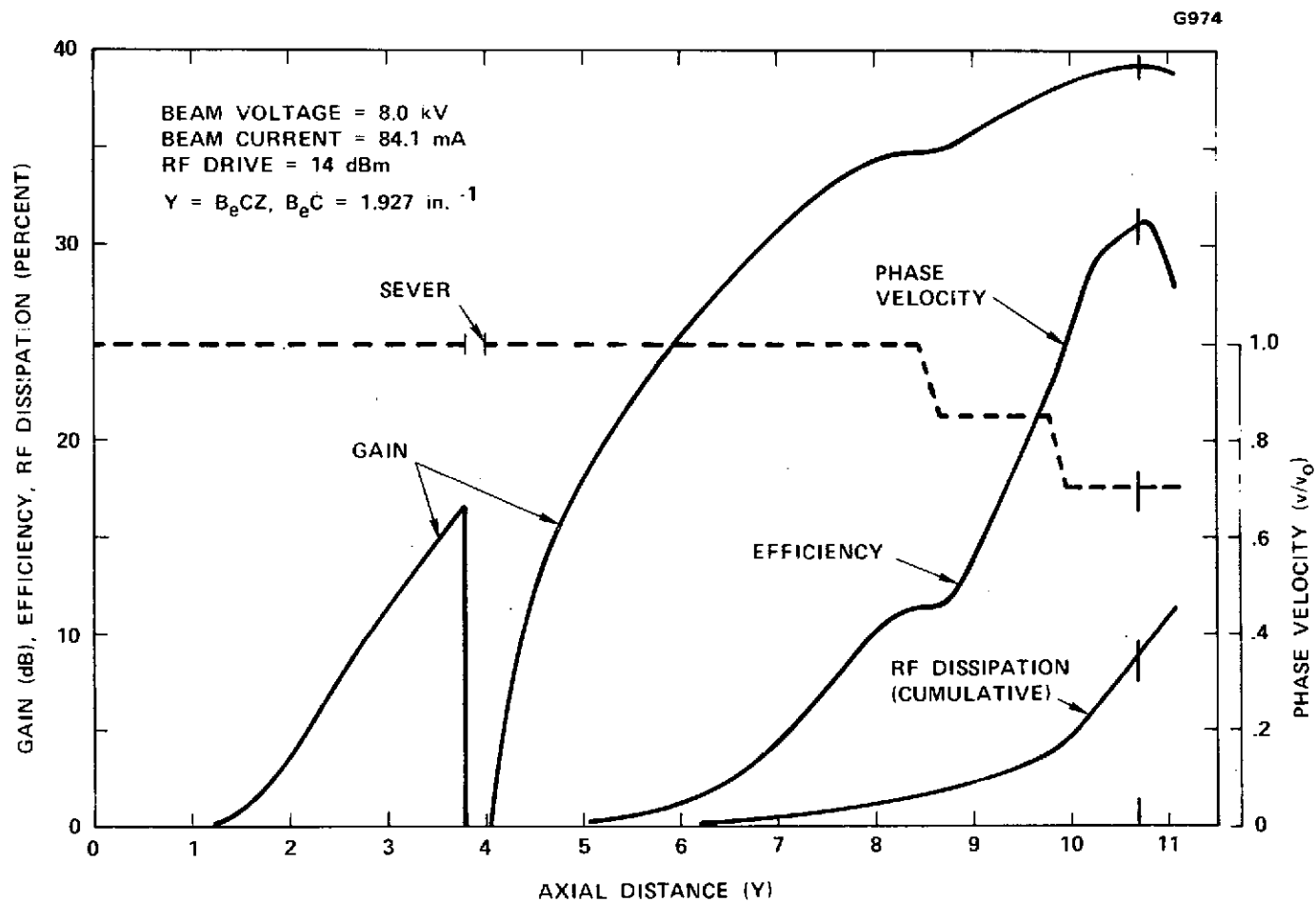


Figure 2-11 284H calculated performance for optimum taper design.



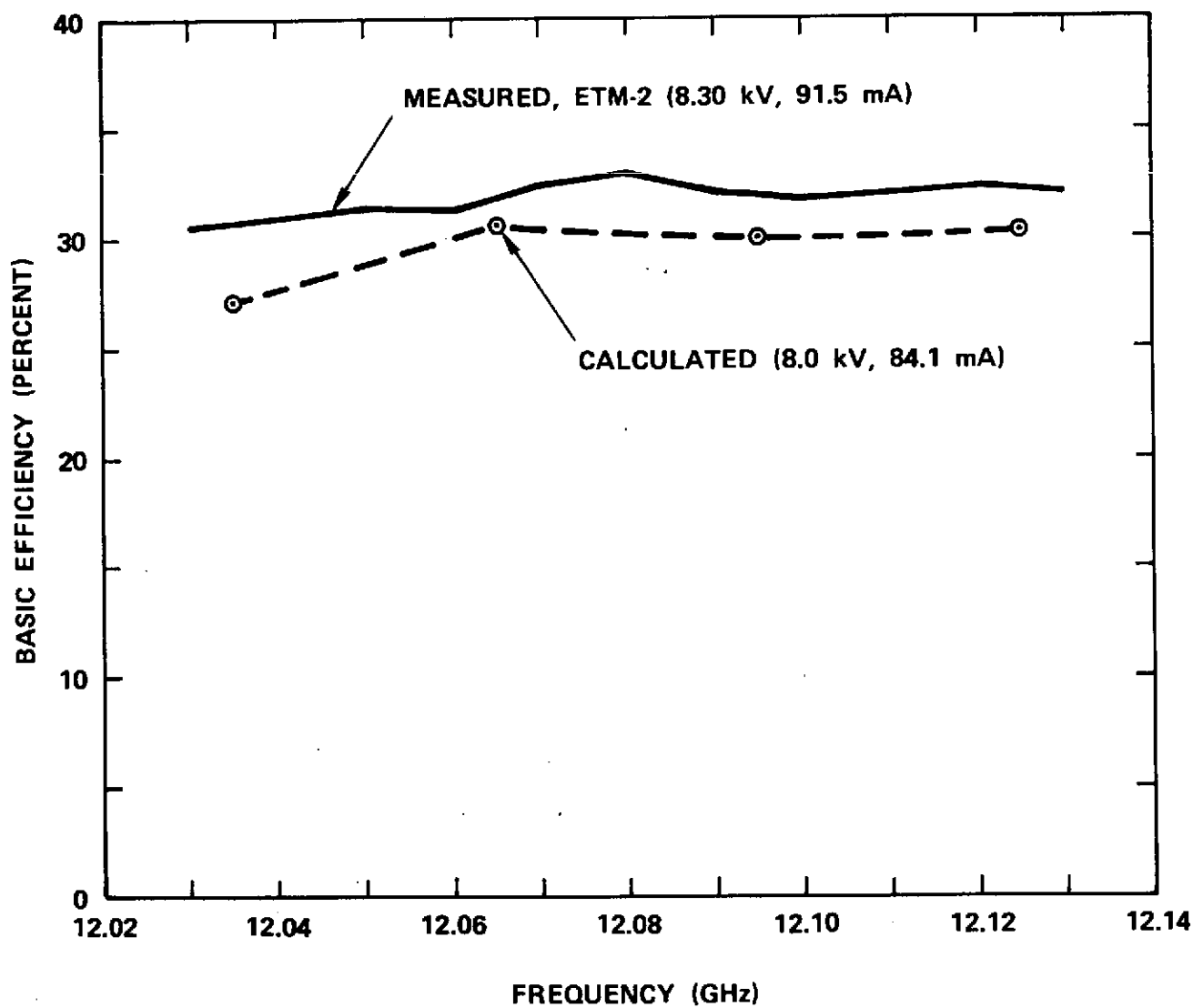


Figure 2-12 284H ETM-2 calculated versus measured basic efficiency.

## 2.2 ELECTRON GUN

A new electron gun design was undertaken for the 284H tube. This gun is a Pierce type, convergent flow design using a potted heater, a type B impregnated tungsten cathode, and a modulating anode. A photograph of the gun assembly (designated the model 197B) is shown in Figure 2-13. The 197B measured gun parameters are given in Table 2-2. The mechanical design of the gun utilized conventional Hughes cylindrical supports for ruggedness and low voltage gradients. Special heat shields were incorporated to minimize filament power.

Initial electrode shapes were designed using a combination of empirical data and electrolytic tank measurements. The results were then analyzed using a digital computer program which computed electron trajectories and beam perveance based on a combination of three basic applications: Laplace Equation solving, Electron optics using fixed starting conditions, and Electron optics using the Langmuir-Child formulation at a space-charge limited spherical cathode. Because of the highly thermal nature of the beam, further analysis was required. Using computed on-axis potentials from the ray tracing program to describe the lense effect of the gun elements, the effect of the thermal velocities of the electrons was analyzed in another digital computer program. Here the beam was studied with and without magnetic field. The computations without a magnetic field were compared with measured beam parameters from the demountable beam analyzer. The correlation between the calculated and measure beam perveance, beam minimum radius, and beam minimum position was excellent. The electron flow as determined by the computer calculation and by measurement was highly laminar with sharp beam edge definition.

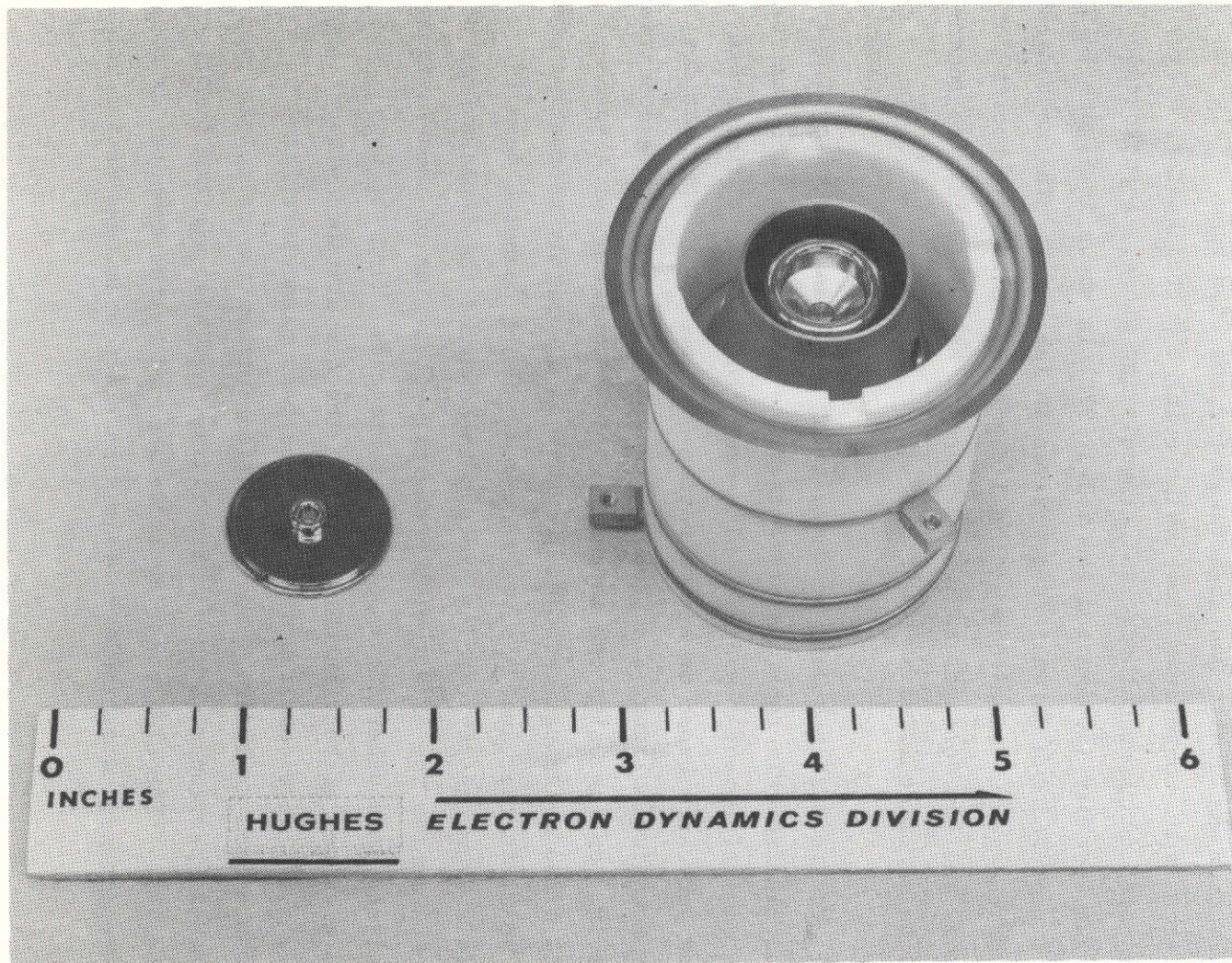


Figure 2-13 284H electron gun.

ORIGINAL PAGE IS  
OF POOR QUALITY

TABLE 2-2

## 197B Electron Gun for the 284H OST

Measured Gun Parameters	
Perveance	$0.116 \text{ } \mu\text{A/V}^{3/2}$
Beam Voltage	8 kV
Cathode Current	83.1 mA
Anode Current	0.04 mA
Minimum Beam Diameter	0.032 in. (0.081 cm)
Cathode Current Density	$1 \text{ A/cm}^2$
Filament Power	5.5 W

### 2.3 PPM FOCUSING DESIGN

The electron beam focusing was one of the most critical design areas in the 284H tube development. The maximum operating temperature of the circuit pole piece ferrules and the heat power flowing into the base plate structure is directly proportional to the beam current interception on the RF slow wave structure. As such, the beam transmission is an important factor in the reliability of both the tube and adjacent spacecraft components.

Extensive theoretical and experimental evidence exists which proves that the basic interaction efficiency is a sensitive function of the beam cross-section and the degree of laminarity. The collection of the electrons at body potential also degrades the overall efficiency of the TWT. Finally, the characteristics of the collector are critically dependent on the electron trajectories of the focused beam near the output of the tube.

The coupled cavity structure provides an excellent magnetic circuit for periodic permanent magnet focusing of the electron beam. The cavity walls are fabricated of vacuum quality electrolytic iron for use as magnetic pole pieces. The focusing magnets are situated between adjacent pole pieces and just outside the copper spacers which form the cylindrical cavity. In this way the focusing field is brought into close proximity to the beam. The magnetic pole pieces are accurately aligned and brazed as part of the normal circuit assembly sequence, minimizing transverse field effects. In addition the coupled cavity circuit is thermally rugged making PPM focusing at the specified power level a conservative design approach.

In the 284H TWT, the required axial magnetic field is provided by a double period permanent magnet (PPM) focusing structure as shown in

Figure 2-14. Double period PPM focusing offers an important advantage over the conventional single period design; a stronger magnetic field can be obtained with a given magnetic material. This is because the magnet length per cavity is increased, resulting in a greater magnetizing force between the pole pieces.

By using double period PPM focusing, it was possible to use ordinary Alnico 8 magnetic material in the standard (untapered) sections of the 284H. In the velocity taper, rare earth magnets (Samarium Cobalt) were used. These were required in order to: (1) provide increased magnetic focusing field near the tube output where the beam space-charge forces are highest; and (2) achieve this field with reduced magnet thickness caused by the velocity taper period reduction. Table 2-3 gives the PPM focusing parameters for the 284H tubes.

Computer computations were made to optimize the beam focusing with magnetic field. These calculations included thermal velocity effects. From measured magnetic field data, computer generated plots were made of various beam envelopes under optimum focusing conditions. These are shown in Figure 2-15. The magnetic field is shown at the top of the plot. The lower portion of the graph shows beam envelopes containing 99.5 percent and 95 percent of the beam current ( $R_{99.5}$  and  $R_{95}$ ), the beam radius at 1/10 peak current density ( $R_{1/10}$ ), and an rms beam radius  $R_0$ .

The near lack of ripple on  $R_0$  indicates optimum focusing conditions. The ripple on the other envelopes is entirely due to the thermal velocities of the electrons.

The computed result indicated greater than 99 percent transmission without RF drive. The typical transmission actually achieved on the 284H tubes was 99 percent. Beam transmission of 93 to 95 percent was obtained at saturation.

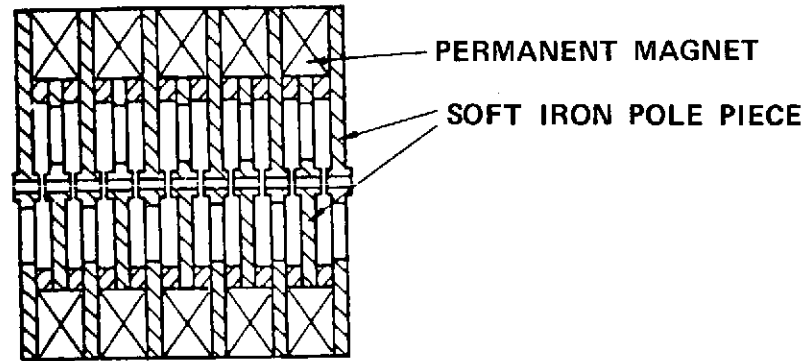
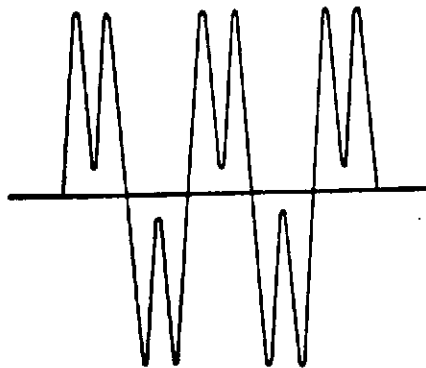
**DOUBLE PERIOD PPM STRUCTURE****AXIAL MAGNETIC FIELD**

Figure 2-14 Double PPM focusing structure and axial magnetic field.



TABLE 2-3

## 284H PPM Focusing Parameters

Period	Material	Field (tesla)		$\lambda P/L$
		Peak	RMS	
Standard	ALNICO 8	.2250	.1170	7.27
Taper 1	SmCo5	.2860	.1487	8.55
Taper 2	SmCo5	.3216	.1672	9.69

The achievement of this excellent focusing was easily done and relatively few magnet shunts were required to maximize transmission. Final adjustments in focusing were made with the tube operating at 60°C baseplate temperature to account for slight thermal changes in the Samarium Cobalt magnets in the velocity taper. These adjustments also improved the focusing at 25°C baseplate temperature. Since the Alnico 8 magnets are insensitive to temperature changes only adjustments at the tube output were found necessary.

2.4 REFOCUSING SOLENOID

In order to optimize the beam entrance conditions into the multi-stage depressed collector, a refocusing solenoid was incorporated just beyond the shielded output pole piece of the 284H TWT. The purpose of this refocusing section was to allow the spent electron beam to expand, reducing the space charge forces and minimizing the beam radial velocity components.

Three acceptable refocusing schemes were defined by Dr. H. Kosmahl of NASA. They are depicted in Figure 2-16.

For the 284H tube, the value of  $B_{rms}$  is

$$B_{rms} = .117 \text{ tesla}$$



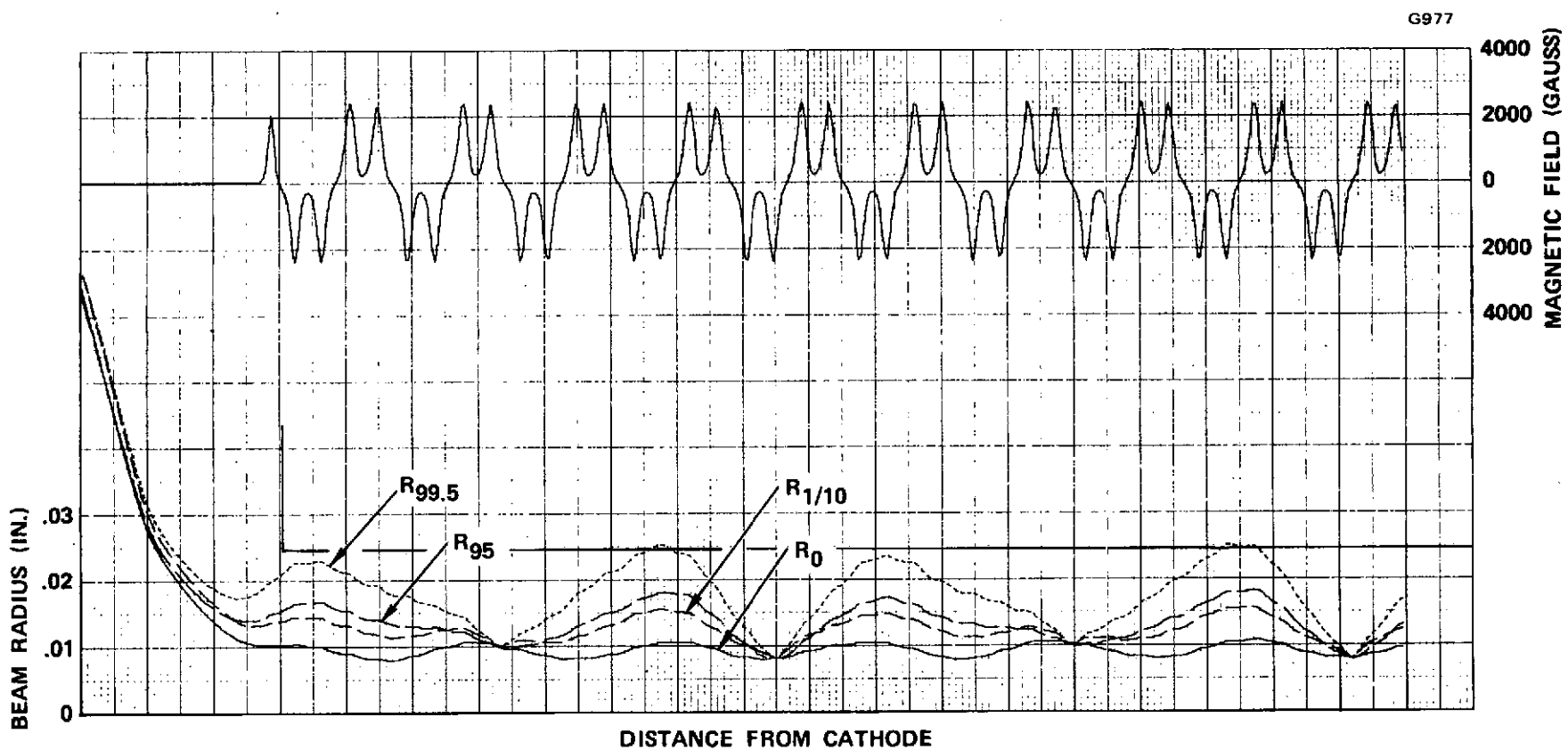


Figure 2-15 Computer analysis of focused electron beam for the 284H.

The values of  $\lambda C$  are calculated from the formula

$$\lambda C = \frac{21.2 \times 10^{-4} \sqrt{V_0/10}}{B} \text{ meters}$$

where B is the magnetic field in tesla and  $V_0$  is the beam voltage in kilovolts.

The calculated values for each refocusing section design are given in Figure 2-16.

Due to package design and weight considerations, Hughes selected to utilize a refocusing section design somewhat like option II with a total length of .0381 meters (like option III).

Two independently adjustable field levels were provided by means of a two section solenoid as shown in Figure 2-17. By operating the two sections with different power supplies, any combination of field levels could be produced.

The axial field configuration that gave maximum depressed collector efficiency for the 284H tubes is shown in the lower curve of Figure 2-17. If one ignores the slightly higher field in the first section, this refocusing section corresponds closely to the design option III.

The refocusing solenoid dissipated 6 watts. An alternate structure utilizing permanent magnets was designed but was not used in any of the 284H tubes. The use of the permanent magnet design would have increased the overall efficiency by as much as 1 percentage point.

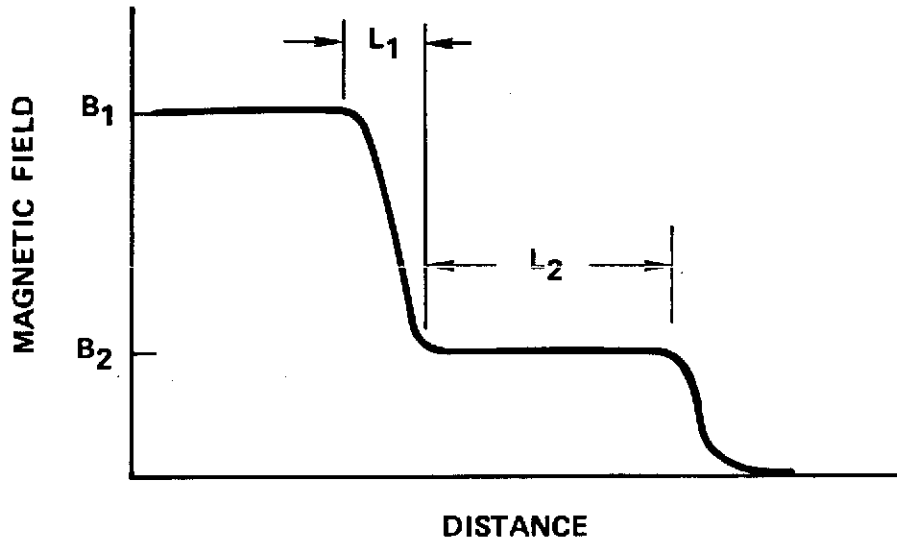


Figure 2-16 Refocusing section designs.

- |      |                    |                               |                            |
|------|--------------------|-------------------------------|----------------------------|
| I.   | $L_1/\lambda_{c1}$ | $= 1.8$                       | $L_1 = .041$               |
|      | $L_2/\lambda_{c2}$ | $= 0.46$                      | $L_2 = .0348 \text{ m}$    |
|      | $B_1$              | $= \text{Brms}$               | $B_1 = .117 \text{ tesla}$ |
|      | $B_2$              | $= .025 - .030 \text{ tesla}$ |                            |
| II.  | $L_1/\lambda_{c1}$ | $= 1.0$                       | $L_1 = .023 \text{ m}$     |
|      | $L_2/\lambda_{c2}$ | $= 0.46$                      | $L_2 = .0348 \text{ m}$    |
|      | $B_1$              | $= \text{Brms}$               | $B_1 = .117 \text{ tesla}$ |
|      | $B_2$              | $= .025 - .030 \text{ tesla}$ |                            |
| III. | $L_1/\lambda_{c1}$ | $= 0$                         | $L_1 = 0$                  |
|      | $L_2/\lambda_{c2}$ | $= 0.5$                       | $L_2 = .0378 \text{ m}$    |
|      | $B_1$              | $= \text{Brms}$               | $B_1 = .117 \text{ tesla}$ |
|      | $B_2$              | $= .025 - .050 \text{ tesla}$ |                            |

# REFOCUSING SOLENOID

G979

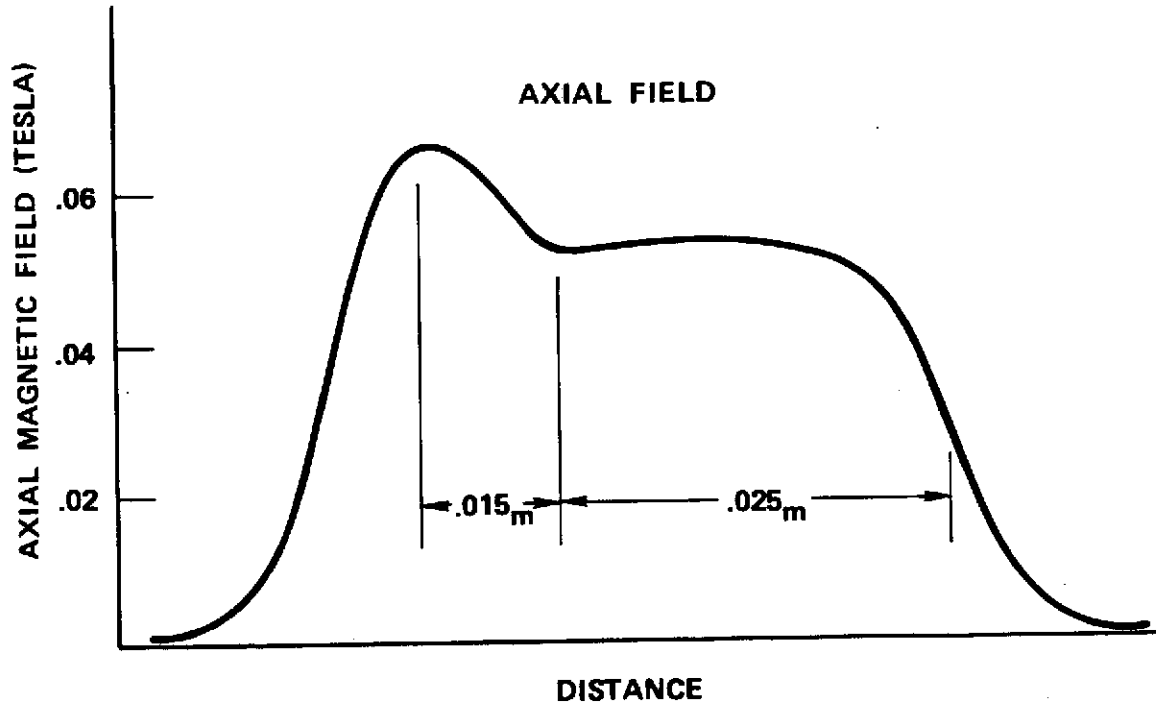
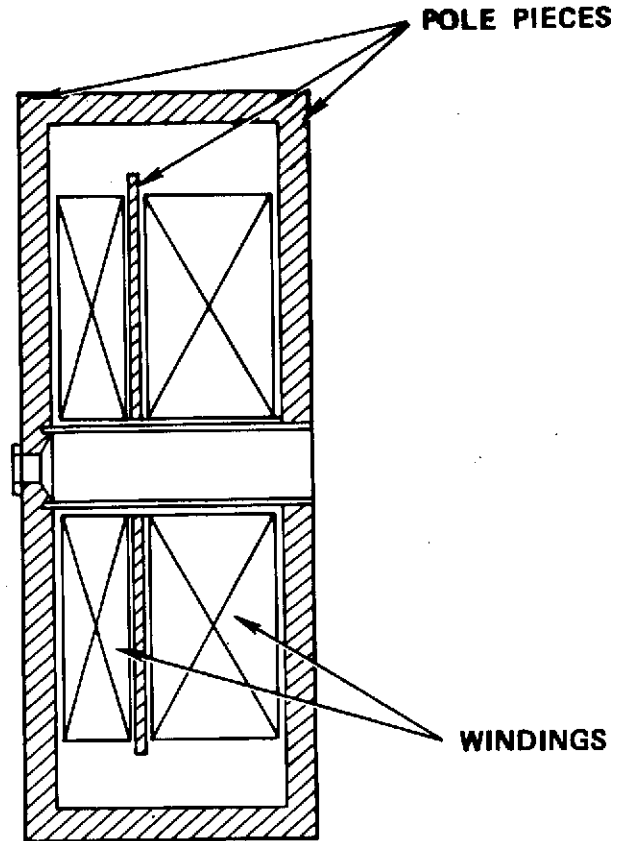


Figure 2-17 284H refocusing section.

## 2.5 RF COUPLERS AND WINDOWS

The RF couplers provide the means of guiding the RF power into and out of the coupled cavity circuit across the vacuum envelope. The design approach used on the 284H was to utilize identical rectangular waveguide, poker chip RF windows, and three-step rectangular waveguide transformers for the input and output couplers.

The waveguide transformer was computer designed for minimum VSWR in the operating frequency band. The height of this transformer is stepped in three sections from full WR-75 waveguide height to the height of the standard circuit cavity.

The poker chip RF window utilizes a thin alumina window in a short section of cylindrical waveguide. Abrupt transitions to WR-75 rectangular waveguide are made on either side of the window. The length of the cylindrical section is adjusted to give minimum VSWR in the frequency band. Typical measured VSWR's of these poker chip windows is less than 1.05:1. The window design used on the 284H was taken directly from a previous Hughes tube.

A dual directional waveguide coupler was incorporated on the output RF coupler of the 284H to permit monitoring the OST output RF power as well as the reflected RF power from the high power circulator beyond the OST.

A photograph of this OST power sensor assembly is shown in Figure 2-18. This unit has two built-in crystal detectors, with a forward coupling of 54 dB, and a reverse coupling of 33 dB.

Table 2-5 summarizes the characteristics of the telemetry power sensor. The crystal detector voltage outputs versus OST RF power output and load VSWR are given in Figure 2-19.

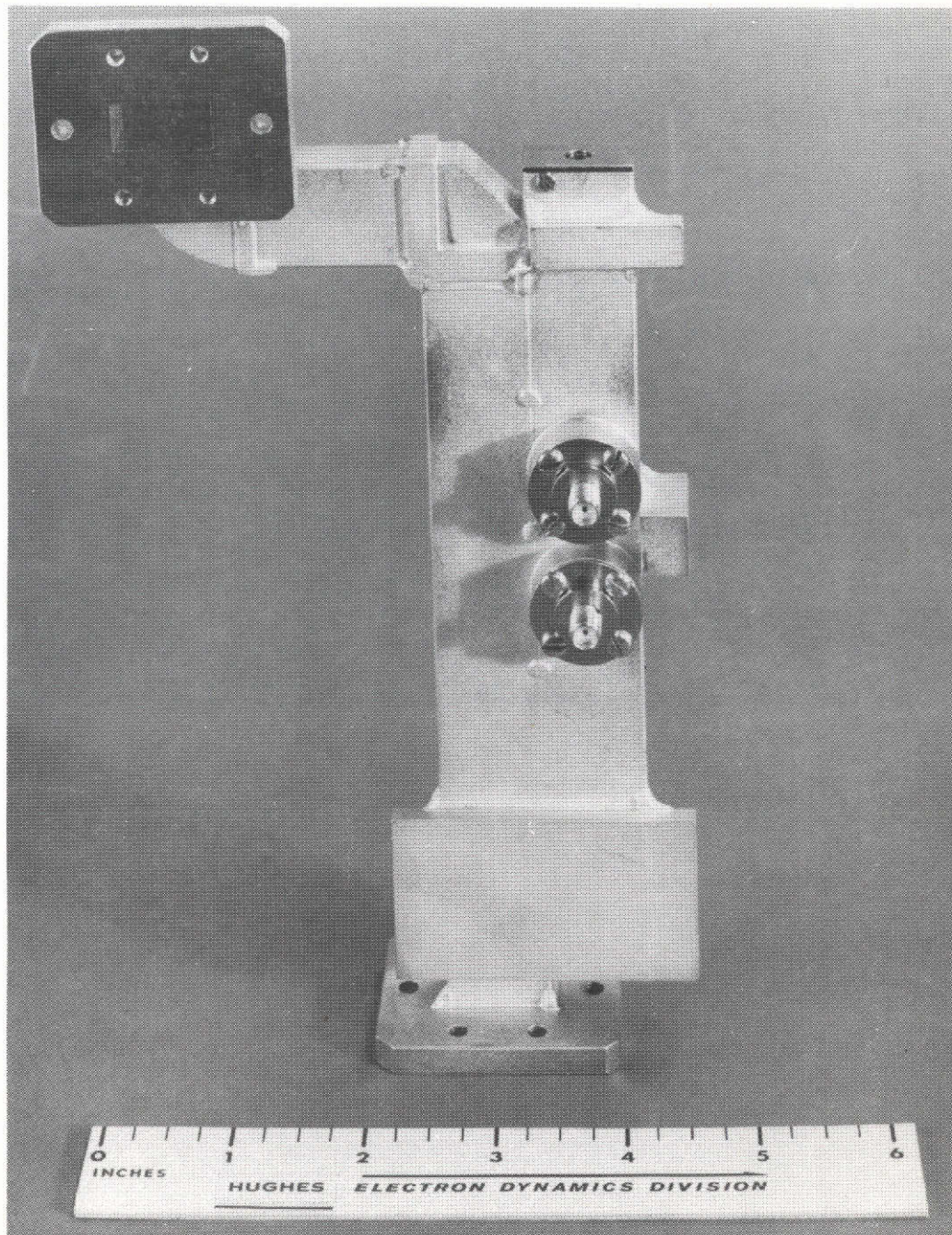


Figure 2-18 284H OST power sensor.

ORIGINAL PAGE IS  
OF POOR QUALITY

TABLE 2-5

OST Power Sensor COUPLER ASSY	
Signal output at 200W $P_{out}$	50 mV
Signal output at 2 W $P_{REFLECTED}$	50 mV
Directivity of reflected sensor	32 dB
Forward insertion loss	0.2 dB
Temperature sensitivity	+55 mV/ $^{\circ}$ C
VSWR	1.05:1
Weight	0.5 lb.

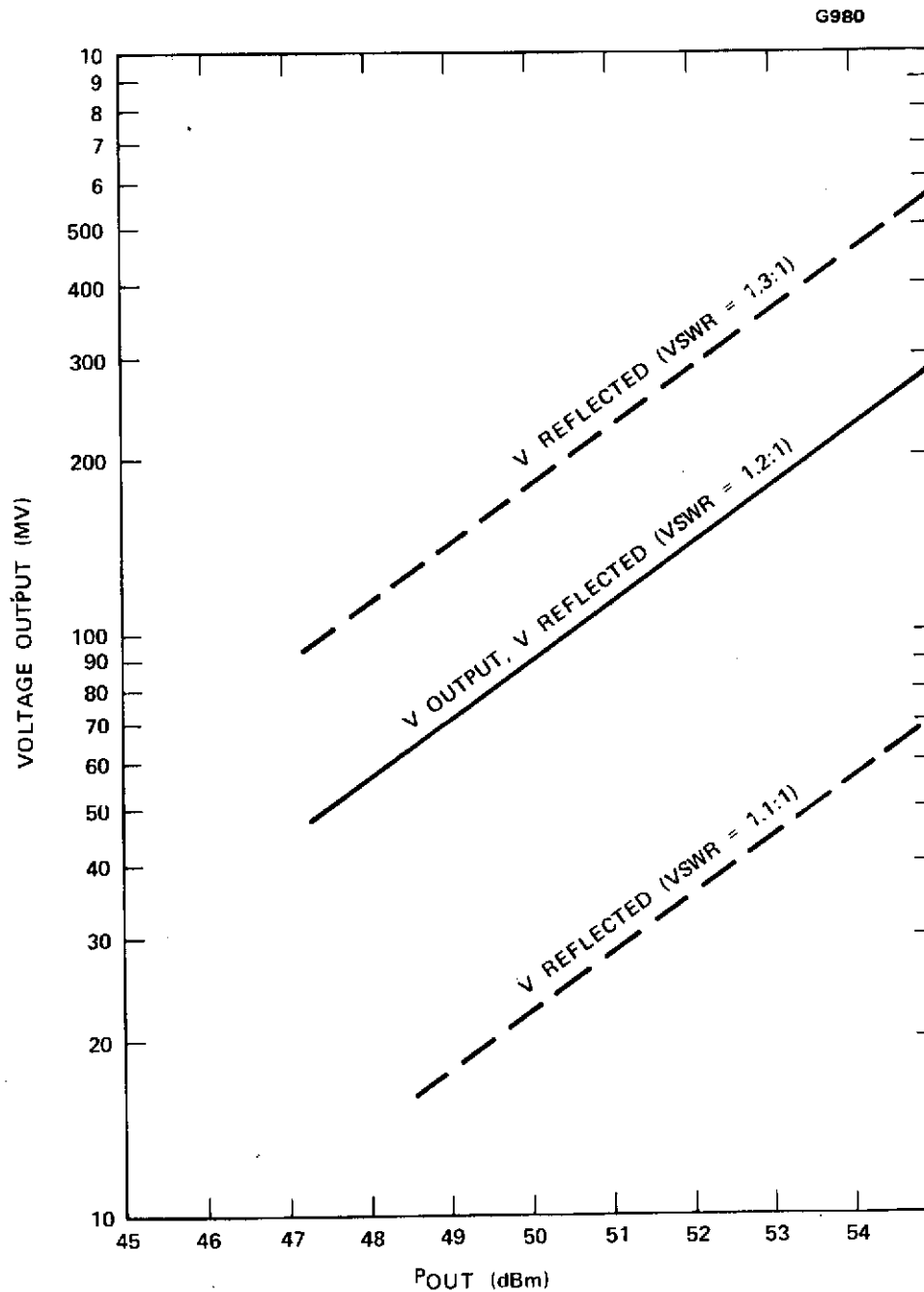


Figure 2-19 284H OST voltage sensor outputs.



## 2.6 MULTI-STAGE DEPRESSED COLLECTOR (MDC)

### 2.6.1 Electrical Design of the MDC

The electrical design of the 284H multi-stage depressed collector (MDC) was done at NASA Lewis Research Center by Dr. H. G. Kosmahl. The design was based on initial values of the 284H TWT characteristics and was defined by a set of equipotentials furnished to Hughes by NASA. These are shown in Figure 2-18. The electrode voltages are normalized to the cathode voltage, with collector number 1 at ground (tube body) and number 10 at cathode potential. The remaining collector voltages are at  $0.2 V_k$ ,  $0.3 V_k$ , etc. to provide a smooth decelerating force on the spent beam electrons. An axial spike on the tenth electrode provides an additional radial force on the high energy electrons. The first and tenth equipotentials were exactly duplicated with hemispherical and conical electrode shapes respectively. The remaining equipotentials were approximated by conical elements as shown in Figure 2-20. The second element (corresponding  $0.1 V_0$  equipotential) was eliminated since a negligible number of electrons were expected in this energy class.

The ten stage depressed collector has three electrical functions:

1. To sort electrons according to their velocities.
2. To slow the electrons so they are collected with the lowest possible kinetic energy.
3. To prevent back-streaming of reflected primary and secondary electrons into the RF circuit.

The electrons are intercepted on the surface of the electrode facing away from the tube. In this way, secondaries are effectively suppressed by the more negative potential of the following electrode.

The important features of the ten stage depressed collector are listed in Table 2-6. A cross-section view of the MDC is shown in Figure 2-21. The first electrode is hemispherically shaped, the rest of the electrodes

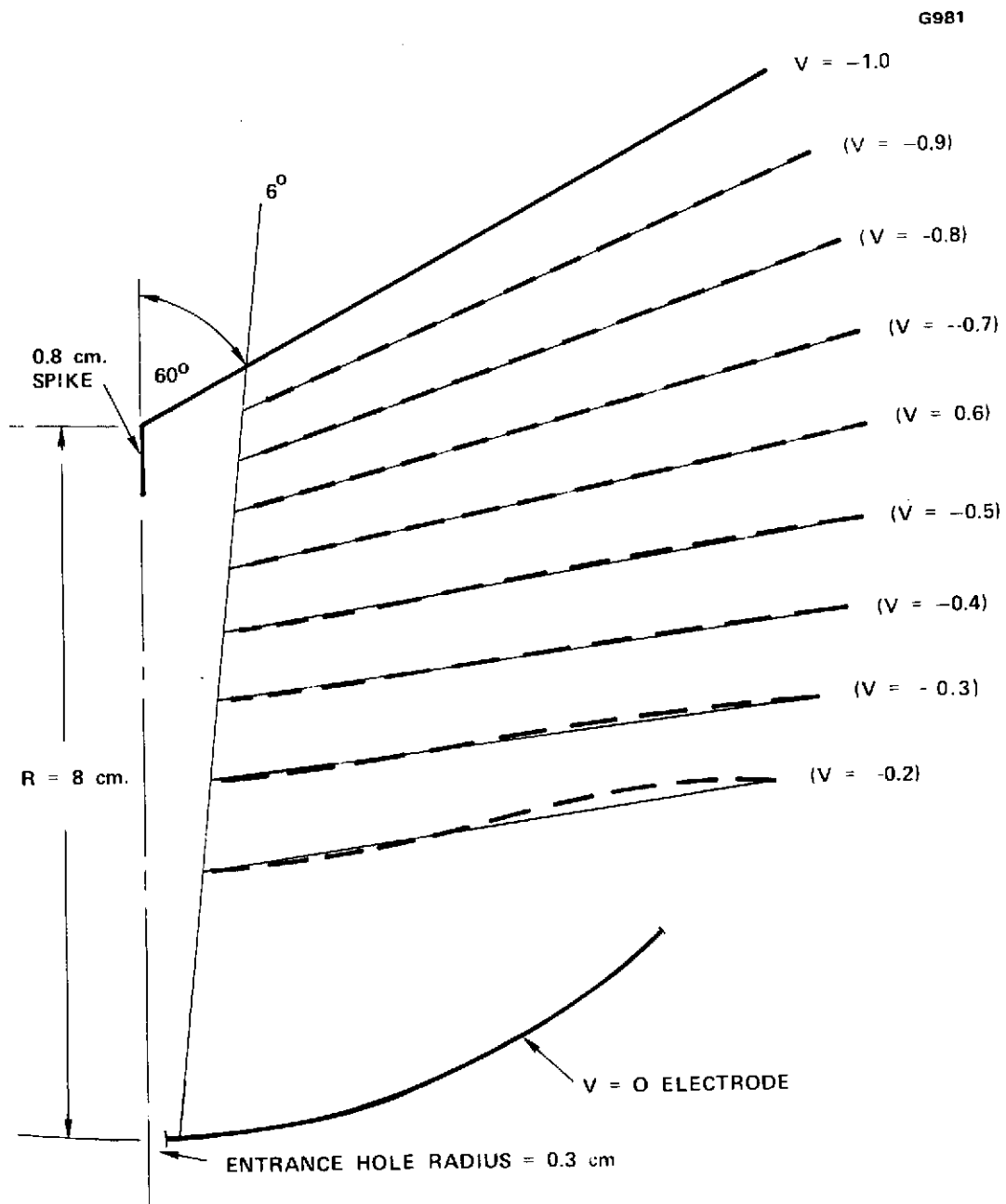


Figure 2-20 284H multistage depressed collector equipotentials.

TABLE 2-6

MDC Design Features

- Spun Molybdenum Electrodes
- Tungsten spike
- Overlapping ion shields
- Stainless steel vacuum envelope
- Special bellows thermal choke
- Internal radiation heat shields

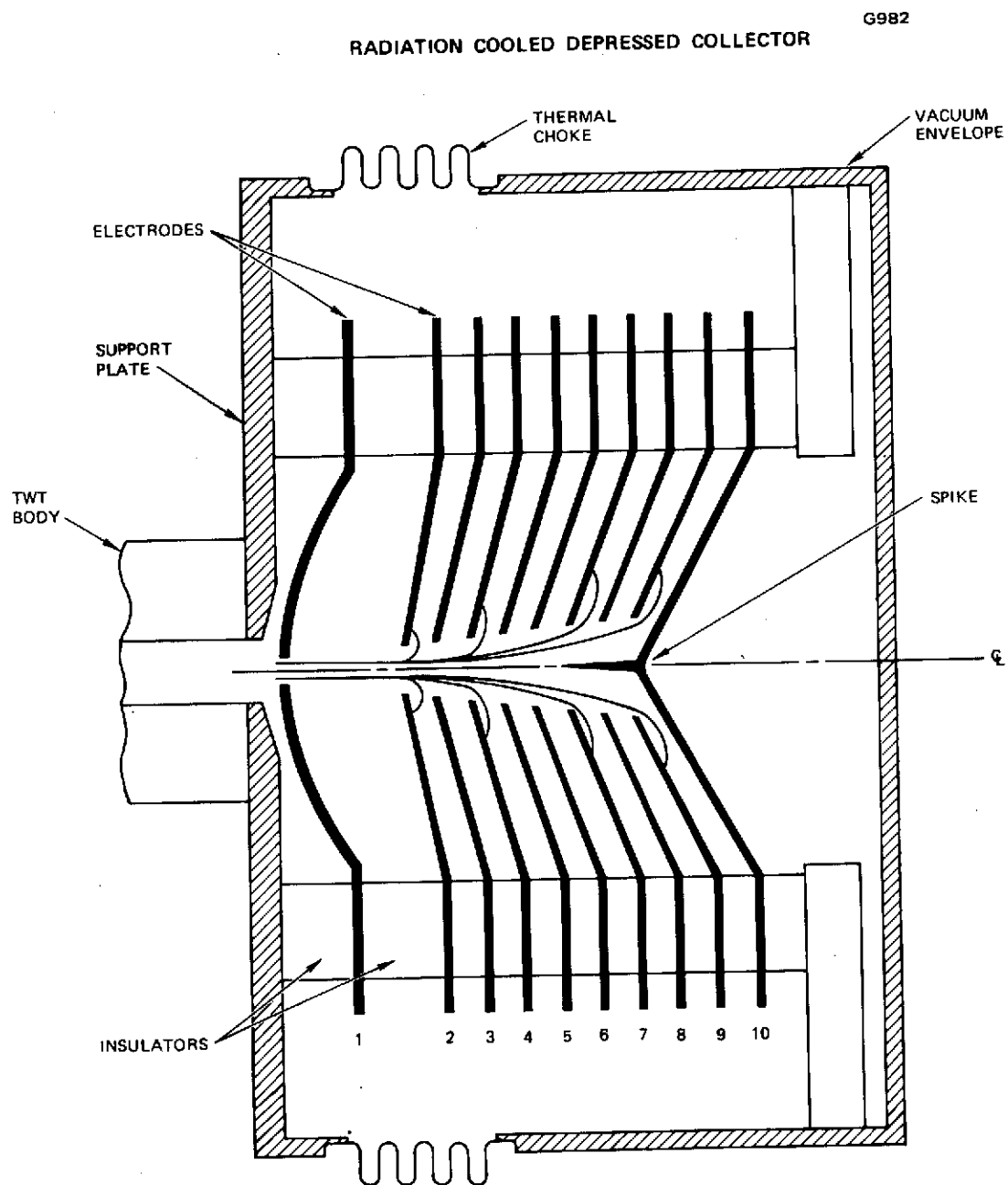


Figure 2-21 284H radiation cooled depressed collector.

ORIGINAL PAGE IS  
OF POOR QUALITY

are conically shaped. There is a flat flange area at the OD to simplify the mechanical support design. The collector elements are electrically and thermally insulated from each other, the TWT body, and the vacuum envelope. The insulators also provide mechanical support for the electrodes. Heat is dissipated by radiation to the other electrodes, to the vacuum envelope, and from there to deep space.

To optimize the MDC performance, tube-to-tube changes were made only to the electrode apertures and to the length of the spike.

A tradeoff exists between size (weight) and operating temperature for the MDC. A larger diameter collector results in greater weight and lower radiated power density, hence lower operating temperature. Conversely, a smaller diameter collector weighs less but operates at a higher temperature.

To produce the desired electrostatic forces on the spent beam electrons, there is a minimum conical electrode size. To determine this size a computer program was used which solves the Laplace equation within a given closed potential boundary. Starting with electrode flange inner diameters of 0.254 meters, the flanges were reduced in successive steps until the potentials at the beam edge changed by 0.1 percent. This occurred at a flange I.D. of 0.095 meters. The electrode design was then fixed at that value. A flange OD of 0.15 meters was selected from mechanical and thermal considerations. Following the design of the electrodes for the MDC, the voltage standoff capability of the assembly was examined. The space between the electrodes was found to be sufficient to stand off more than 2 kV in vacuum. The insulators between the electrode flanges were also voltage stress analyzed. All of these were of sufficient length to stand off at least two times the required voltage difference (1.6 kV).

To prevent material from volatilizing off of the hot collector surfaces, coating the spacer insulators and thereby causing voltage breakdown, ion shields are incorporated into the design. These ion shields are embodied as overlapping concentric cylinders outside the insulators. The geometry is such that the ion shields provide complete optical blockage from most of the electrode surfaces. The radial spacings of these ion shields are conservatively designed to stand off greater than 1.6 kilovolts across the vacuum gap.

On the preliminary OST's, the spike in the tenth electrode was mounted on an insulated micrometer mechanism to permit adjustment during test. The spike length was fixed in the ETM OST's.

#### 2.6.2 Mechanical Design of the MDC

The mechanical design of the MDC is shown in Figure 2-21. The entire assembly is attached to the TWT by means of the support plate. The electrodes and vacuum envelope are supported by equally spaced tubular posts. The assembly is positioned on these posts, then held permanently in place by welded fasteners at the ends. The electrodes are insulated from the supports by ceramic tubing as shown. This arrangement provides easy assembly and accurate alignment of the electrode apertures using a special fixture.

The pressure applied to the electrodes and insulator spacers was carefully controlled to assure that no transverse movement could occur under operating and non-operating vibration or shock. Due to the temperature differences of the insulators and the support posts, the compressive forces on the electrode stack increases for both hot (operating) and cold (non-operating) conditions. The cross sections of the supports and insulators are designed for safe stress levels under all conditions. The various conditions analyzed and the resulting stresses are summarized in Table 2-7.

The high voltage attachments were made with conductors from the feedthrus to each electrode. The connection to the electrode is heli-arc welded at assembly. The longer conducting rods are supported by one or two radial tabs welded to intermediate electrodes. Ceramic sleeves over the rods serve as insulators. The mechanical support for the vacuum envelope is primarily from radial spokes between the envelope and the support posts. Very little support comes from the support plate due to the flexibility of the thermal choke.

The vacuum envelope is essentially a 0.050 thick stainless steel can. The thickness was chosen as the best compromise between minimum weight, stress with an internal vacuum, maximum thermal conductance, and reliable vacuum integrity.

TABLE 2-7

MDC Thermal Differential Expansion Effects

Condition	Differential Expansion	Force On Electrodes	Stress On Support Tubes
Uniform 25°C	.000 cm	4,740 lbs	10,000 psi
OST on w/oRF	+.0187 cm	22,200 lbs	42,500 psi
OST on w RF	-.0114 cm	14,200 lbs	30,000 psi
OST off (MDC can -200°C)	+.0116 cm	14,360 lbs	30,340 psi

A mass model of the OST was fabricated as part of the 284H program. This model included a representative mock-up of the collector assembly and used actual OST package parts. A photograph of the mass model is shown in Figure 2-22. Vibration tests were performed on this mass model early in the program and also on one of the preliminary OST's (P-1) several months later.



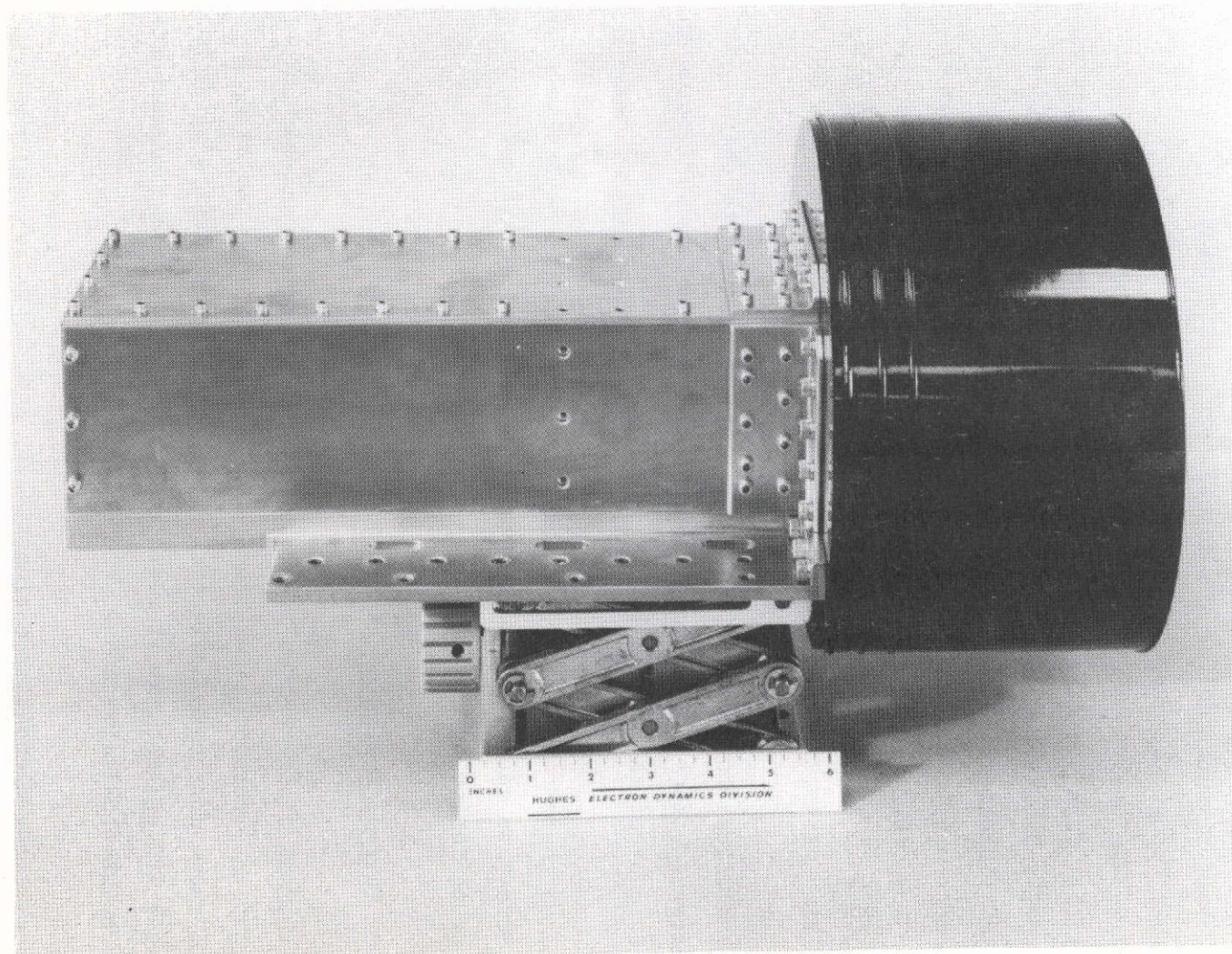


Figure 2-22 284H mass model.

ORIGINAL PAGE IS  
OF POOR QUALITY



The mass model vibration tests were conducted with the baseplate attached to a rigid fixture, unlike the actual space craft which utilizes a flexible honeycomb panel. These tests were also performed without the truss member used in the TEP. The results are summarized in Figure 2-23. For axial vibration (thrust axis), the lowest resonant frequency was 950 MHz; indicative of a very low energy effect. At the critical TWT-MDC interface location 3, the amplification was only 5.5. The collector electrode resonance was 1000 Hz with an amplification of only 1.5. For vibration in the lateral axis (transverse) the lowest resonance was 360 Hz. At the critical interface 1 the amplification was 6.5. The resulting deflection is well within safe stress limits for the OST.

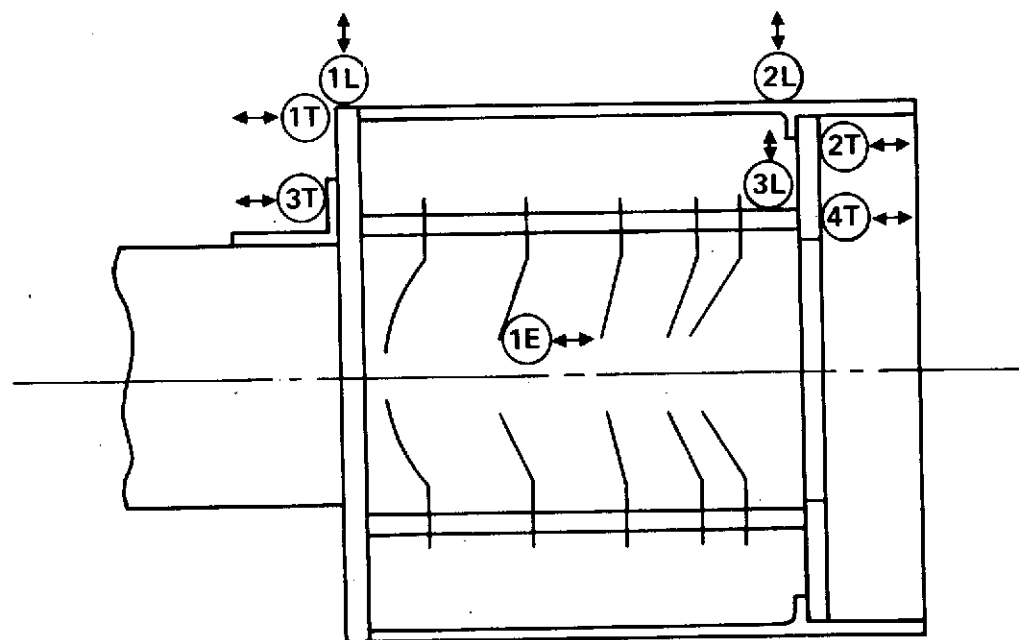
The amplification at positions 2 and 3 are higher due to the cantilever effect. The stress levels are nevertheless well below the yield point of the materials.

Based on these results, it was concluded that the MDC mechanical design was more than adequate to withstand the specified qualification vibration and acceleration levels.

### 2.6.3 Thermal Design of the MDC

The thermal design was as important as the electrical and mechanical designs in determining the final configuration of the radiation cooled multi-stage depressed collector. Several design tradeoffs were made between weight, mechanical rigidity, size and operating temperatures before the final dimensions were selected.

The collector elements are electrically and thermally insulated from each other, the tube body, and the vacuum envelope. The insulators also provide thermal isolation and mechanical support for the electrodes.



	LATERAL AXIS			THRUST AXIS				ELECTRODE
	1L	2L	3L	1T	2T	3T	4T	1E
"G" MAGNIFICATION	6.5	40.0	40.0	11.0	11.5	5.5	5.0	1.5
RESONANT FREQUENCY	950 Hz			360 Hz				1000 Hz

Figure 2-23 284H Mass model resonance tests.

The heat generated by the incident electron beam is dissipated entirely by radiation to the other electrodes, to the vacuum envelope, and from there to deep space. The element and vacuum envelope temperatures are strongly influenced by the TWT RF output power as well as the thermal characteristics of the surrounding environment and the elements themselves. This is because the distribution of current to the various electrodes is determined by the beam energy spread which, in turn, is a function of the RF power output.

The design of the MDC proceeded in the following sequence:

1. The electrical design constraints were determined.
2. The initial mechanical design was established.
3. The thermal characteristics of the MDC design were analyzed.

Based on the results of the thermal design the initial mechanical design was modified as required to optimize the overall collector performance.

One problem that occurred in the thermal design of the MDC was the reduction of heat conduction from the MDC vacuum envelope to the TWT support plate. Due to the radiation cooling, the vacuum envelope operates at several hundred degrees centigrade while the TWT temperature must be maintained below  $100^{\circ}\text{C}$ . Without an effective thermal isolator, a large percentage of the collector power dissipation flows to the TWT, drastically reducing the effectiveness of the radiation cooling approach.

To solve this problem Hughes designed an improved thermal isolator. The design consists of a series of large holes through the side of the envelope to reduce the effective cross section area and yet provide the necessary mechanical strength. A vacuum tight envelope is maintained by a bellows that is electron beam welded over the holes. The

long conduction path length of the bellows is also an effective barrier to heat transfer. A photograph showing this thermal choke is shown in Figure 2-24.

The thermal analysis of the 284H radiation cooled multi-stage depressed collector was done by Mr. A. N. Curran of NASA Lewis Research Center. The computations were performed using a modified version of an existing model thermal analysis computer program. The model of the MDC consisted of flat electrode dishes inside a metal vacuum envelope. No heat transfer from the electrodes and the envelope to the support plate was assumed. Conservative estimates of the emissivities of the elements ( $\epsilon = .30$ ) and the envelope ( $\epsilon = .90$ ) were used. The steady state analysis was performed for two types of OST operation: (1) RF output power of 200 watts (at saturation), and, (2) RF output power of 0 watts (no RF drive).

The results for  $P_{out} = 200 \text{ W}$  are shown in Figure 2-25. The graph on the left gives the electrode temperature versus radial distance for each of the elements and for the end of the vacuum envelope (container). The maximum predicted temperature is less than  $400^{\circ}\text{C}$ . The graph on the right gives the vacuum envelope cylinder temperature versus distance along the envelope. The maximum temperature  $282^{\circ}\text{C}$  ( $540^{\circ}\text{F}$ ).

The results for  $P_{out} = 0 \text{ W}$  are shown in Figure 2-26. This is the worst case condition due to the higher spent beam power and the higher concentration of beam interception on the most depressed elements. The maximum electrode temperature is  $570^{\circ}\text{C}$  on element number 8. The maximum vacuum envelope temperature is  $343^{\circ}\text{C}$  ( $650^{\circ}\text{F}$ ).

An additional analysis was performed at Hughes to evaluate the heat transfer from the MDC to the TWT support plate. This analysis used the electrode temperatures from the NASA calculations. Included in this



Figure 2-24 284H MDC vacuum envelope with thermal choke.

ORIGINAL PAGE IS  
OF POOR QUALITY

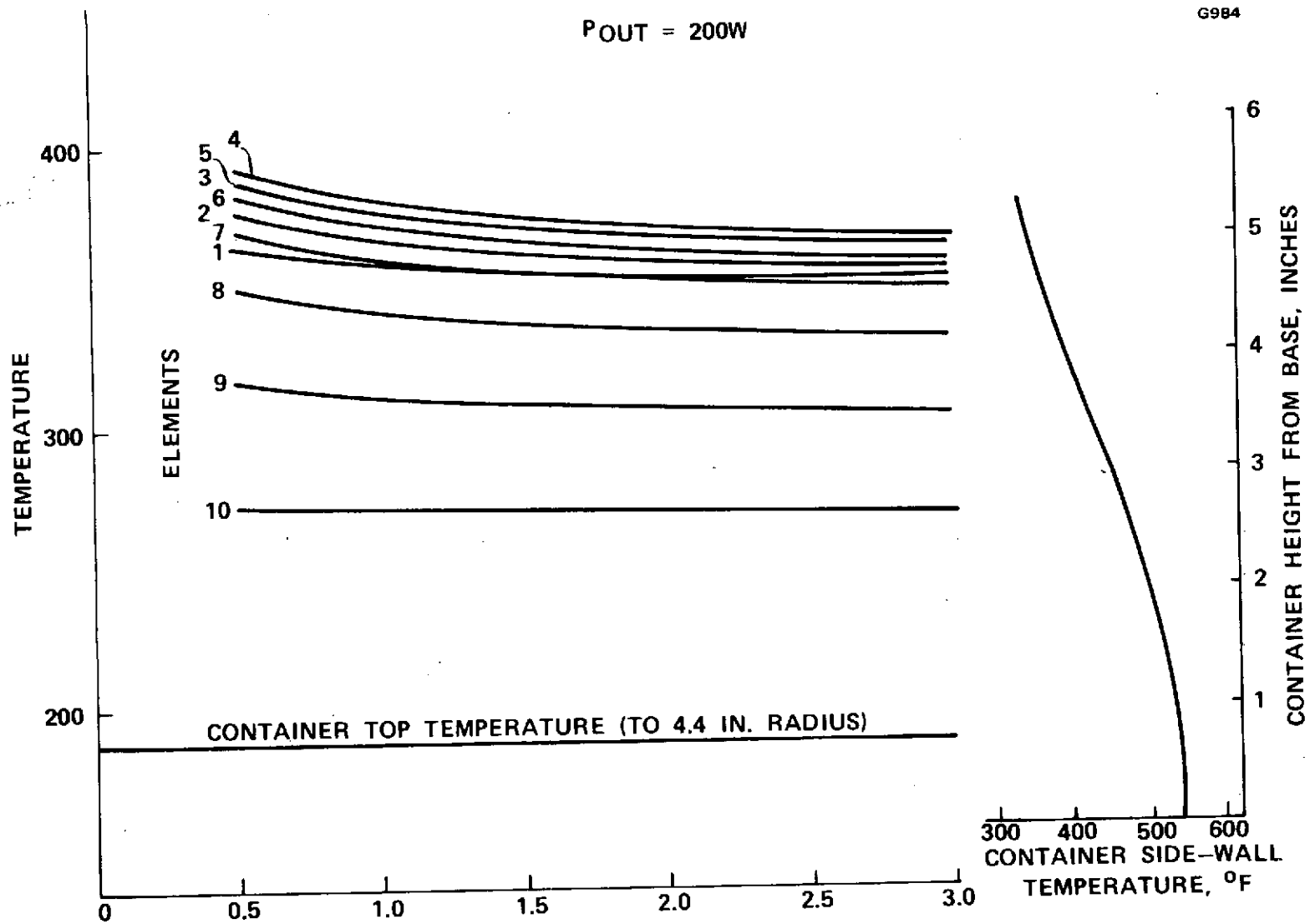


Figure 2-25 Computed MDC steady-state temperature profiles.

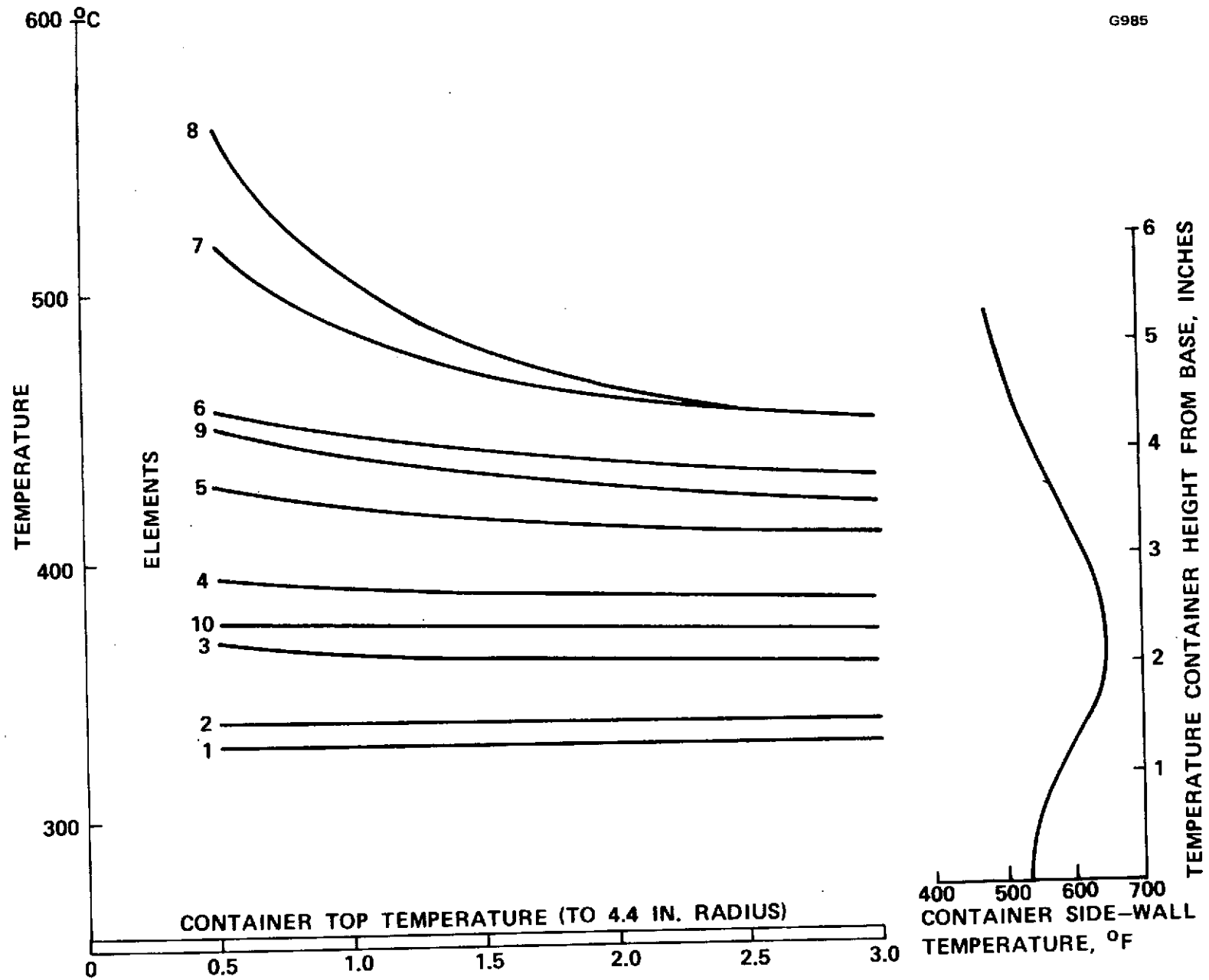


Figure 2-26 Computed MDC steady-state temperature profiles.



model were the heat shield and the thermal choke used to minimize the heat transfer from the MDC to the TWT. The results of this analysis are given in Figure 2-27. For  $P_{out} = 200$  watts, the heat transferred is  $P = 6.4$  watts (7.8%). For  $P_{out} = 0$  watts the heat transferred is  $P = 8.9$  watts (6.0%).

## 2.7 OST PACKAGE DESIGN

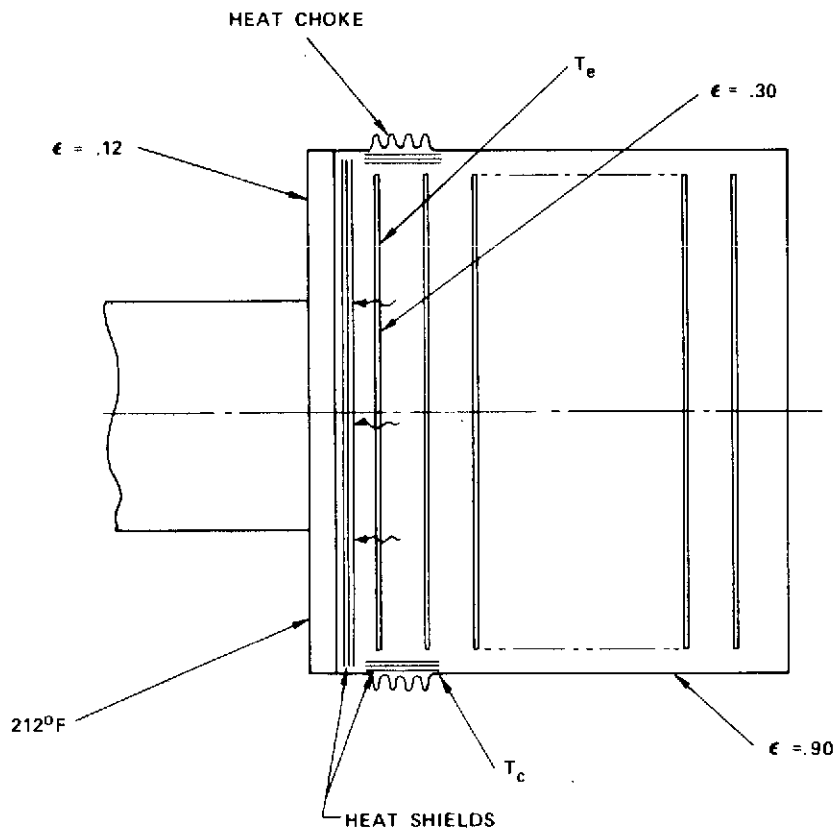
The package for the TWT performs three important functions:

1. Maintains rigid support and accurate alignment of the collector and the TWT body.
2. Provides conduction cooling for the tube RF circuit and evenly distributes the dissipated heat along the baseplate.
3. Distributes the cantilevered collector load over the length of the TWT baseplate.

A picture of the packaged 284H OST with the cover removed is shown in Figure 2-28. The packaged tube body is 4 inches by 4 inches by 12.5 inches; the collector is 9 inches in diameter by 5.6 inches long. The packaged 284H tube weighs 26.2 pounds. The OST component weights are listed in Table 2-8.

The tube body is clamped into a cradle which is integral to the baseplate for support and heat transfer. The TWT heat dissipation is evenly distributed along the baseplate with less than a  $2^{\circ}\text{C}$  temperature differential at  $60^{\circ}\text{C}$ . The power dissipation density is less than 4 watts per square inch. The collector is rigidly attached to the tube baseplate on the "I" beam side panels to minimize flexing of the collector-tube interface during vibration.





MDC TO TWT					
$P_{out}$ (RF)	$T_E$ °C	$T_C$ °C	$P_{diss}$ W	$P_{cond}$ W	$P_{rad}$ W
0 W	362	390	149	6.9	2.0
200 W	388	313	82	3.9	2.5

Figure 2-27 MDC to TWT heat transfer analysis.

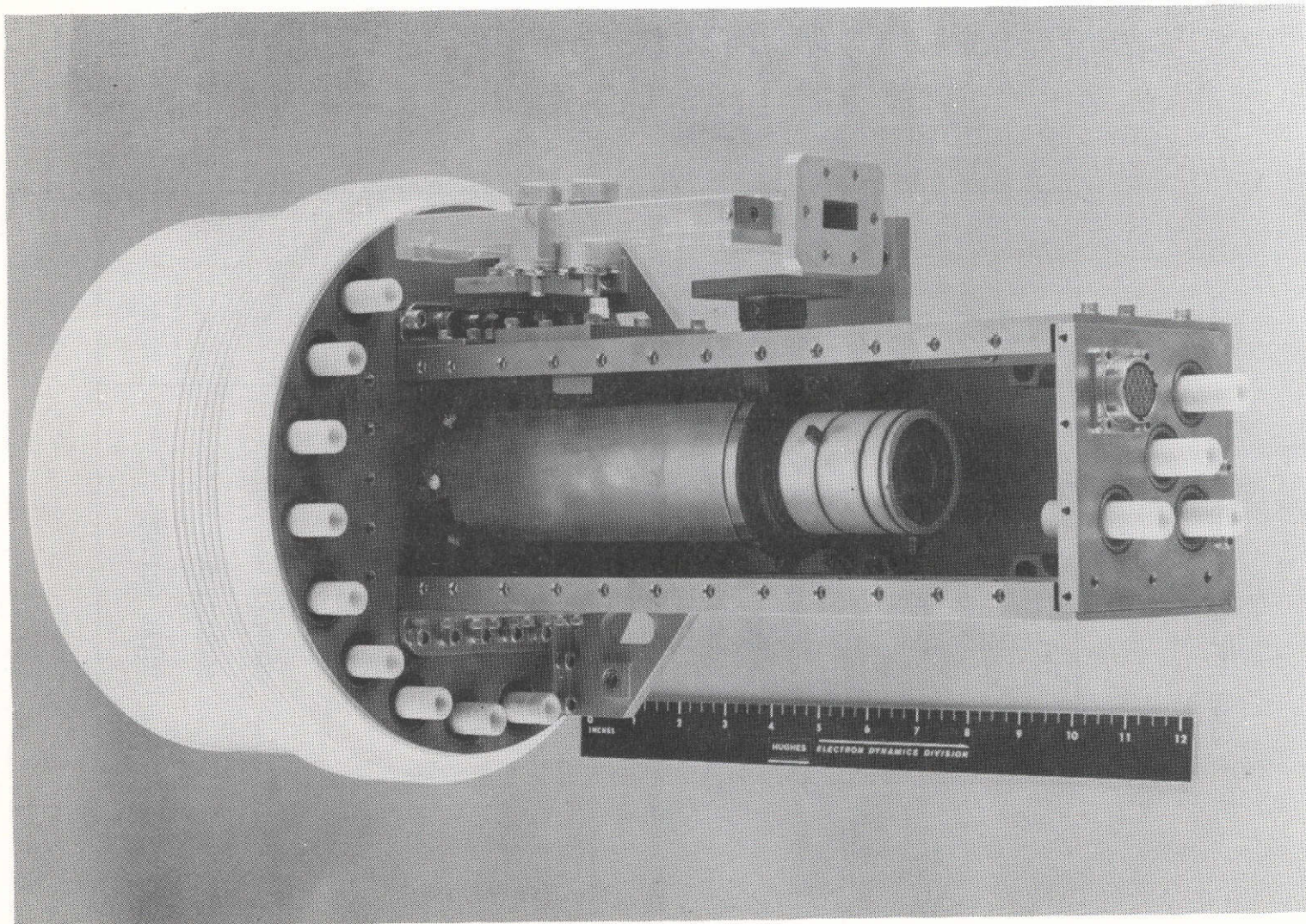


Figure 2-28 Photo of 284H with cover removed.

TABLE 2-8

284H OST Component Weights (lbs.)

TWT	
Gun	1.2
Circuit	2.7
Magnets	<u>1.1</u>
	5.0
MDC	
Electrodes	3.4
Supports	4.0
Support Plate	3.5
Can	<u>2.1</u>
	13.0
PACKAGE	
Baseplate	3.0
Right Side	.6
Left Side	.6
Top	.6
End	.7
Brackets and Screws	<u>1.8</u>
	7.3
COUPLER	.5
EQUALIZER	<u>.4</u>
TOTAL WEIGHT	26.2

The 284H mechanical design was proven to be satisfactory by subjecting the complete P-1 OST to specified qualification sinusoidal and random vibration levels. These test levels are summarized in Table 2-9.

The only significant resonances detected were in the lateral (transverse) direction. The resulting deflections and amplifications at the two lowest resonant frequencies are shown in Figure 2-29. All of these are within safe limits. After being subjected to the qualification vibration levels, the OST was examined for damage. No damage or deformation was observed. The cold circuit match was also checked with no measurable changes detected.

TABLE 2-9

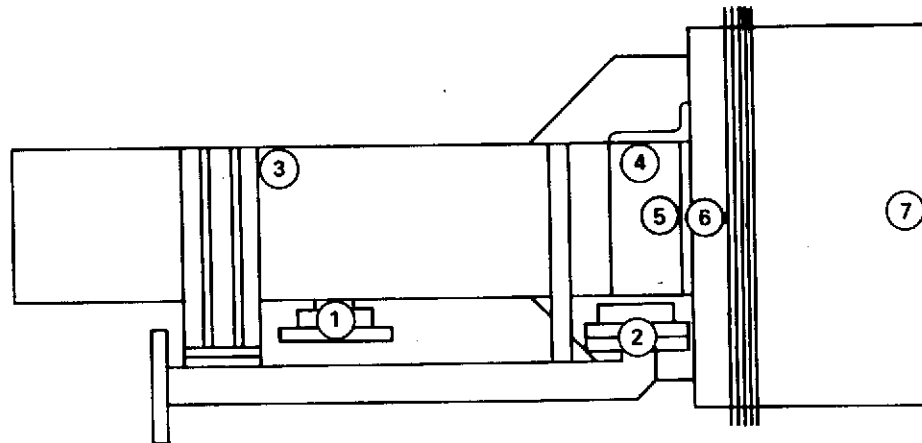
## Qualification Vibration Test Levels

<u>Sinusoidal</u> Sweep Rate 2 oct/min	
Thrust Axis	
Frequency (Hz)	Acceleration g's
5-23	.5" DA to 12.0 g
23-120	12.0
120-200	4.5
200-2000	5.0
Lateral Axis	
5-15	.5" DA to 4.5 g
15-200	4.5
200-2000	5.0
<u>Random</u> 2 min/axis	
Thrust and Lateral Axes	
Frequency (Hz)	PSD ( $g^2/Hz$ )
20-300	+3 dB/OCT
300-2000	0.045

G987

	①	②	③	④	⑤	⑥	⑦
"G" MAGNIFICATION	4.0	3.0	5.5	2.5	5.0	5.0	22.0
1 G DEFLECTION	.0006	.0004	.0008	.0004	.0007	.0007	.0032
5 G DEFLECTION	.0029	.0022	.0040	.0018	.0036	.0036	.0160

RESONANT FREQUENCY 260 Hz



	①	②	③	④	⑤	⑥	⑦
"G" MAGNIFICATION	2.0	1.5	2.5	1.5	2.5	3.0	6.0
1 G DEFLECTION	< .0001"					.0001	.0002
5 G DEFLECTION	.0003	.0002	.0004	.0002	.0004	.0004	.0009

RESONANT FREQUENCY 580 Hz

Figure 2-29 284H OST resonance deflections.



## 2.8 FABRICATION TECHNIQUES

The fabrication of the 284H OST's utilized procedures and techniques similar to all coupled cavity tubes at Hughes EDD. The major task was the adjustment of the loose RF circuit cavity parts to obtain the proper frequency centering and a low VSWR in the operating band.

### 2.8.1 RF Circuit Fabrication

Once the theoretical design of the RF circuit was completed and the periods, cold bandwidth and  $\beta L/\pi$  at midband were determined, cavity parts were iteratively machined until the desired characteristics were achieved. The dimensions that were adjusted were the coupling hole angle and the ferrule length. Slightly different ferrule dimensions were used in each of the velocity taper sections to achieve the same  $\omega-\beta$  characteristic with the reduced cavity period.

The cold matching of each circuit section was performed in the following sequence:

- (1) A complete section of loose parts is matched with an adjustable coupler and wave guide transformer at each end. Symmetrical adjustments are made to the coupling holes and ferrule lengths at both ends of the section until a minimum VSWR is achieved.
- (2) The matched section (without the adjustable couplers) is brazed and the VSWR is rechecked.
- (3) A termination and sever is clamped to one end of the section and again the coupling hole and ferrule length are adjusted to provide a low VSWR.
- (4) The matched termination assembly is brazed and the VSWR is rechecked.
- (5) A fixed coupler is made to the same dimensions as the optimized adjustable coupler and the VSWR is checked.

- (6) The coupler is brazed and the VSWR is rechecked.
- (7) In the output section each of the taper sections is matched and brazed separately.
- (8) After all the circuit subassemblies are matched and brazed, the complete structure is brazed together (stack brazed). The final input and output VSWRs are then measured.

During circuit section and stack brazing, it was necessary to control the flow of the braze material into the cavities. Any excess braze material inside the cavities circuit resulted in increased RF losses which reduced the basic tube efficiency dramatically. To control the braze flow, two techniques were utilized which resulted in the lowest insertion loss and reliable, vacuum tight braze joints. A nickel-copper-silver alloy was used together with a higher temperature schedule which stabilized the entire assembly just below the liquidus temperature then quickly heated it to make the braze.. The assembly was then immediately cooled below the solidus temperature to prevent excessive flow of the material into the cavities.

#### 2.8.2 Collector Vacuum Envelope Fabrication

Electron beam welding was used to attach the bellows thermal choke to the machined vacuum envelope. This operation was performed by an outside vendor using straight forward techniques. Great care had to be taken to assure a very close fit (no gap greater than 0.005 inch) between the two mating cylindrical surfaces.

#### 2.8.3 OST Assembly Procedure

The 284H OST was assembled in much the same way as conventional coupled cavity tubes at Hughes EDD. Furnace brazing, RF induction brazing, and heli-arc welding were the methods used. The final assembly sequence was as follows:



- (1) RF circuit subassembly brazes
- (2) RF circuit stack braze including the refocusing section RF windows and collector support plate
- (3) Multi-stage depressed collector assembly onto the collector support plate
- (4) Heli-arc welding of the collector vacuum envelope to the collector support plate.
- (5) Heli-arc welding of the electron gun to the input pole piece of the OST.

### 3.0 OST DESIGN STUDY

A design study of the 284H characteristics and interface requirements was undertaken to allow definition of the TEP interfaces and PPS requirements early in the program. For completeness, the final results of this study, dated December 5, 1972, are included in this section of the final report.

REVISED OST DESIGN STUDY  
DATA ITEMS

1. OST weight - 27.0 lbs<sub>m</sub> (12.23 kg)
2. Method of Mounting
  - A. OST baseplate mounted to TEP baseplate by means of 8-32 flat head screws--hole pattern shown on OST interconnection drawing B108919.
  - B. OST tied to PPS by means of angle at gun end of OST.
  - C. OST tied to TEP by bracket going over OST which connects to TEP baseplate near S/C hinges.
3. Thermal Interface
  - A. Baseplate of OST mounted directly to TEP baseplate--no filler used between surfaces.
  - B. OST Baseplate Temperatures

Non-operating (survival)	-55°C to +125°C
Operating (no damage)	-20°C to +100°C - +125°C
Operating (full spec)	+25°C to +100°C *

\*Hughes calculations and experience indicate that full spec performance can be achieved up to 100°C. However, until actual tests can be performed on an OST, Hughes cannot guarantee such performance.

These temperatures to be monitored on the OST baseplate adjacent to the output RF window.

## C. Thermal Dissipation of OST

Most Probable Heat Input (TWT Baseplate)

Power in equals 100 MW

Power out equals 200 W

Cathode	5.5 W
Anode	3.25 W
Input interception	12.0 W
Output interception	16.2 W
Input termination	5.0 W
Output termination	.5 W
RF loss	45.0 W
Coupler loss	5.6 W
Refocus solenoid	5.0 W
Collector to body	6.4 W
	<hr/>
	104.5 W

Power in equals 25 MW

Power out equals 100 W

Cathode	5.5 W
Anode	3.25 W
Input interception	12.0 W
Output interception	12.0 W
Input termination	1.0 W
Output termination	.25 W
RF loss	15.0 W
Coupler loss	2.5 W
Refocus solenoid	5.0 W
Collector to body	8.0 W
	<hr/>
	64.5 W

## C. Thermal Dissipation of OST (continued)

Most Probable Heat Input (TWT Baseplate) (continued)

Power in equals 8 MW noise

Power out equals 63 W noise

Cathode	5.5	W
Anode	3.25	W
Input interception	12.0	W
Output interception	4.0	W
Input termination	.5	W
Output termination	0	W
RF loss	9.5	W
Coupler loss	1.6	W
Refocus solenoid	5.0	W
Collector to body	9.0	W
	<hr/>	
	50.3	W

Heater half power

Cathode	2.75	W
All others	0	W
	<hr/>	
	2.75	W

Zero power

All elements	0	W
--------------	---	---

Maximum Heat Input (TWT Baseplate)

Power in equals 100 MW

Power out equals 200 W

Cathode	7.0	W
Anode	8.0	W
Input interception	12.3	W
Output interception	24.5	W
Input termination	5.0	W
Output termination	2.0	W
RF loss	50.0	W
Coupler loss	15.0	W
Refocus solenoid	5.0	W
Collector to body	13.5	W
	<hr/>	
	142.3	W

## C. Thermal Dissipation of OST (continued)

Maximum Heat Input (TWT Baseplate) (continued)

Power in equals 25 MW

Power out equals 100 W

Cathode	7.0	W
Anode	8.0	W
Input interception	12.3	W
Output interception	16.5	W
Input termination	1.0	W
Output termination	1.0	W
RF loss	20.0	W
Coupler loss	6.0	W
Refocus solenoid	5.0	W
Collector to body	15.5	W
	<hr/>	
	92.3	W

Power in equals 8 MW noise

Power out equals 63 W noise

Cathode	7.0	W
Anode	8.0	W
Input interception	12.3	W
Output interception	8.2	W
Input termination	.5	W
Output termination	.5	W
RF loss	12.6	W
Coupler loss	3.8	W
Refocus solenoid	5.0	W
Collector to body	15.5	W
	<hr/>	
	73.4	W

Heater half power

Cathode	3.5	W
All others	0	W
	<hr/>	
	3.5	W

Zero power

All elements	0	W
--------------	---	---

## C. Thermal Dissipation of OST (continued)

Most Optimistic Heat Input (TWT Baseplate)

Power in equals 100 MW

Power out equals 200 W

Cathode	5.0 W
Anode	2.0 W
Input interception	7.8 W
Output interception	9.7 W
Input termination	2.5 W
Output termination	.5 W
RF loss	40.00 W
Coupler loss	3.0 W
Refocus solenoid	5.0 W
Collector to body	6.4 W
	<hr/>
	81.9 W

Power in equals 25 MW

Power out equals 100 W

Cathode	5.0 W
Anode	2.0 W
Input interception	7.8 W
Output interception	7.8 W
Input termination	.5 W
Output termination	.25 W
RF loss	15.0 W
Coupler loss	1.5 W
Refocus solenoid	5.0 W
Collector to body	8.0 W
	<hr/>
	52.9 W

## C. Thermal Dissipation of OST (continued)

Most Optimistic Heat Input (TWT Baseplate) (continued)

Power in equals 8 MW noise

Power out equals 63 W noise

Cathode	5.0 W
Anode	2.0 W
Input interception	7.8 W
Output interception	3.9 W
Input termination	.25 W
Output termination	0 W
RF loss	9.5 W
Coupler loss	.6 W
Refocus solenoid	5.0 W
Collector to body	9.0 W
	<hr/>
	43.0 W

Heater half power

Cathode	2.5 W
All others	0 W
	<hr/>
	2.5 W

Zero power

All elements	0 W
--------------	-----

Assumptions

1. MDC radiation calculated assuming
  - a.  $\epsilon = .87$  for most probable and minimum cases.  
Negligible heat transfer from MDC to TWT.
  - b.  $\epsilon = .41$  for maximum case.  
Negligible heat transfer from MDC to TWT.
  - c. 50% blockage of radiation due to S/C.
2. MDC to TWT heat transfer calculated from MDC temperatures obtained in (1) and thermal resistances.



4. TWT and MDC voltages, currents, regulation and ripple are summarized in Tables 2-1 and 2-2.

Turn on sequence for cathode turn on:

- a. OST sensors on--particularly vac-ion pump.
- b. Heater on to half power. Limit surge current to 1.8 A.  
Allow vac-ion current to stabilize below 2.0 microamps.
- c. Heater on to full power. Limit surge current to 1.8 A.  
Allow vac-ion current to stabilize below 2.0 microamps.  
Refocusing coil on.
- d. Cathode, collector, anode voltages on. Collector voltages should remain proportional to cathode voltage during turn on. Cathode voltage must stabilize within regulation band within 10 milliseconds.

Do not perform this operation at OST baseplate temperatures below  $-20^{\circ}\text{C}$  or above  $+125^{\circ}\text{C}$  or vac-ion currents above 2.0 microamps. Allow vac-ion current to stabilize below 2.0 microamps.

- e. RF drive signal on.

During beam turn-on, anode current may increase to 2.0 mA max. Steady state anode current will be less than 1.0 mA.

During beam turn-on, body current may increase to as much as 20 mA at about .5 operating cathode voltage. The steady state body current will be less than 4.0 mA.

When RF drive is applied, body current will increase monotonically to steady state value of 4.0 mA or less.

When RF drive is applied, the MDC electrode currents will change approximately as indicated in Table 2-2.

## 4. (continued)

## Normal shut down sequence:

- a. Remove RF drive.
- b. Turn off cathode, collector, and anode voltages. Cathode voltage must stabilize at 0 volts within 10 milliseconds.
- c. Turn off refocusing coil.
- d. Reduce heater to half power.

## Automatic shut down sequence:

- a. Turn off cathode, collector and anode voltages. Cathode voltage must stabilize at 0 volts within 10 milliseconds.
- b. Turn off RF drive and refocusing coil.

## OST Protection Requirements:

1. Limit heater current surge to 1.8 A max.
2. Limit arc currents to 1000 A peak.
3. Limit stored energy in all high voltage power supplies to 40 joules or less.
4. Turn off OST when body current exceeds 10.0 mA.
5. Turn off OST when vac ion current exceeds 5.0 microamperes.
6. Turn off OST in the event of a sustained high voltage arc.

## 5. Telemetry Signals

## A. RF output power and reflected power sensor

Detectors	IN415E crystals
IF impedance	335 - 465 $\Omega$
Load resistance	10 K $\Omega$
Burn out ratings	
CW power	325 mW
Peak	7.5 microsec watt
RF output power coupling	-54 dB
Reflected power coupling	-33 dB
Crystal voltage output vs. OST RF power output--output power sensor	Figure 2

## 5. (continued)

## A. (continued)

Crystal voltage output vs. OST RF power      Figure 3-2  
 output and load VSWR-reflected power  
 sensor

Connectors      SMA female

## B. OST pressure sensor

$V_{IP}$       3.0 kV

$I_{IP}$  versus pressure      Figure 3-3

Connector      Mates with AMP LGH-1/2 lead assembly

## C. Thermistor temperatures

Temperature Range

OST baseplate thermistor       $-55^{\circ}\text{C}$  to  $+125^{\circ}\text{C}$

MDC envelope thermistor 1       $-75^{\circ}\text{C}$  to  $+150^{\circ}\text{C}$

MDC envelope thermistor 2       $+100^{\circ}\text{C}$  to  $+300^{\circ}\text{C}$

MDC envelope thermistor 3       $+100^{\circ}\text{C}$  to  $+300^{\circ}\text{C}$

Coupler thermistor       $0^{\circ}\text{C}$  to  $+125^{\circ}\text{C}$

TRW should recommend thermistor resistance that will provide  
 maximum sensitivity over indicated range.

## D. MDC envelope opening device

Linear actuator squib device all stainless steel with bellows  
 to contain all combustion products. Typical electrical re-  
 quirements are as follows:

Firing circuit	2 bridge wires (one redundancy)
All-fire current (thru each or both bridge wires)	4.5 A for 10 milliseconds
No-fire current (thru each or both bridge wires)	1.0 A
Bridge wire resistance	$1.05 \pm .10$ ohm
Pin to case resistance	2 megohm at 500 V DC
Pin to case no-fire	1000 V RMS max.

## 6. Electrical Input Power, Voltages, Currents

See revised Tables 3-1 and 3-2.

Type and location of connectors--see revised B108919 (final).

## 7. Magnetic Moment

$$1.5 \times 10^{-7} \text{ Wb-m}$$

## 8. OST Component Weight Breakdown

<u>Component</u>	<u>Lbs.</u>	<u>kg</u>
TWT circuit	2.7	1.22
Magnets	1.1	.50
Electron gun	1.2	.55
MDC electrodes	3.4	1.55
MDC supports	4.0	1.80
MDC support plate	5.0	2.27
MDC envelope	2.6	1.17
TWT package	5.8	2.63
Coupler assembly	0.8	0.36
MDC opening device	0.4	0.18
Total OST weight	<u>27.0</u> $\begin{smallmatrix} +0.0 \\ -3.0 \end{smallmatrix}$	<u>12.23</u> $\begin{smallmatrix} +0.0 \\ -1.3 \end{smallmatrix}$

## OST Center of Mass

Tolerance

$\bar{x} = +.24 \text{ in.} = .61 \times 10^{-2} \text{ m}$	$\pm .25 \text{ in}$
$\bar{y} = +2.04 \text{ in.} = +5.18 \times 10^{-2} \text{ m}$	$\pm .25 \text{ in}$
$\bar{z} = +.75 \text{ in.} = 1.91 \times 10^{-2} \text{ m}$	$\pm .50 \text{ in}$

## Collector Center of MASS

Tolerance

$\bar{x} = 0 = 0 \text{ m}$	$\pm .25 \text{ in}$
$\bar{y} = 2.12 \text{ in.} = 5.39 \times 10^{-2} \text{ m}$	$\pm .25 \text{ in}$
$\bar{z} = -2.30 \text{ in.} = 5.85 \times 10^{-2} \text{ m}$	$\pm .50 \text{ in}$

## 8. OST Component Weight Breakdown (continued)

TWT Center of Mass	<u>Tolerance</u>
$\bar{x} = +.57 \text{ in.} = 1.45 \times 10^{-2} \text{ m}$	$\pm .25 \text{ in}$
$\bar{y} = +1.92 \text{ in.} = 4.88 \times 10^{-2} \text{ m}$	$\pm .25 \text{ in}$
$\bar{z} = +5.10 \text{ in.} = 13.00 \times 10^{-2} \text{ m}$	$\pm .50 \text{ in}$

## Moment of Inertia About OST Center of Mass

$I_x = 628.4 \text{ in}^2 - \text{lb} = .184 \text{ kg-m}^2$	$\pm 6 \text{ in}^2 - \text{lb}$
$I_y = 636.8 \text{ in}^2 - \text{lb} = .186 \text{ kg-m}^2$	$\pm 6 \text{ in}^2 - \text{lb}$
$I_z = 142.9 \text{ in}^3 - \text{lb} = .042 \text{ kg-m}^2$	$\pm 1.5 \text{ in}^2 - \text{lb}$

Note: For coordinate system see Figure 3-1.

## 9. OST Power Requirements

Tube on with zero RF drive (63 W noise output)

	<u>Most Probable</u>	<u>Maximum</u>
Refocus coil power	5.0 W	5.0 W
Heater power	5.5 W	7.0 W
Anode power	3.25 W	8.0 W
Body power	16.0 W	20.5 W
Vac ion	Negligible	Negligible
Collector 1	16.0	17.0
Collector 2	19.2	20.4
Collector 3	22.4 W	25.0
Collector 4	19.2	20.4
Collector 5	28.0	30.0
Collector 6	22.4	25.0
Collector 7	40.8	43.5
Collector 8	48.0	51.0
Collector 9	4.0	4.2
Collector 10	<u>0</u>	<u>0</u>
	249.75	277.0

## 9. OST Power Requirements (continued)

Tube on full RF drive (200 watts output)

	<u>Most Probable</u>	<u>Maximum</u>
Refocus coil	5.0 W	5.0 W
Heater power	5.5	7.0
Anode power	3.25	8.0
Body power	28.2	36.8
Vac ion power	Negligible	Negligible
Collector 1	40.0	42.5
Collector 2	64.0	68.0
Collector 3	56.0	60.0
Collector 4	48.0	51.0
Collector 5	40.0	42.5
Collector 6	32.0	34.0
Collector 7	24.0	25.0
Collector 8	12.8	13.5
Collector 9	4.0	4.2
Collector 10	<u>0</u>	<u>0</u>
	362.7 W	397.5 W

Assumptions for paragraphs 3C and 9

Most probable case

Nominal voltages, currents, and losses per Tables 3-1 and 3-2.

Maximum case

Maximum possible for full spec OST.

Maximum voltages, currents, and losses.

Paragraphs 3C and 9 use same assumed currents and voltages to OST elements.

Tube off S/C in sunlight

Heater power	3.5 W max
Temperature control power	0

Tube off S/C in shadow

Heater power	3.5 W max
Temperature control power	0

## 10. Gain versus Frequency (estimated)

<u>Frequency</u>	<u>Sat. Gain</u>	<u>-3 dB Gain</u>	<u>-5 dB Gain</u>
12,038	33.9	36.5	38.4
12.0805	33.6	36.0	37.3
12.123	33.0	37.5	36.3

## 11. Tube Parameters to Detect Overdrive

For overdrive condition, body current will increase and should be used to protect OST.

Maximum body current	10 mA
Response time	1 millisecond

## 12. Estimate of Maximum and Minimum Temperatures for OST Baseplate

Operating-full spec	Maximum	100°C *
	Minimum	25°C
Operating-no damage	Maximum	125°C
	Minimum	-20°C
Non-operating - survival	Maximum	125°C
	Minimum	-55°C

\*This temperature is an estimate. It should be confirmed by actual OST testing.

13. Estimate of Maximum and Minimum Expected Temperatures for MDC Envelope  
Assumes  $\epsilon = .41$ , MDC voltages and currents as in Table 3-2, improved thermal design.

Operating - RF	Maximum	320°C
Operating - DC	Maximum	390°C
Non-operating - survival	Minimum	-200°C *

\*This temperature is expected at -55°C OST baseplate temperature and 3.5 watts heat flow from OST to MDC.

TABLE 3-1

## HUGHES 284H ELECTRICAL REQUIREMENTS

			NOM.	MIN.	MAX.	REG.	RIPPLE
$V_k$	Cathode Voltage *	kV	-8.0	-7.8	-8.2	$\pm 1\%$	.01%
$I_k$	Cathode current	mA	84	81	87		
$V_a$	Anode voltage (off) *	kV	-8.0	$-V_k$	$-(V_k + .5)$	$\pm 1$	$\pm 2\%$
$V_a$	Anode voltage (on) *	V	350	150	550	$\pm 1\%$	$\pm 1\%$
$I_a$	Anode current (on)	mA	.4	.05	1		
$V_f$	Filament voltage	V	5.0	4.5	5.5		
$I_f$	Filament current	A	1.1	.9	1.5	$\pm 1\%$	$\pm 1\%$
$V_{sol}$	Refocusing voltage *	V	1.66	1.50	1.83		
$I_{sol}$	Refocusing current	A	3.0	2.7	3.3	$\pm 1\%$	$\pm 1\%$
$I_b$	Body current	mA	4	.5	5		
$I_c$	Total collector current	mA	79	75	87		
$V_{ip}$	Ion pump voltage *	kV	3.0	2.7	3.3	10%	10%
$I_{ip}$	Ion pump current (start)	mA	.05	.001	5		
$I_{ip}$	Ion pump current	$\mu A$	.2	.05	5		

\*Voltages with respect to TWT body except  $V_f$  which is with respect to cathode.

$$\frac{\Delta \phi}{\Delta V_k} = 0.5^\circ/\text{volt max.}$$

$$\text{AM-PM} = 6^\circ/\text{dB max.}$$

$$\frac{\Delta P_o}{\Delta V_{kA}} = .025 \text{ dB/volt}$$

$$\frac{\Delta F}{\Delta V_k} = .060 \text{ MHz/volt}$$

$$\frac{\Delta I_k}{\Delta V_{k-a}} = .017 \text{ mA/volt}$$

$$\frac{\Delta P_o}{\Delta I_k} = .055 \text{ dB/mA}$$



TABLE 3-2

## NOMINAL MDC VOLTAGES AND CURRENTS

<u>OST Electrode</u>	<u>Voltage Ku</u>	<u>Current mA</u>				
		<u>RF Pout</u>	<u>200W</u>	<u>100W</u>	<u>50W</u>	<u>0 W</u>
Filament	5		2	2	2	2
Cathode	-8.0		84	84	84	84
Anode	0		1	1	1	1
Body	0		4	3	2	2
Collector 1	0		5	3	2	0
Collector 2	-1.6		10	8	3	0
Collector 3	-2.4		10	9	4	2
Collector 4	-3.2		10	9	4	2
Collector 5	-4.0		10	8	7	5
Collector 6	-4.8		10	8	7	5
Collector 7	-5.6		10	13	17	20
Collector 8	-6.4		8	15	30	40
Collector 9	-7.2		5	5	5	5
Collector 10	-8.0		1	1	1	1

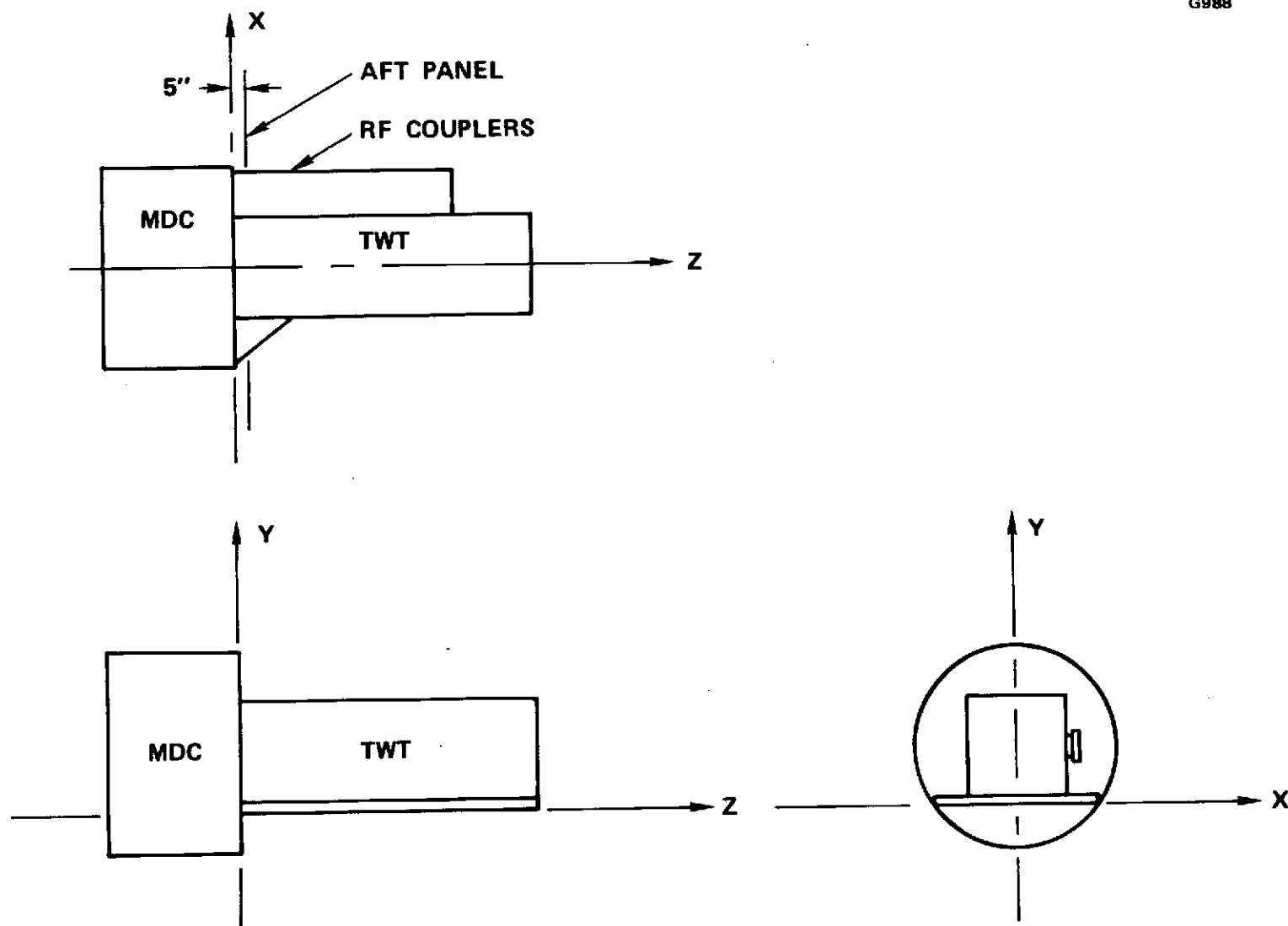


Figure 3-1 Definitions of axes.

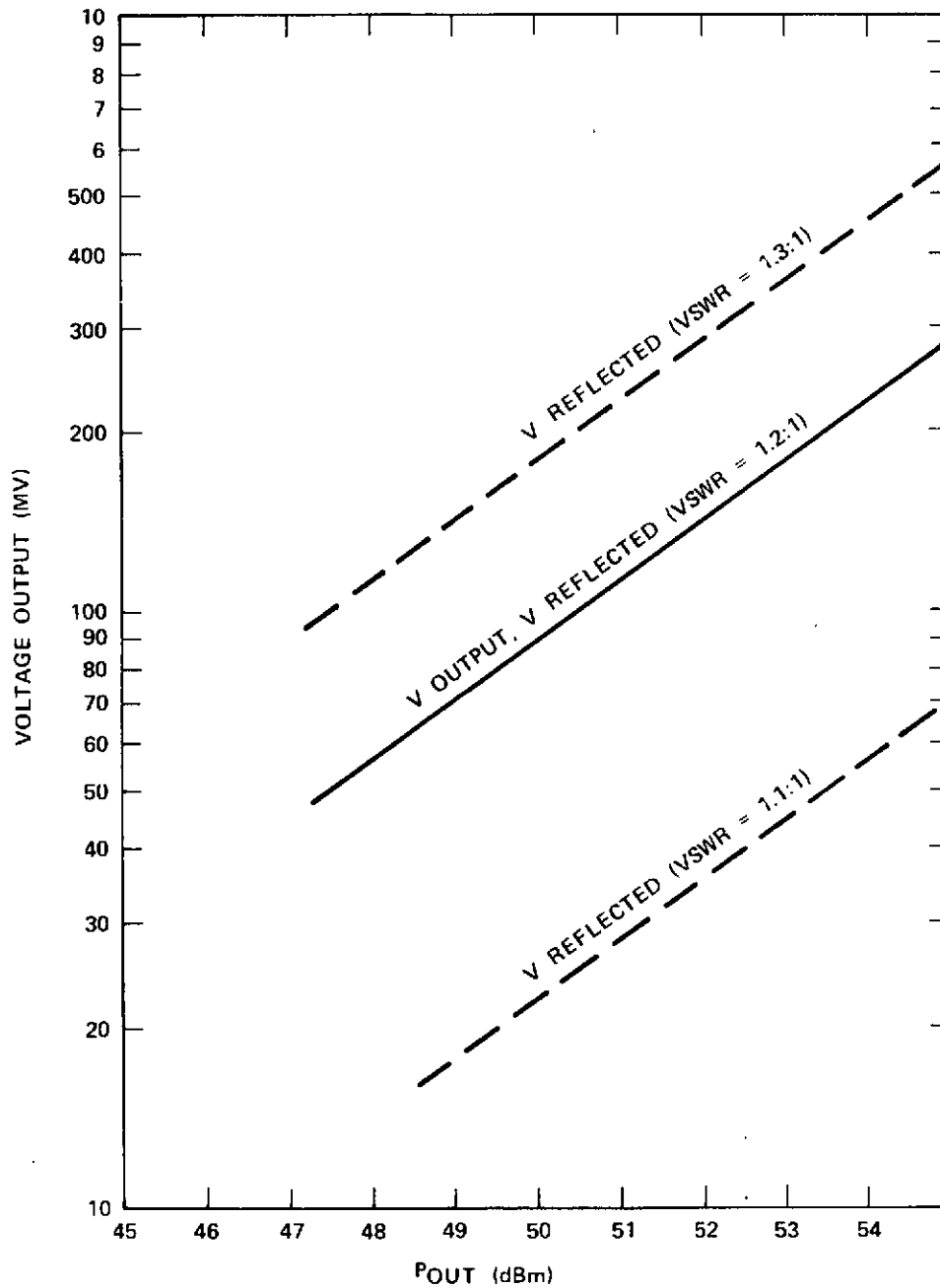


Figure 3-2 Voltage sensor outputs.

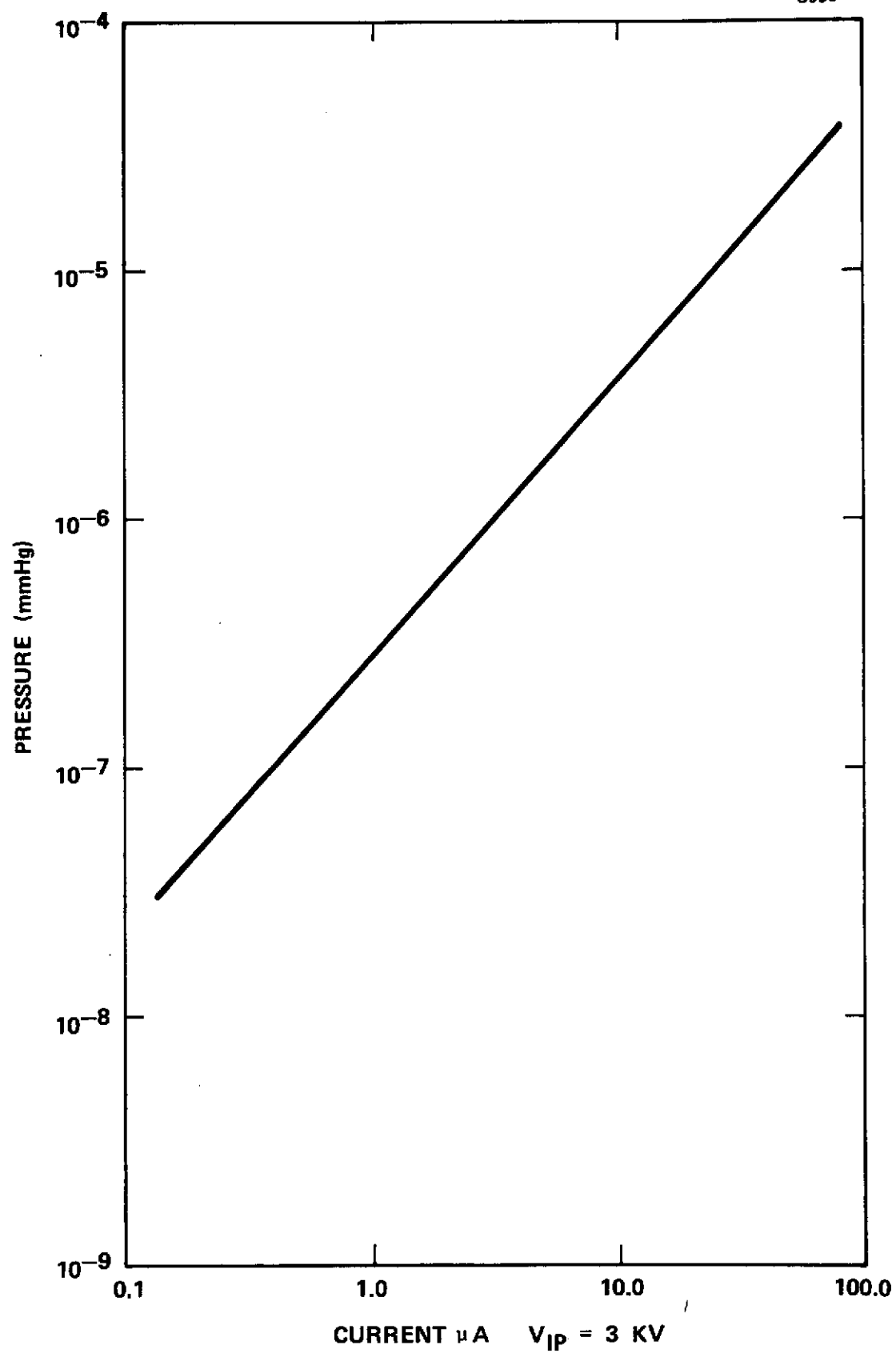


Figure 3-3 Pressure sensor.

#### 4.0 284H OST DEVELOPMENT RESULTS AND DISCUSSION OF RESULTS

##### 4.1 SUMMARY

This section of the final report describes the design, fabrication, and test results of each of the 284H tubes built during the development program. Five tubes were constructed and tested. Their serial numbers were:

E-1  
P-1  
P-2  
ETM-1  
ETM-2

The E-1 tube was an experimental TWT having a single stage water-cooled bucket type collector and a two section RF circuit without a velocity taper. This tube was built to obtain fundamental circuit interaction data, to prove out the electron gun and PPM focusing design and to permit accurate calibration of the large signal computer program.

The design of 284H OST serial number P-1 was identical to that of E-1 except that a velocity taper was incorporated into the output of the RF circuit. This tube was first tested with the single stage bucket collector and was thereafter integrated with the first MDC.

284H OST serial number P-2 was constructed similar to P-1 but with design changes to the RF coupled cavity circuit and to the MDC aperatures. These iterations were made to improve the overall performance of the OST.

284H tube serial numbers ETM-1 and ETM-2 were the third and fourth OST's built during the development phase. Changes were made in the RF circuit

**PRECEDING PAGE BLANK NOT FILMED**

oscillation suppression distribution, the circuit brazing techniques (to reduce in band losses) and the collector aperture sizes. The original contract required three engineering test model (ETM) tubes, however work was terminated by NASA after the delivery of ETM-2. The performance of the 284H ETM OST's came closest to meeting the requirements of the contract.

In addition to these tubes, dynamic mass and thermal models of the 284H were constructed and delivered to NASA for spacecraft simulation testing.

#### 4.2 284H SERIAL NUMBER E-1

The first tube constructed and tested was 284H serial number E-1. All the components of this tube except the RF coupled cavity circuit and the collector were identical to the initial OST design used in serial number P-1. The RF coupled cavity circuit was a two section design using only standard (untapered) cavities; the velocity taper was omitted on this tube. A standard water cooled undepressed bucket collector was used in place of the MDC. A photograph of the 284H serial number E-1 is shown in Figure 4-1.

The fabrication of E-1 proceeded without any difficulty. The measured final cold match and transmission loss of the output section are shown in Figure 4-2. The electron gun design used on this tube was tested in the electrostatic demountable beam analyzer to verify the perveance, minimum beam diameter and beam minimum position. These characteristics were all found to be identical to the design values. The E-1 TWT was completed and baked out in September, 1974.

The electron beam focusing results achieved on 284H serial number E-1 are listed in Table 4-1. The beam transmission without RF input drive was 98.2 percent; with saturation RF drive the transmission was greater

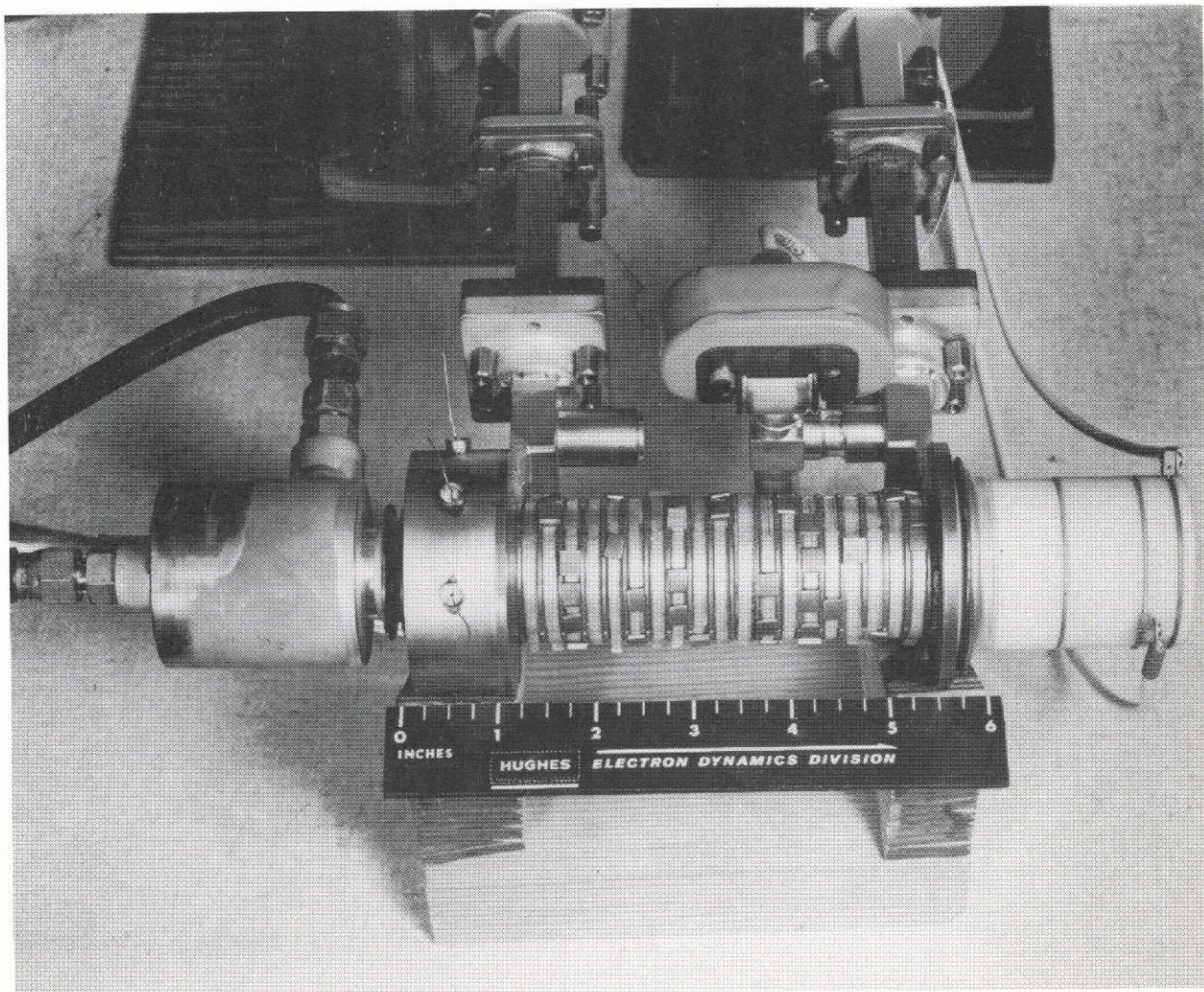


Figure 4-1 284H E-1 on test.

ORIGINAL PAGE IS  
OF POOR QUALITY

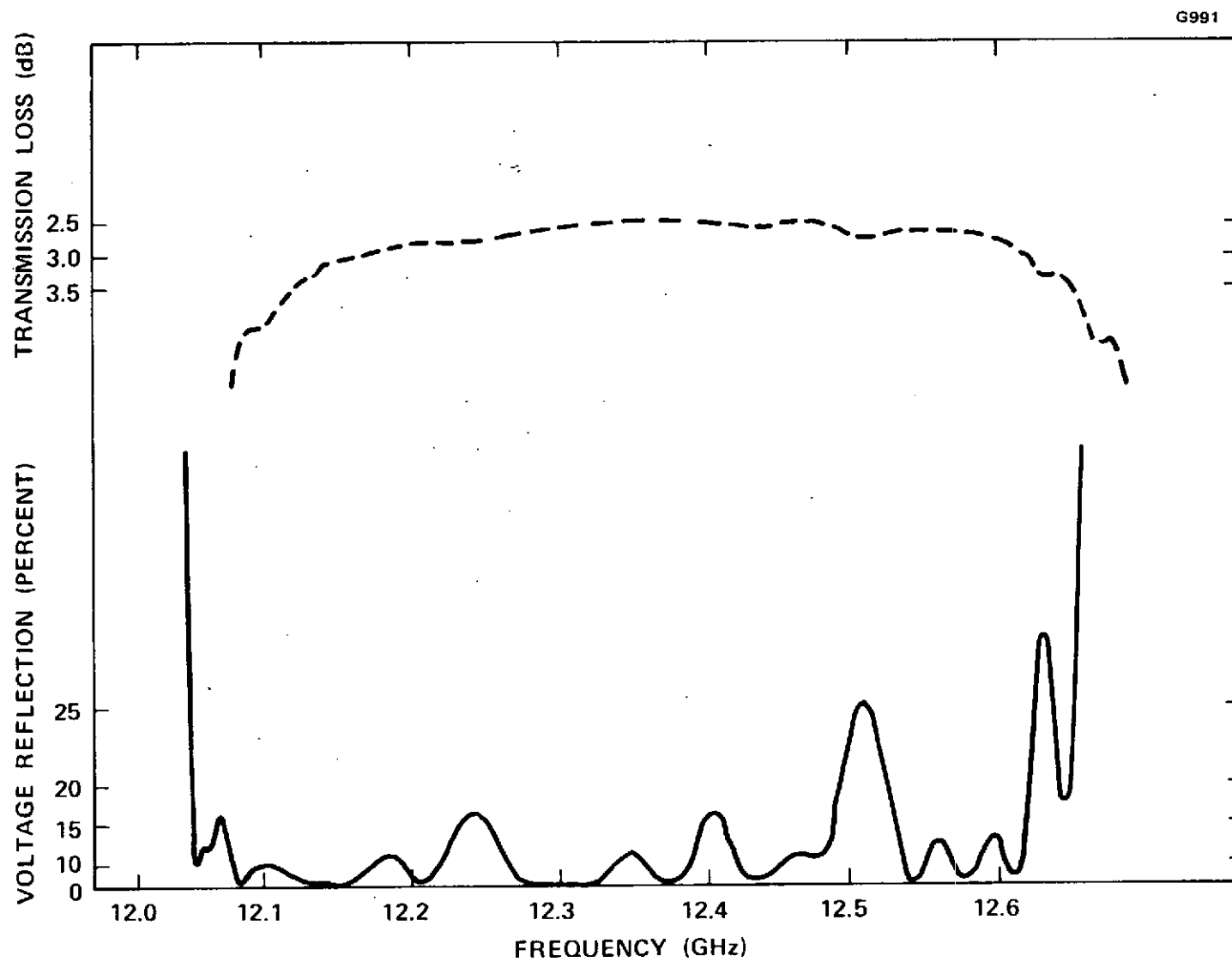


Figure 4-2 284H E-1 Output section.



TABLE 4-1

284H S/N E-1 Focusing Results	
Beam Voltage	8.0 kV
Beam Current	85.0 mA
Peak Field, Input	2000 GAUSS
Output	2370 GAUSS
Transmission, Without RF Drive	98.2%
With Saturated RF Drive	95.3%
Max. Body Current versus Beam Voltage	20 mA @ 4.5 kV

than 95.3 percent. This focusing was achieved with an optimized axial magnetic field of 2000 gauss tapering up to 2370 gauss at the output. This field strength was predicted to give best focusing based on computer analysis including thermal velocity effects. The maximum intercepted body current during the turn-on transient was 20 MA at a beam voltage of -4.5 kV.

The saturated output power versus frequency for three beam voltages is shown in Figure 4-3. A maximum output power of 118 watts was obtained at the design voltage of  $E_k = -8.0$  kV. The basic (undepressed) efficiency of the TWT is shown in Figure 4-4. The maximum efficiency of this untapered circuit was 17 percent at the design beam power of  $P_k = 682$  W.

The comparison of measured performance of 284H serial number E-1 and the computer predictions is given in Figure 4-5. With the calculations corrected for the TWT output RF coupler loss, excellent correlation was obtained.

#### 4.3 284H SERIAL NUMBER P-1

The 284H S/N P-1 design was identical to that of S/N E-1 except for the incorporation of a two step velocity taper into the output section. This tube was first assembled and tested with an undepressed bucket collector, and was thereafter integrated with the initial MDC to make the first complete OST.

The construction and matching of the RF circuit for P-1 went smoothly until the final RF circuit braze. Following this braze, the in-band cold match degraded to 30 percent, the result of slight changes in the taper cavity ferrule gaps due to differential expansion. While this mismatch was not excessive, it was overly sensitive to dimensional changes in the output coupler and sever termination. With fixed coupler

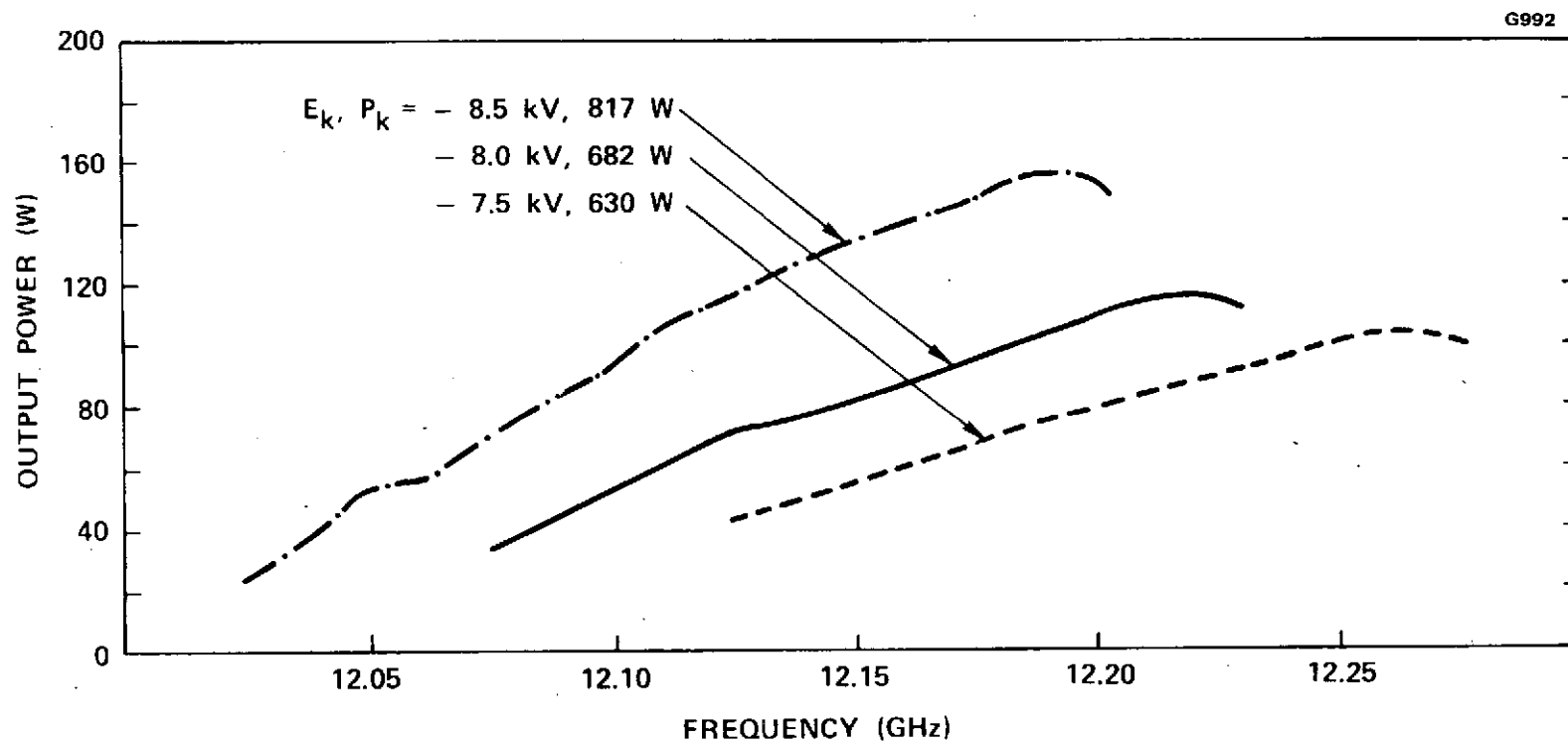


Figure 4-3 284H E-1 saturated output power.

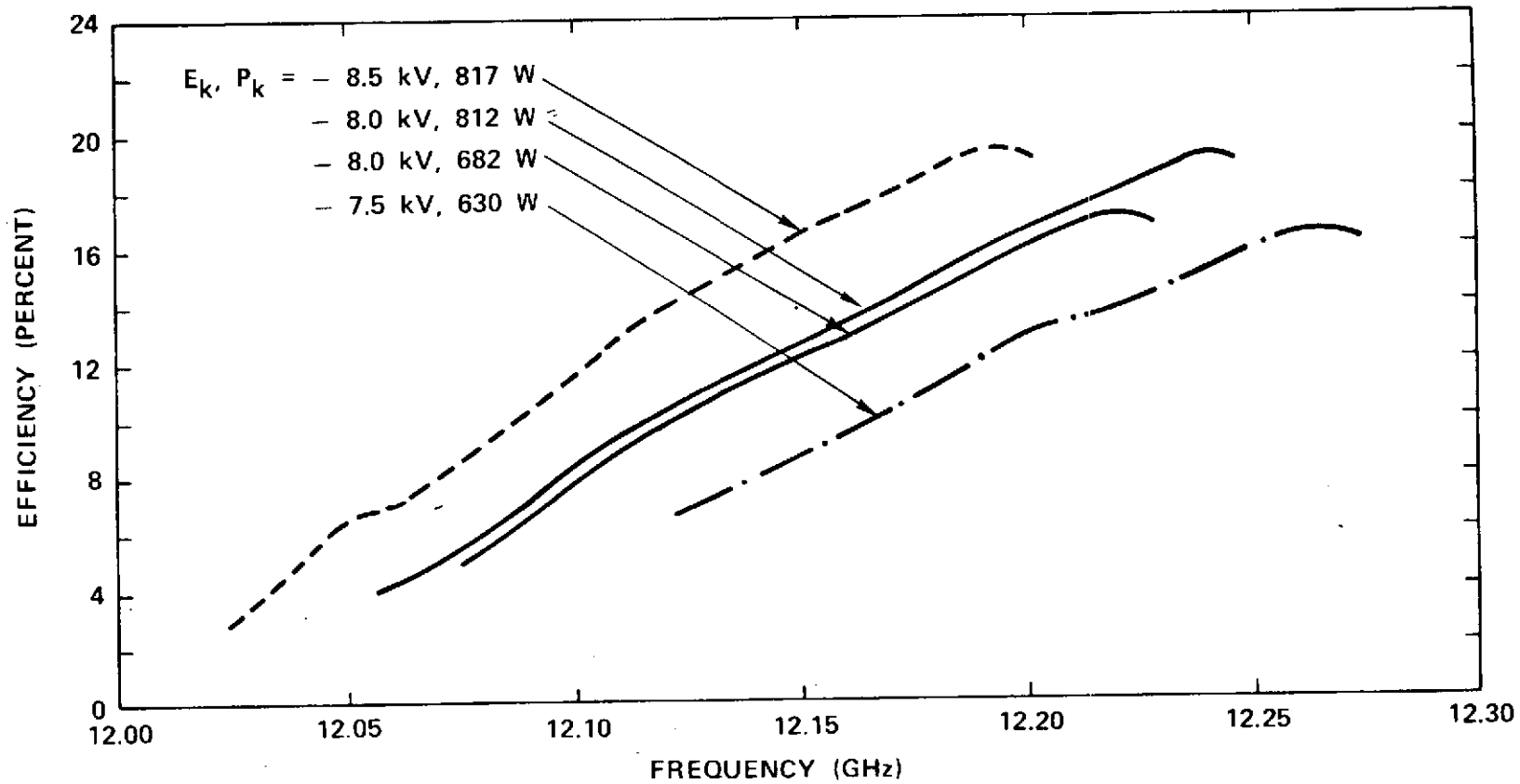


Figure 4-4 284H E-1 basic saturated efficiency.

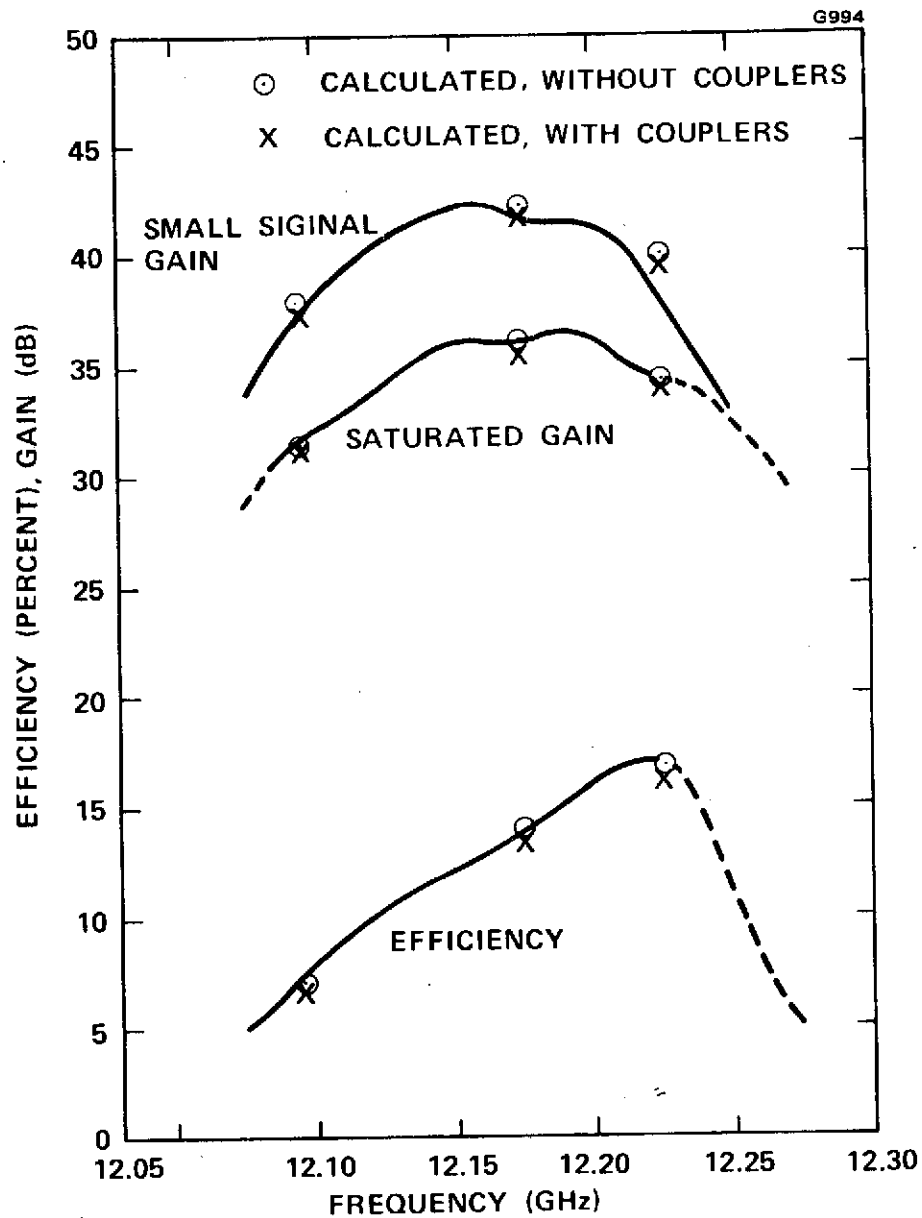


Figure 4-5 284H E-1 Computer calibration ( $E_k = -8.0$  kV).

parts, the mismatch was 45 percent voltage reflection. In addition, the coupler configuration that provided an acceptable match had high RF losses.

The final output section voltage reflection and transmission loss versus frequency are shown in Figure 4-6. The high RF circuit losses were due to the following: (1) The low design value of phase shift per cavity at midband; (2) the presence of copper-gold braze alloy fillets within the cavities (these alloys have one fifth the electrical conductivity of OFHC copper so that even small amounts can significantly increase the loss); and, (3) the high coupler loss resulting from the RF circuit matching problems.

The focusing results from 284H S/N P-1 were nearly as good as those achieved with the untapered S/N E-1. These results are summarized in Table 4-2, at a beam voltage of  $E_k = -8.0$  kV, the beam current was  $I_k = 89.8$  mA (slightly higher than S/N E-1). Beam transmissions of 99.7 percent without RF drive and 93.2 percent with saturation RF drive were achieved with essentially the same magnetic field as 284H S/N E-1. The maximum turn-on body current was on  $I_w = 13$  mA.

The saturated output powers versus frequency for cathode voltages of  $E_k = -8.0$ ,  $-8.2$ , and  $-8.4$  kV are shown in Figure 4-7. The nominal output power at the optimum beam voltage of  $-8.2$  kV was only  $P_{out} = 130$  W. This corresponds to a basic (undepressed) efficiency of 17 percent. The maximum efficiency which occurred at  $E_k = -8.0$  kV and 12.165 GHz was 19.5 percent. The low efficiency and output power obtained on the tube was due to the large RF losses in the circuit velocity taper and output coupler and the output mismatch. This is shown in Figure 4-8 where measured and computed efficiencies (undepressed) are compared. Including only the circuit RF losses the computed maximum efficiency is 24 percent. When the circuit and coupler losses and mismatch effects are included, the predicted efficiency of 17 percent agrees with the measured value.

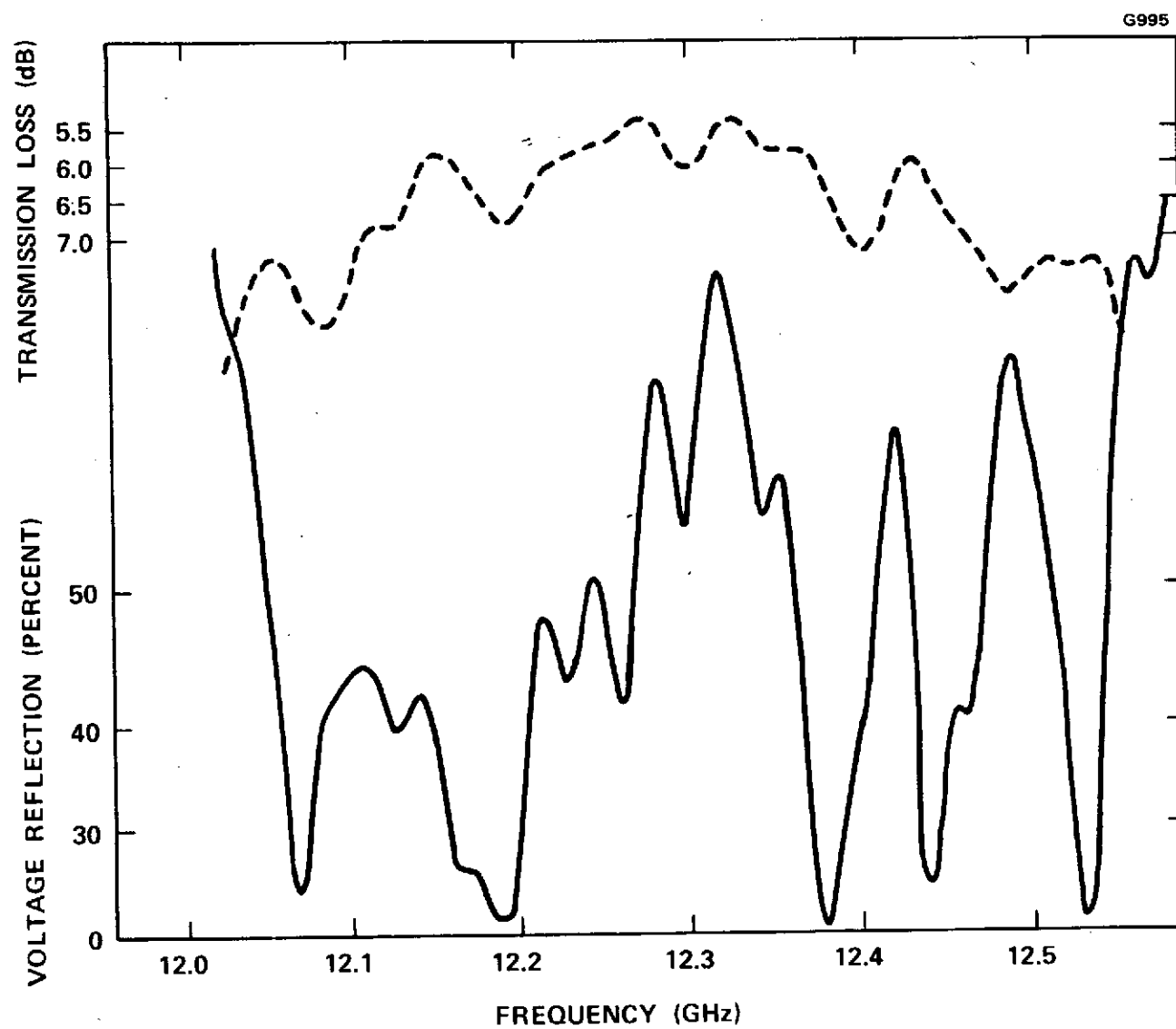


Figure 4-6 Final 284H P-1 output match and transmission loss.

TABLE 4-2

284H S/N P-1 Focusing Results	
Beam Voltage	8.0 kV
Beam Current	89.8 mA
Peak Field, Input	2125 GAUSS
Output	2370 GAUSS
Transmission, Without RF Drive	99.7%
With Saturated RF Drive	93.2%
Max. Body Current versus Beam Voltage	13 mA @ 5.5 kV



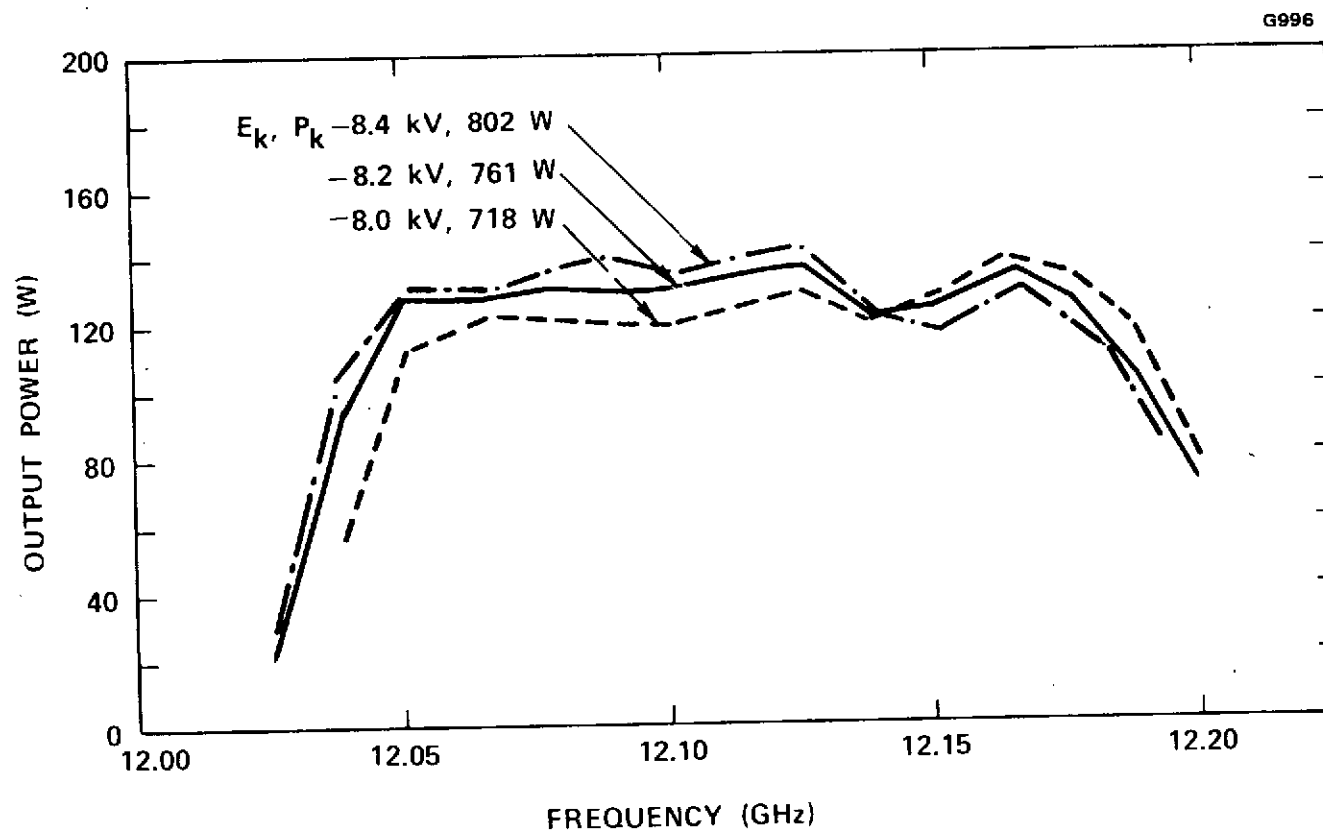


Figure 4-7 284H S/N P-1 Saturated output power.

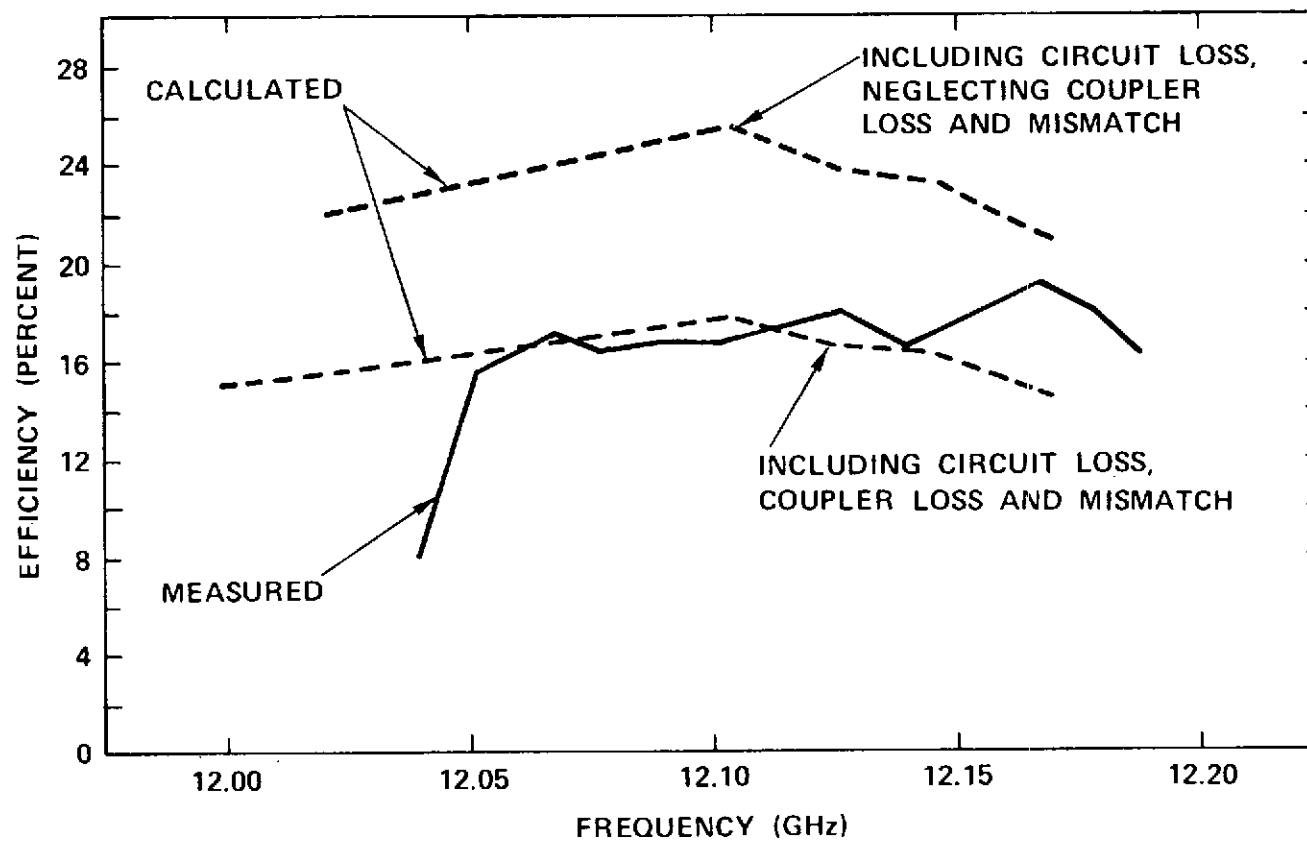


Figure 4-8 284H S/N P-1 basic saturated efficiency.

The swept output powers with constant input powers are shown in Figure 4-9. The amplitude variation from 12.05 GHz to 12.10 GHz was quite small; the large variations in the vicinity of 12.15 GHz were a result of the poor output match.

The small signal gain versus frequency for a constant input RF power of  $P_{in} = 2$  dBm and a cathode voltage of  $E_k = -8.2$  kV is shown in Figure 4-10. The gain variations, unequalized, were less than 1.4 dB from 12.06 to 12.13 GHz. The 3 dB bandwidth was 80 MHz, being somewhat reduced by the poor match. The center frequency of the hot band was approximately 20 MHz high.

Following completion of 284H S/N P-1 hot testing with the undeepressed bucket collector, this collector was removed and the first multistage radiation cooled depressed collector (MDC) was assembled. The OST was then baked out again at 450°C.

During bakeout, the bell jar vacuum pump to the external vacuum failed while the OST was hot. The resulting atmospheric condition on the outside surfaces of the tube at 450°C caused extreme oxidation of the circuit. This resulted in several pin-hole vacuum leaks and an internal tube pressure of approximately  $10^{-5}$  mm Hg. None of the attempts to stop these leaks were successful, so the tube could not be tested with the MDC.

To obtain additional confidence in the mechanical design of the OST, 284H S/N P-1 was packaged and thereafter subjected to the flight acceptance and qualification vibration test levels. The detailed results of these tests are given in Section 2.7; the OST survived these vibration levels with no visible damage. The 284H S/N P-1 OST was then delivered to NASA Lewis Research Center.

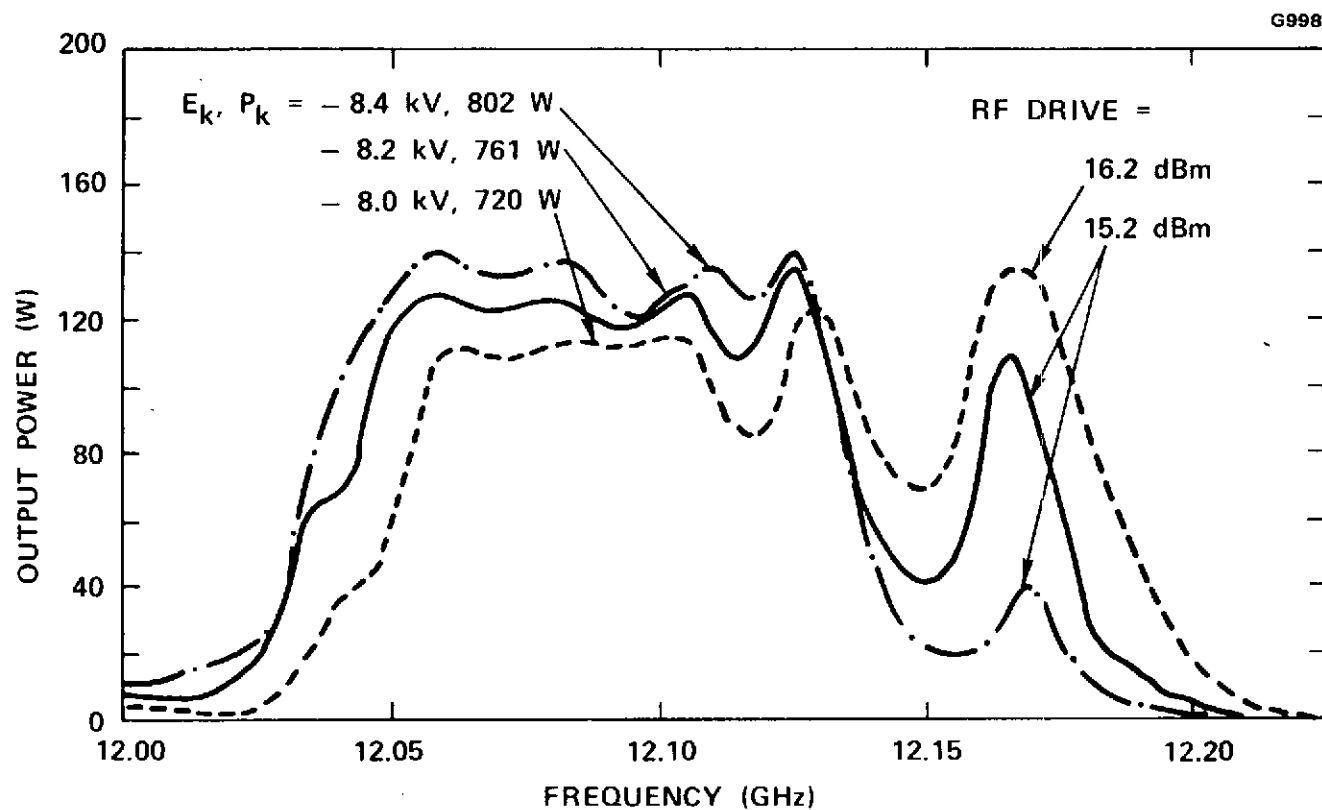


Figure 4-9 .284H S/N P-1 output power with constant drive.

#### 4.4 284H SERIAL NUMBER P-2

Two changes were incorporated in 284H OST S/N P-2. The RF circuit periods (cavity heights) in the standard and velocity taper sections were increased by 6 per cent in order to obtain a higher value of midband phase shift per cavity. In addition, different brazing alloys and modified time-temperature schedules were used to reduce the amount of braze material flowing into the cavities. These changes were made to reduce the circuit loss. The gun and MDC designs were identical to those used on 284H S/N P-1. The permanent magnet thicknesses were increased to accommodate the circuit period change.

Excellent cold circuit matches were achieved on both the input and output sections prior to final braze. The output section was adjusted for low voltage reflection with a coupler configuration having minimum loss.

After final braze, the output match degraded somewhat from that measured before braze (in the same fashion as P-1). The voltage reflection, in the operating frequency band, however, was significantly improved over P-1. The final match (lower curve) is shown in Figure 4-11. Except for a 45 percent peak mismatch at 12.06 GHz the reflections were less than 30 percent across the operating frequency band.

The transmission loss (upper curve) for the 284H S/N P-2 output section is also shown in Figure 4-11. The loss at 12.080 GHz was 3.8 dB, compared with 8.0 dB loss in the P-1 circuit. This dramatic improvement resulted from the circuit period change and the reduced braze material in the brazed coupled-cavity circuit. 284H S/N P-2 construction and bakeout were completed during the second week of March, 1973.

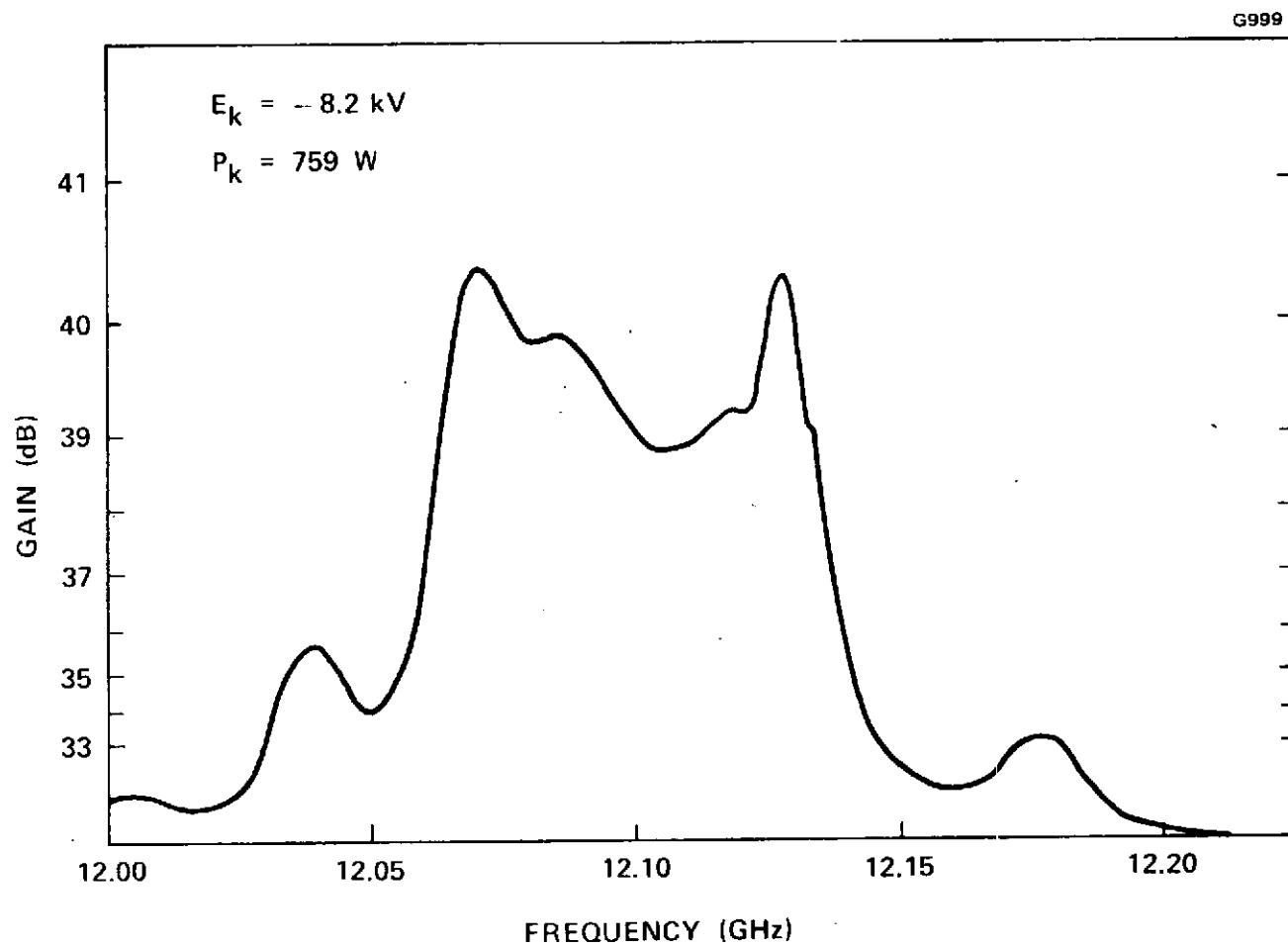


Figure 4-10 284H S/N P-1 small signal gain.

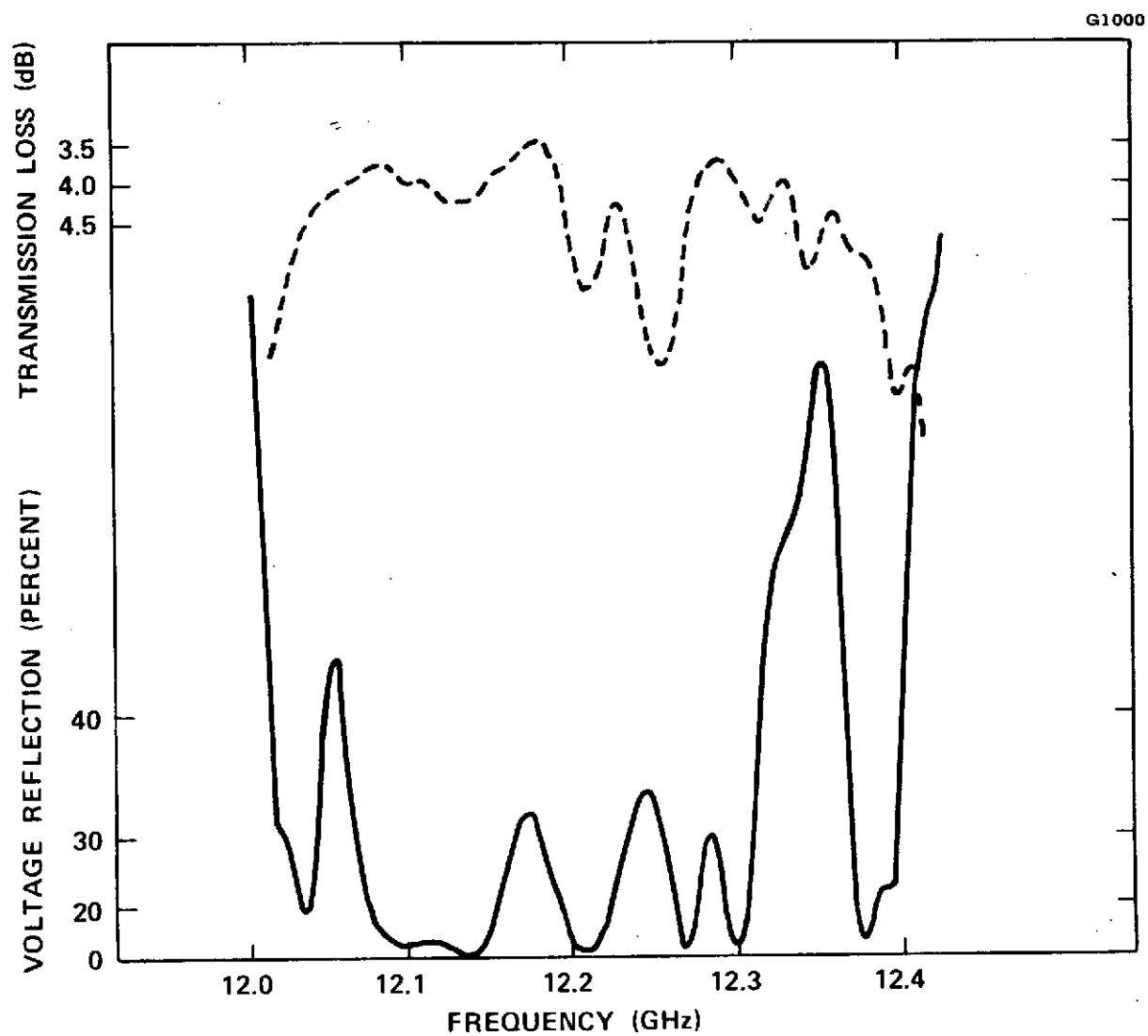


Figure 4-11 284H S/N P-2 output section match and transmission loss.

The focusing characteristics (without RF drive) of 284H S/N P-2 were the same as S/N P-1. However, the measured RF output power and gain were very low. Examination of the RF output pulse during low duty cathode pulsed operation revealed a breakup of the trailing edge for all levels of RF input power. Sensitive spectral measurements of the OST output indicated an oscillation at 27.8 GHz in the output section. This frequency corresponds to the cutoff of the  $TM_{020}$  cylindrical cavity mode of the circuit. The  $TM_{020}$  oscillation in the output section was capturing the beam, making efficient interaction at the fundamental frequencies impossible.

The transmission loss data in the region of 28 GHz of 284H S/N P-2 was compared with that of S/N P-1 to determine the cause of this unexpected oscillation problem. The data for the P-1 OST showed that the resonant loss distribution used to suppress the slot mode at approximately 22 GHz also had significant loss at 28 GHz. On the other hand, the loss distribution used in OST S/N P-2 was centered lower in frequency and therefore has reduced loss at the  $TM_{020}$  cutoff frequency. The reduced braze material in the cavities may also have contributed to the effect by lowering the high frequency skin effect losses. Several attempts were made to suppress the oscillation by reducing the beam current (using the modulating anode) and increasing the magnetic field to reduce the beam diameter. None of these modifications produced any noticeable change in the tubes fundamental output or oscillation power. Further testing of this OST was deferred for testing of 284H S/N ETM-1.

#### 4.5 284H SERIAL NUMBER ETM-1

The matching and final assembly of 284H S/N ETM-1, the first engineering test model OST, was done in a parallel effort with the construction of the P-2 OST. No design changes were made to the RF circuit or velocity taper except for the high frequency oscillation suppression loss which



was increased at the  $TM_{020}$  cutoff frequency of 27.8 GHz. The collector electrode apertures were decreased to a four degree half-angle envelope at the recommendation of Dr. H. Kosmahl of NASA. A fixed tenth electrode spike was also used. A minor increase in the electron gun focus electrode inner diameter was made to prevent interference with the OD of the cathode.

Excellent circuit matches were achieved on S/N ETM-1 as shown in Figure 4-12. After final braze the voltage reflection of the output section was below 30 percent over the entire operating frequency band. The inband transmission loss was approximately the same as for S/N P-2.

Initial testing of 284H S/N ETM-1 began in April, 1973. Due to the change in the focus electrode, the gun perveance was low resulting in a cathode current of only  $I_k = 72.5$  mA. (The design value was  $I_k = 84$  mA.)

During the tests no OST instabilities were observed, and the tube processed to CW duty with no difficulty.

The focusing of this tube was satisfactory; beam transmissions with and without RF drive were 90.5 percent and 97.6 percent respectively.

The saturated output power for S/N ETM-1 is shown in Figure 4-13 at the optimum beam voltage of  $E_k = -8.20$  kV. The minimum output power is  $P = 140$  watts at 12.123 GHz while the maximum output power is  $P = 175$  watts at 12.070 GHz.

The basic interaction efficiency and the overall depressed efficiency including refocusing solenoid and filament powers are given in Figure 4-14. The basic efficiency varies from  $\eta_o = 22.6$  percent at 12.123 GHz to  $\eta_o = 28.3$  percent at 12.070 GHz. The overall efficiency range is a minimum of 36 percent up to a maximum of 44.7 percent. The OST currents

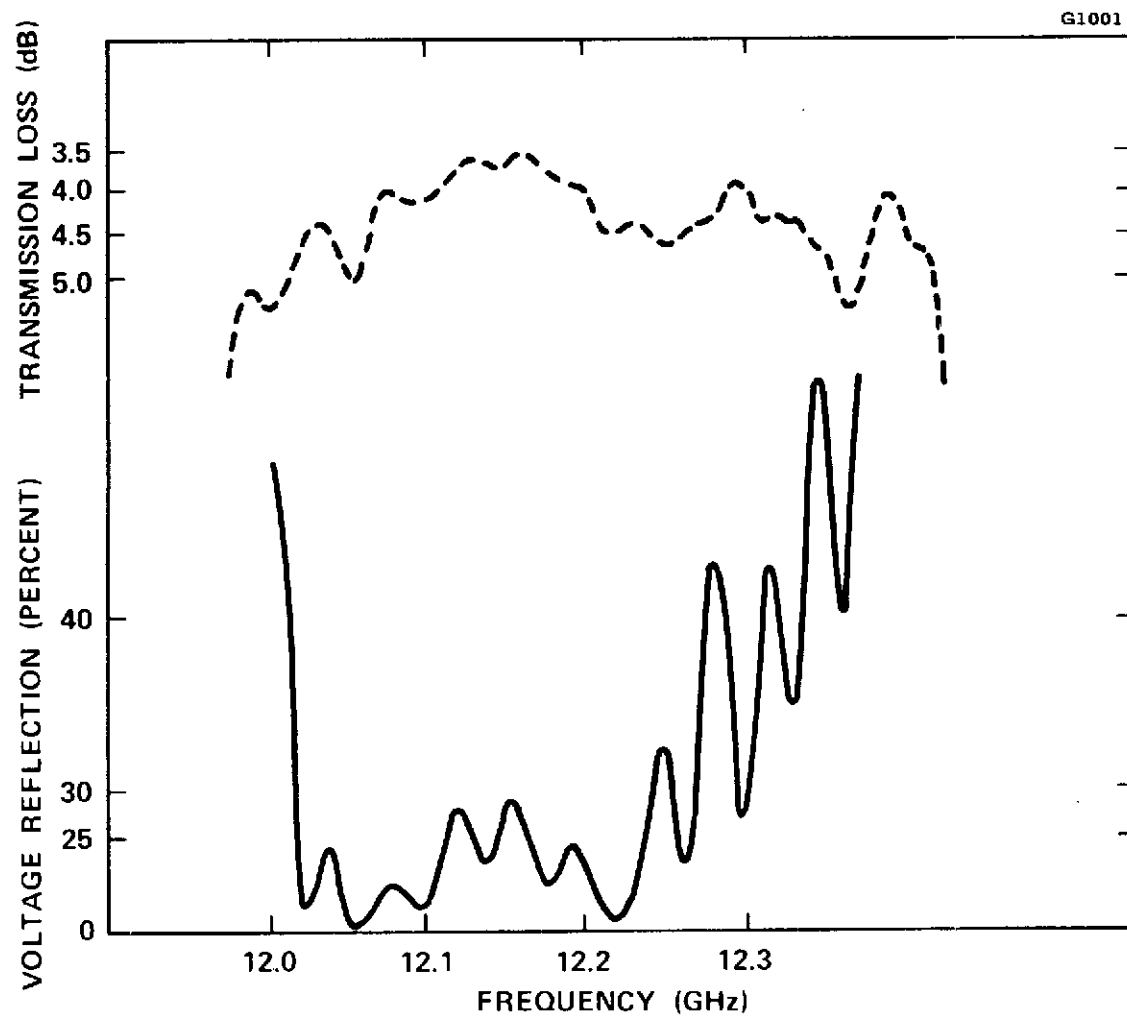


Figure 4-12 284H S/N ETM-1 output section match and transmission loss.

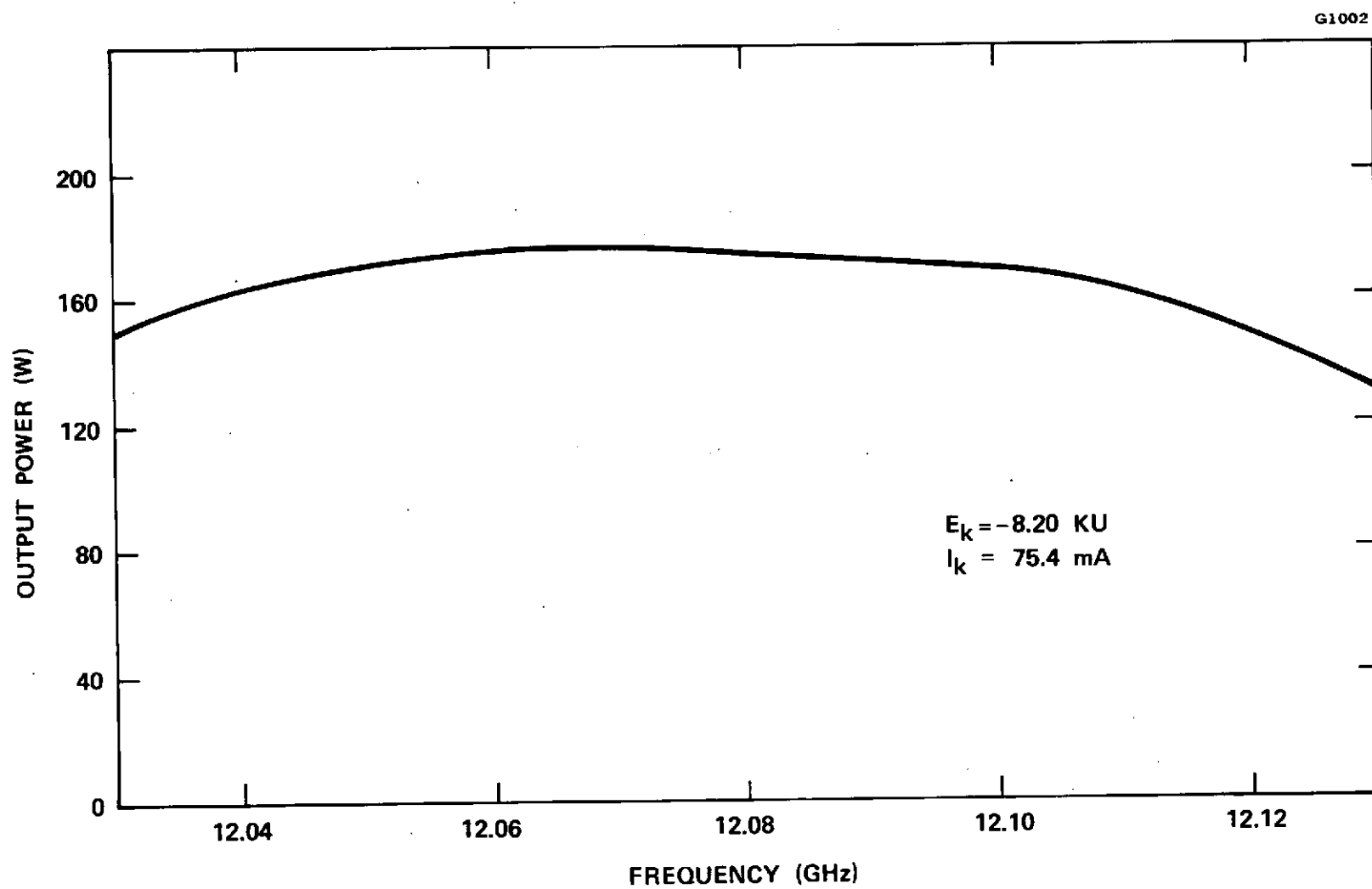


Figure 4-13 Saturated output power for 284H S/N ETM-1.

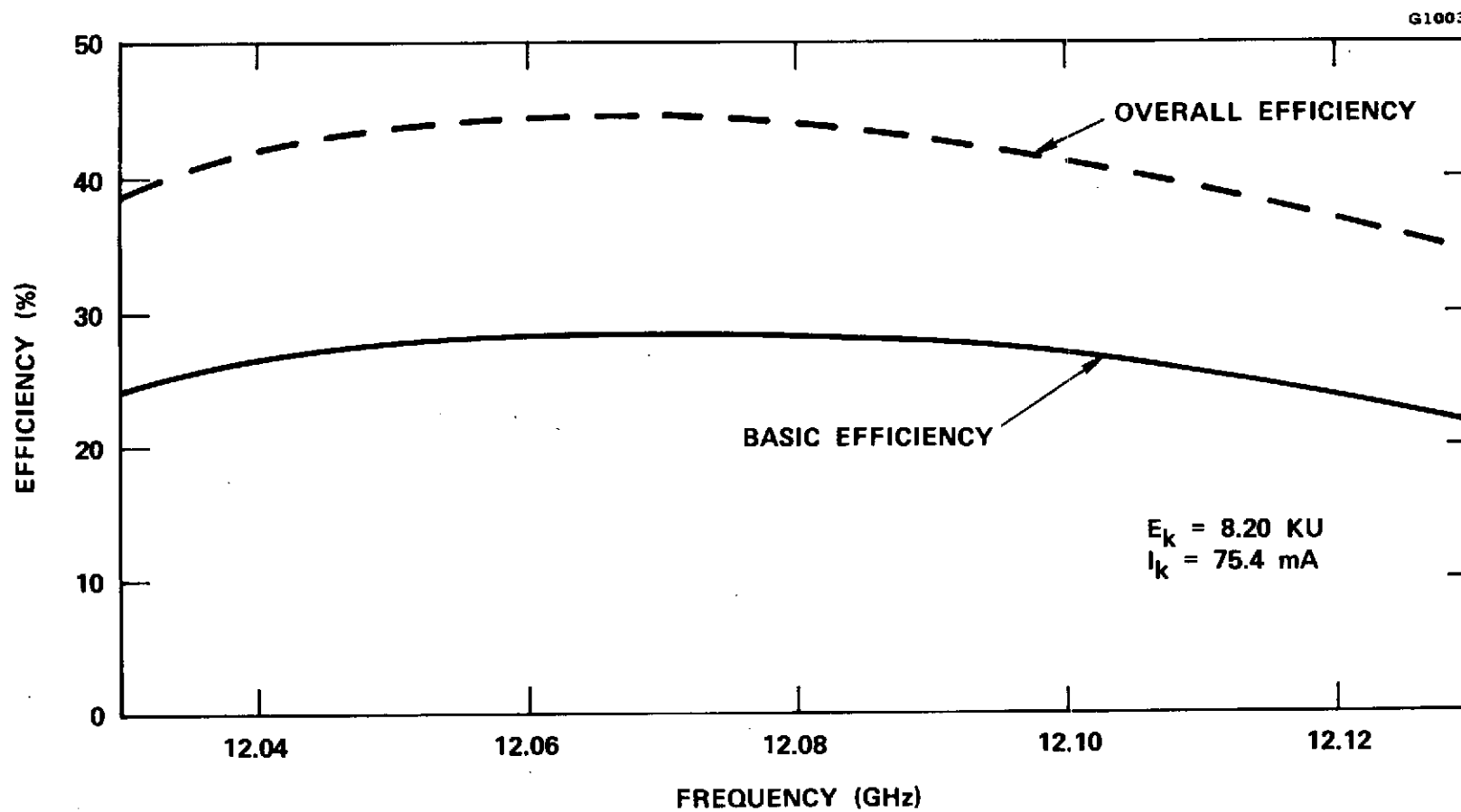


Figure 4-14 284H S/N ETM-1 Saturated efficiencies.

and voltages for saturation at 12.038, 12.070, and 12.123 GHz are given in Table 4-3. The tube parameters for no RF drive are given in Table 4-4. Under these conditions, the calculated collector efficiency was  $\eta_{coll}=73.6$  percent.

The swept output power versus frequency characteristics of 284H S/N ETM-1 are shown in Figure 4-15 for three RF drive levels 1 dB apart. At the optimum input RF power level of  $P_{in} = 15.7$  dBm the output power varies 1.0 dB from 175 watts at 12.070 GHz to 136 watts at 12.123 GHz.

The output power for swept input RF power 10 dB below the optimum value is given in Figure 4-16. From this curve it appears that the frequency centering of this OST is about 20 MHz low.

The RF power out versus RF power in curves for the 284H S/N ETM-1 are shown in Figure 4-17. The saturation curve's untypical shape is due to the circuit velocity taper.

Figure 4-18 is the phase deviation from linear for optimum RF drive. The total deviation across the frequency band is less than  $\pm 12^\circ$ . For RF drive 10 dB below optimum the phase linearity is as shown in Figure 4-19.

After completion of testing, 284H S/N ETM-1 was delivered to NASA Lewis Research Center. All of the data was confirmed by test at NASA. This OST was subsequently integrated with the breadboard power supply at TRW.

#### 4.6 284H SERIAL NUMBER ETM-2

Several changes were made in the design of 284H S/N ETM-2 to increase the output power to greater than 200 watts and to further reduce the circuit RF losses. The electron gun perveance was increased by decreasing the

TABLE 4-3  
284H ETM-1 OPERATING PARAMETERS

OUTPUT POWER ( $P_o$ )	160 W
INPUT POWER ( $P_{in}$ )	40 mW
FREQUENCY (F)	12.038
CATHODE VOLTAGE ( $E_k$ )	-8.20 KV
CATHODE CURRENT ( $I_k$ )	75.7 mA
ANODE VOLTAGE ( $E_A$ )	+300 V
FILAMENT VOLTAGE ( $E_f$ )	5.1 V
FILAMENT CURRENT ( $I_f$ )	1.18 A
SOLENOID (1) VOLTAGE ( $E_s$ )	1.0 V
SOLENOID (1) CURRENT ( $I_s$ )	3.7 A
SOLENOID (2) VOLTAGE ( $E_s$ )	.6V
SOLENOID (2) CURRENT ( $I_s$ )	3.7 A
TWT ION PUMP VOLTAGE	3.0 KV
TWT ION PUMP CURRENT	0.0 mA
MDC .2L/S ION PUMP VOLTAGE	3.0 KV
MDC .2L/S ION PUMP CURRENT	0.0 mA
MDC 8L/S ION PUMP VOLTAGE	3.0 KV
MDC 8L/S ION PUMP CURRENT	0.0 mA
BODY CURRENT	6.2 mA

MDC VOLTAGES (KV)	
NO. 1	0.0
NO. 2	1.63
NO. 3	2.44
NO. 4	3.30
NO. 5	4.13
NO. 6	4.92
NO. 7	5.75
NO. 8	6.55
NO. 9	7.40
NO. 10	8.21

MDC CURRENTS (mA)	
NO. 1	5.0
NO. 2	3.8
NO. 3	10.0
NO. 4	26.5
NO. 5	8.3
NO. 6	4.1
NO. 7	3.1
NO. 8	5.2
NO. 9	3.8
NO. 10	-.3

TABLE 4-3 (con't)

## 284H ETM-1 OPERATING PARAMETERS

OUTPUT POWER ( $P_o$ )	175 W
INPUT POWER ( $P_{in}$ )	25 mW
FREQUENCY (F)	12.070
CATHODE VOLTAGE ( $E_k$ )	-8.20 KV
CATHODE CURRENT ( $I_k$ )	75.4 mA
ANODE VOLTAGE ( $E_A$ )	+300 V
FILAMENT VOLTAGE ( $E_f$ )	5.1 V
FILAMENT CURRENT ( $I_f$ )	1.18 A
SOLENOID (1) VOLTAGE ( $E_s$ )	1.0 V
SOLENOID (1) CURRENT ( $I_s$ )	3.7 A
SOLENOID (2) VOLTAGE ( $E_s$ )	0.6V
SOLENOID (2) CURRENT ( $I_s$ )	3.7 A
TWT ION PUMP VOLTAGE	3.0 KV
TWT ION PUMP CURRENT	0.0 mA
MDC .2L/S ION PUMP VOLTAGE	3.0 KV
MDC .2L/S ION PUMP CURRENT	0.0 mA
MDC 8L/S ION PUMP VOLTAGE	3.0 KV
MDC 8L/S ION PUMP CURRENT	0.0 mA
BODY CURRENT	5.9 mA

## MDC VOLTAGES (KV)

NO. 1	0.0
NO. 2	1.64
NO. 3	2.47
NO. 4	3.30
NO. 5	4.11
NO. 6	4.91
NO. 7	5.74
NO. 8	6.54
NO. 9	7.39
NO. 10	8.19

## MDC CURRENTS (mA)

NO. 1	5.3
NO. 2	4.7
NO. 3	15.6
NO. 4	22.4
NO. 5	6.2
NO. 6	4.1
NO. 7	3.3
NO. 8	5.0
NO. 9	3.4
NO. 10	- .5

# 284H ETM-1 OPERATING PARAMETERS

OUTPUT POWER ( $P_o$ )	140 W
INPUT POWER ( $P_{in}$ )	63 mW
FREQUENCY (F)	12.123
CATHODE VOLTAGE ( $E_k$ )	-8.20 KV
CATHODE CURRENT ( $I_k$ )	75.7 mA
ANODE VOLTAGE ( $E_A$ )	+300 V
FILAMENT VOLTAGE ( $E_f$ )	5.1 V
FILAMENT CURRENT ( $I_f$ )	1.18 A
SOLENOID (1) VOLTAGE ( $E_s$ )	1.0 V
SOLENOID (1) CURRENT ( $I_s$ )	3.7 A
SOLENOID (2) VOLTAGE ( $E_s$ )	0.6 V
SOLENOID (2) CURRENT ( $I_s$ )	3.7 A
TWT ION PUMP VOLTAGE	3.0 KV
TWT ION PUMP CURRENT	0.0 mA
MDC .2L/S ION PUMP VOLTAGE	3.0 KV
MDC .2L/S ION PUMP CURRENT	0.0 mA
MDC 8L/S ION PUMP VOLTAGE	3.0 KV
MDC 8L/S ION PUMP CURRENT	0.0 mA
BODY CURRENT	7.4 mA

## MDC VOLTAGES (KV)

NO. 1	0.0
NO. 2	1.63
NO. 3	2.42
NO. 4	3.30
NO. 5	4.12
NO. 6	4.93
NO. 7	5.75
NO. 8	6.53
NO. 9	7.38
NO. 10	8.16

## MDC CURRENTS (mA)

NO. 1	4.9
NO. 2	3.8
NO. 3	9.4
NO. 4	23.5
NO. 5	7.6
NO. 6	5.4
NO. 7	5.2
NO. 8	5.3
NO. 9	3.7
NO. 10	- .5



TABLE 4-4  
284H ETM-1 OPERATING PARAMETERS

OUTPUT POWER ( $P_o$ )	0
INPUT POWER ( $P_{in}$ )	0
FREQUENCY (F)	-
CATHODE VOLTAGE ( $E_k$ )	8.20 KV
CATHODE CURRENT ( $I_k$ )	76 mA
ANODE VOLTAGE ( $E_A$ )	+300 V
FILAMENT VOLTAGE ( $E_f$ )	5.1 V
FILAMENT CURRENT ( $I_f$ )	1.18 A
SOLENOID (1) VOLTAGE ( $E_s$ )	1.0 V
SOLENOID (1) CURRENT ( $I_s$ )	3.7 A
SOLENOID (2) VOLTAGE ( $E_s$ )	0.6 V
SOLENOID (2) CURRENT ( $I_s$ )	3.7 A
TWT ION PUMP VOLTAGE	3.0 KV
TWT ION PUMP CURRENT	0.0 mA
MDC .2L/S ION PUMP VOLTAGE	3.0 KV
MDC .2L/S ION PUMP CURRENT	0.0 mA
MDC 8L/S ION PUMP VOLTAGE	3.0 KV
MDC 8L/S ION PUMP CURRENT	0.0 mA
BODY CURRENT	1.8 mA

MDC VOLTAGES (KV)

NO. 1	+0.00
NO. 2	1.59
NO. 3	2.33
NO. 4	3.15
NO. 5	4.06
NO. 6	4.94
NO. 7	5.84
NO. 8	6.76
NO. 9	7.46
NO. 10	8.23

MDC CURRENTS (mA)

0 NO. 1	0.9
.2 NO. 2	0.7
.3 NO. 3	0.9
.4 NO. 4	1.5
.5 NO. 5	2.2
.6 NO. 6	7.0
.7 NO. 7	14.8
.8 NO. 8	34.3
.9 NO. 9	11.9
1.0 NO. 10	0.0

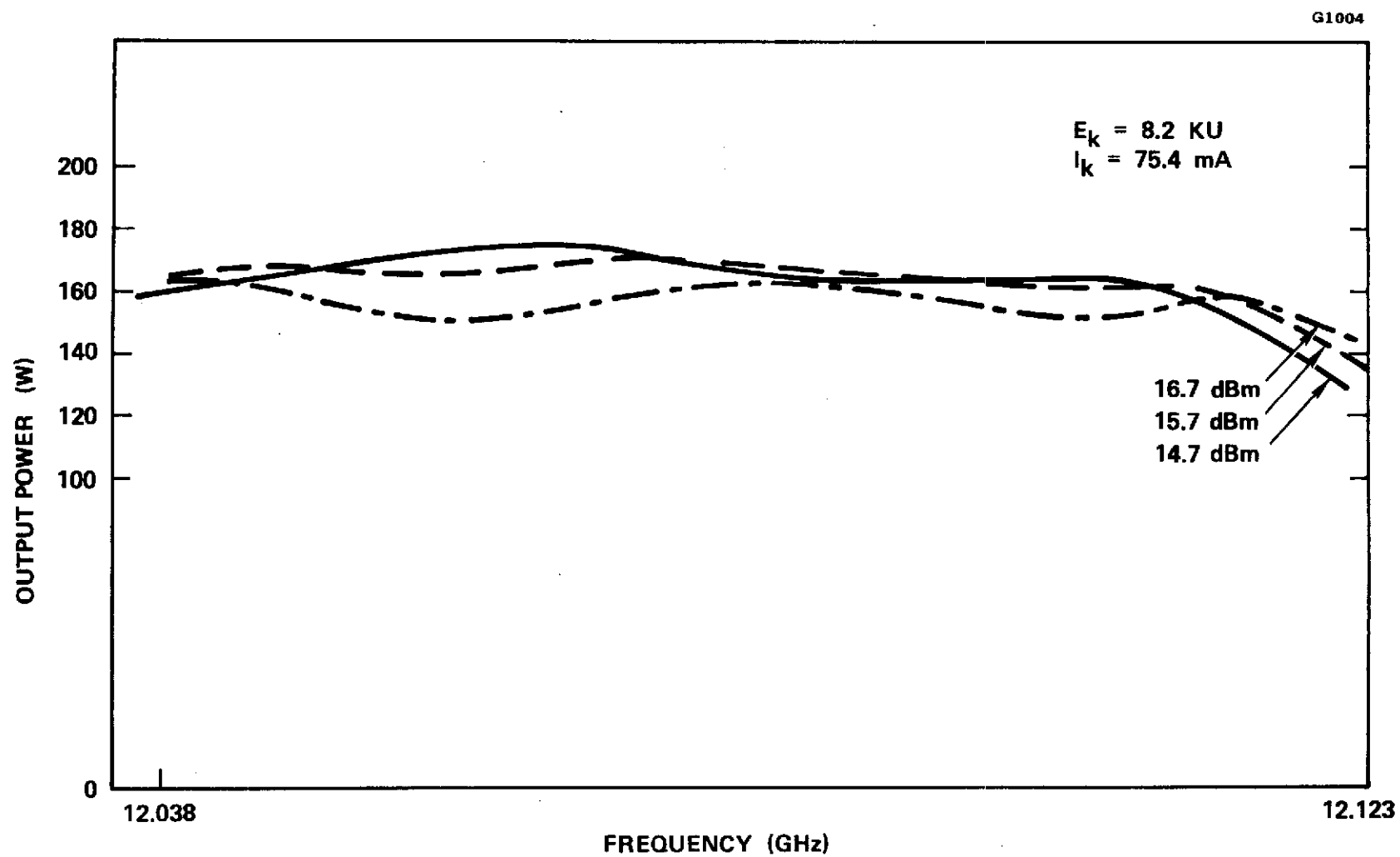


Figure 4-15 284H ETM-1 swept power output for constant power.

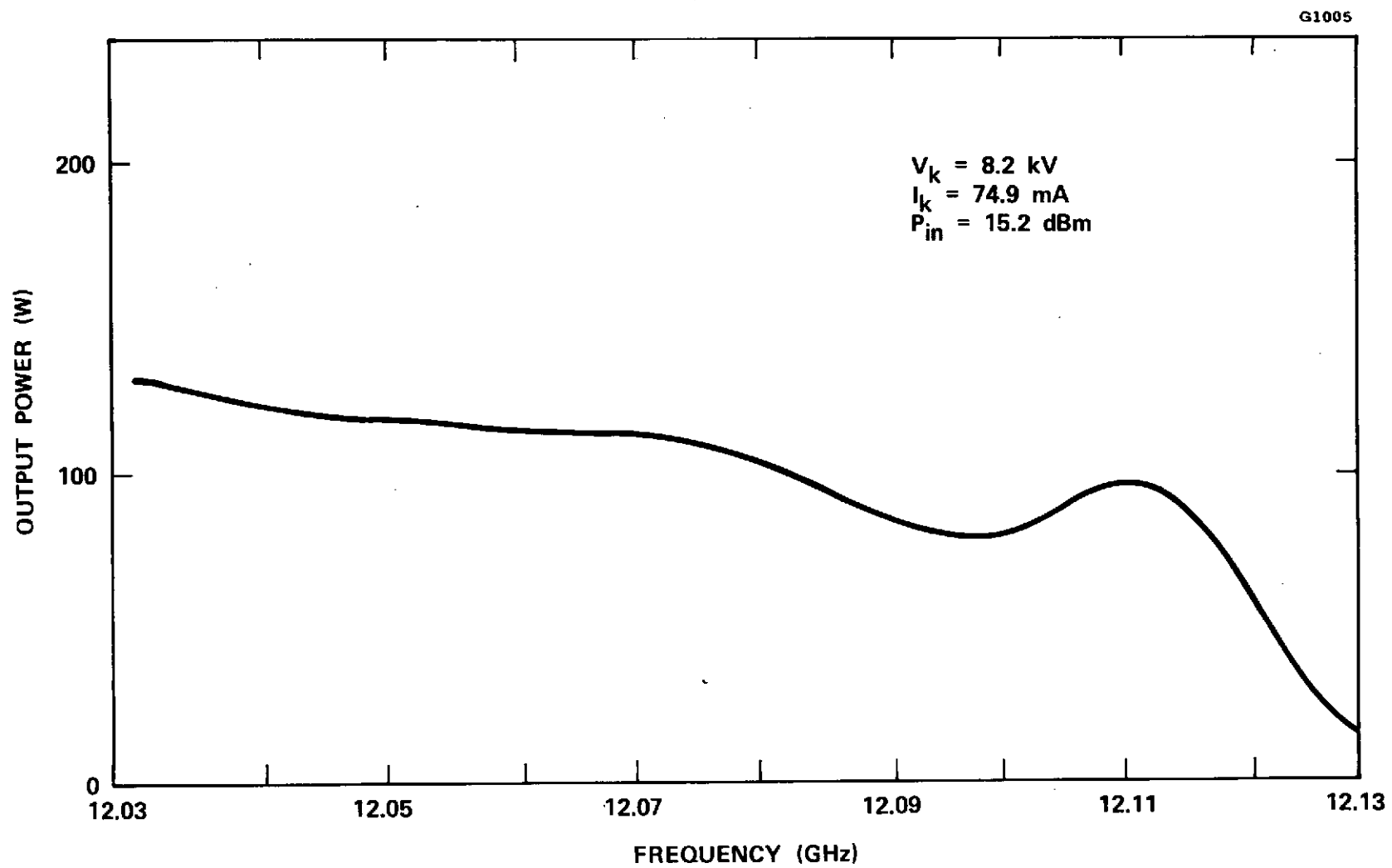


Figure 4-16 Output power of 284H ETM-1  
at 10 dB below optimum drive.

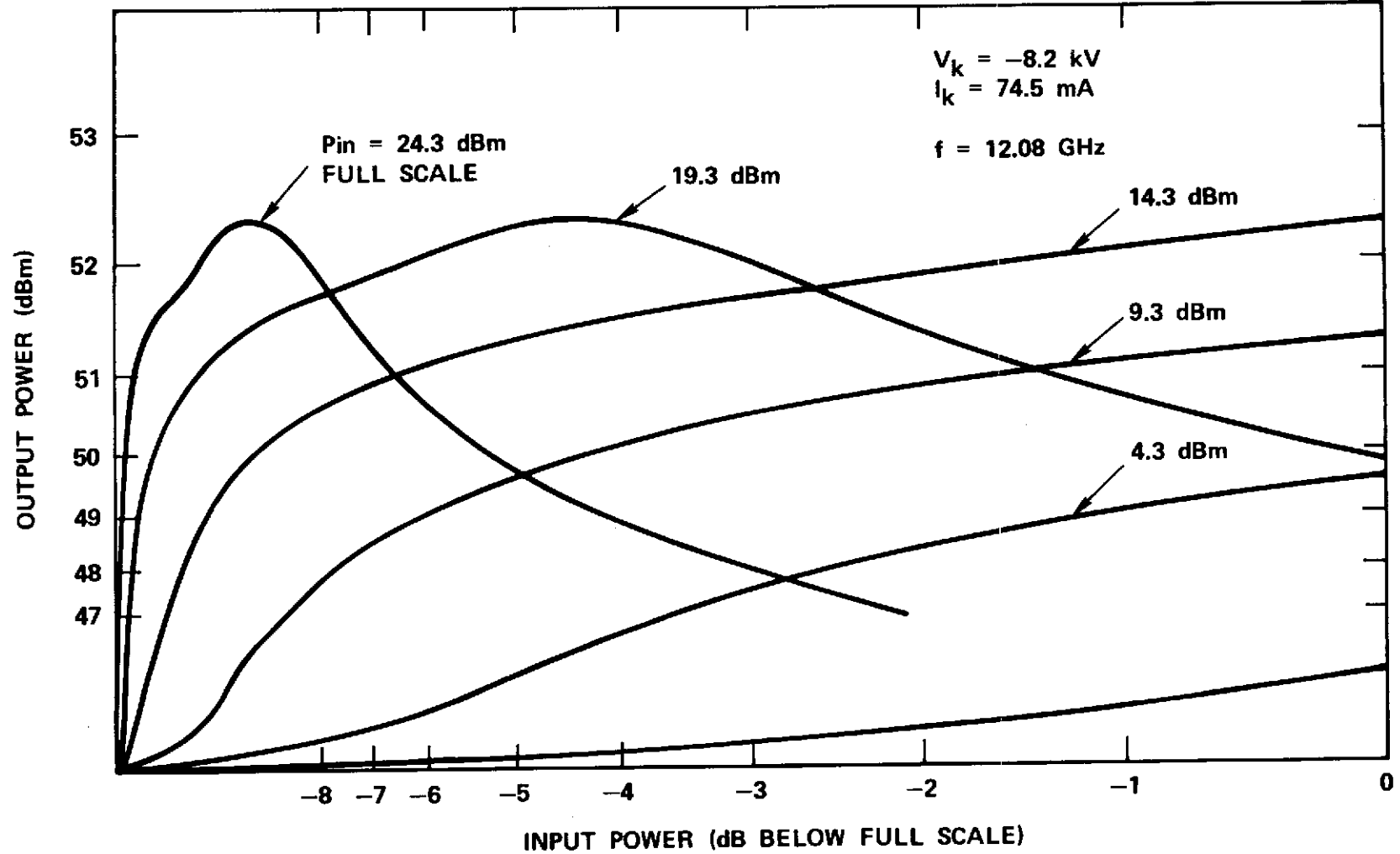


Figure 4-17 Power out versus power in for 284H S/N ETM-1.

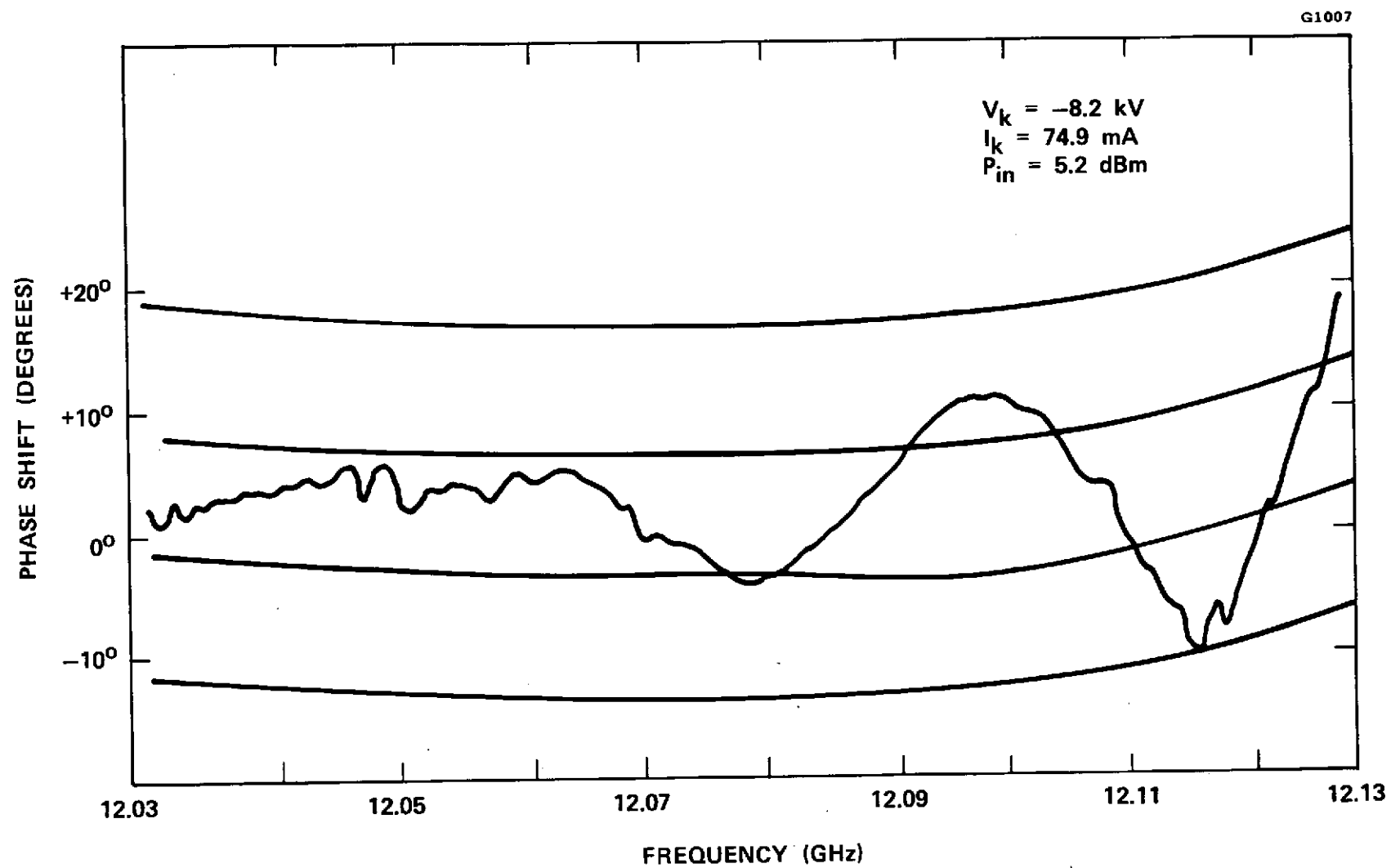


Figure 4-18 Phase linearity at optimum drive for 284H ETM-1.

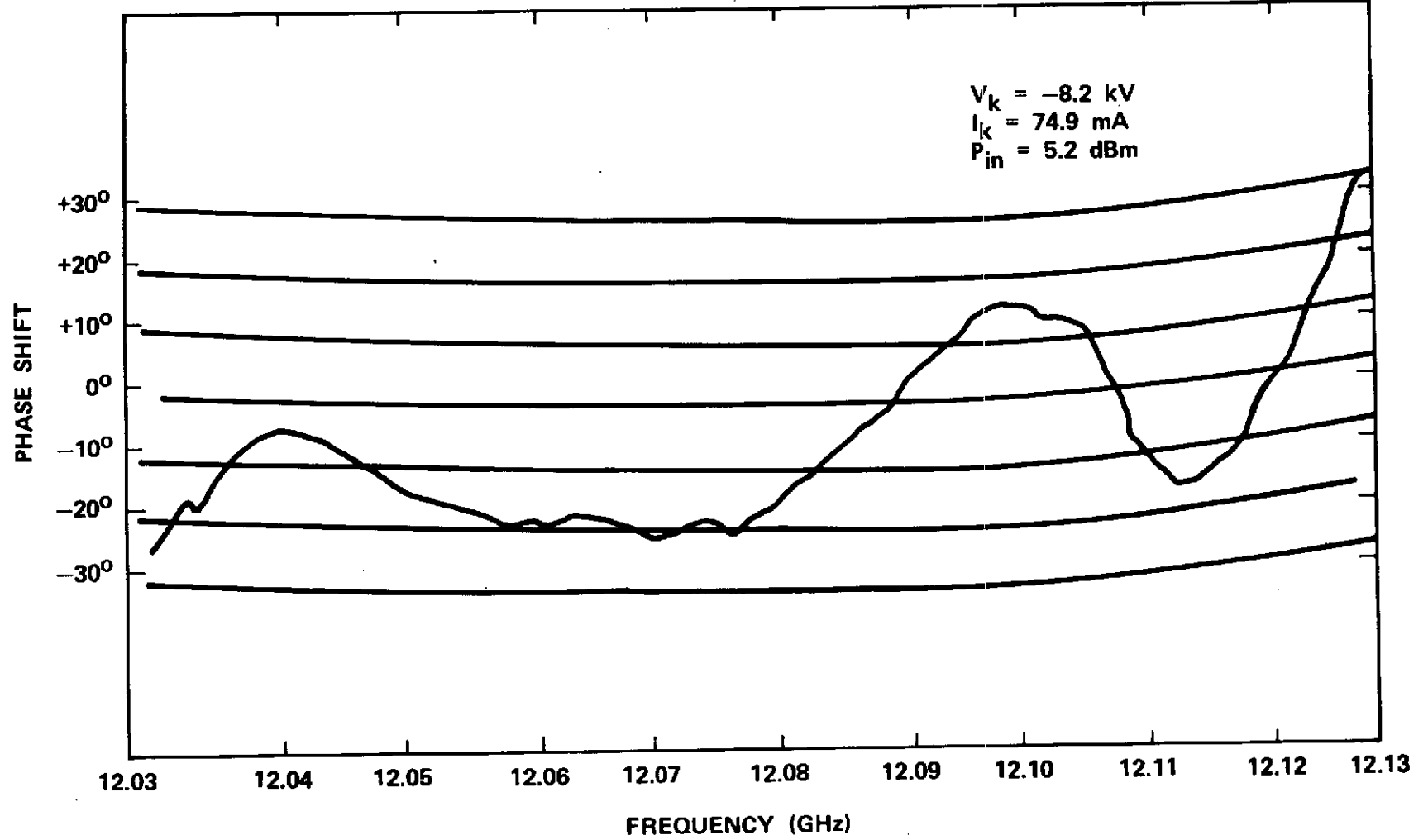


Figure 4-19 Phase linearity at 10 dB below optimum drive for 284H ETM-1.

cathode to anode spacing. Based on computer analyses the second velocity taper section was shortened by one cavity to reduce the RF losses and thereby increase the depressed efficiency.

The monel output waveguide transformer was copper plated on the inside surfaces to also reduce skin effect losses. The center frequency of the RF circuit was increased by about 20 MHz.

The MDC electrode apertures used were the original design, having a half angle envelope of  $6^\circ$ . This was done to improve the performance with the higher perveance gun. A fixed spike for the last collector electrode was also used in this tube.

Excellent in-band matches were obtained with 284H S/N ETM-2. The brazed output circuit voltage reflection, shown in Figure 4-20, was below 20 percent. The measured transmission loss of the circuit was identical to the loss of S/N ETM-1. However, this measurement did not include the copper plated waveguide transformer. The tube assembly, bakeout and initial test were completed without difficulty.

The modified electron gun performed well, providing a beam current of  $I_k = 87$  mA at a beam voltage of  $V_k = -8.0$  kV. Using the same axial magnetic field as 284H S/N ETM-1, a beam transmission without RF drive of 98 percent was achieved. At saturation, the transmission was greater than 93 percent.

The 284H S/N ETM-2 OST produced between 235 watts and 250 watts of saturated output power across the required 85 MHz frequency band, shown in Figure 4-21. For the beam voltage of  $E_k = -8.30$  kV and beam current of  $I_k = 91.9$  mA, this output power corresponds to minimum and maximum interaction efficiencies of 30 percent and 33 percent respectively.

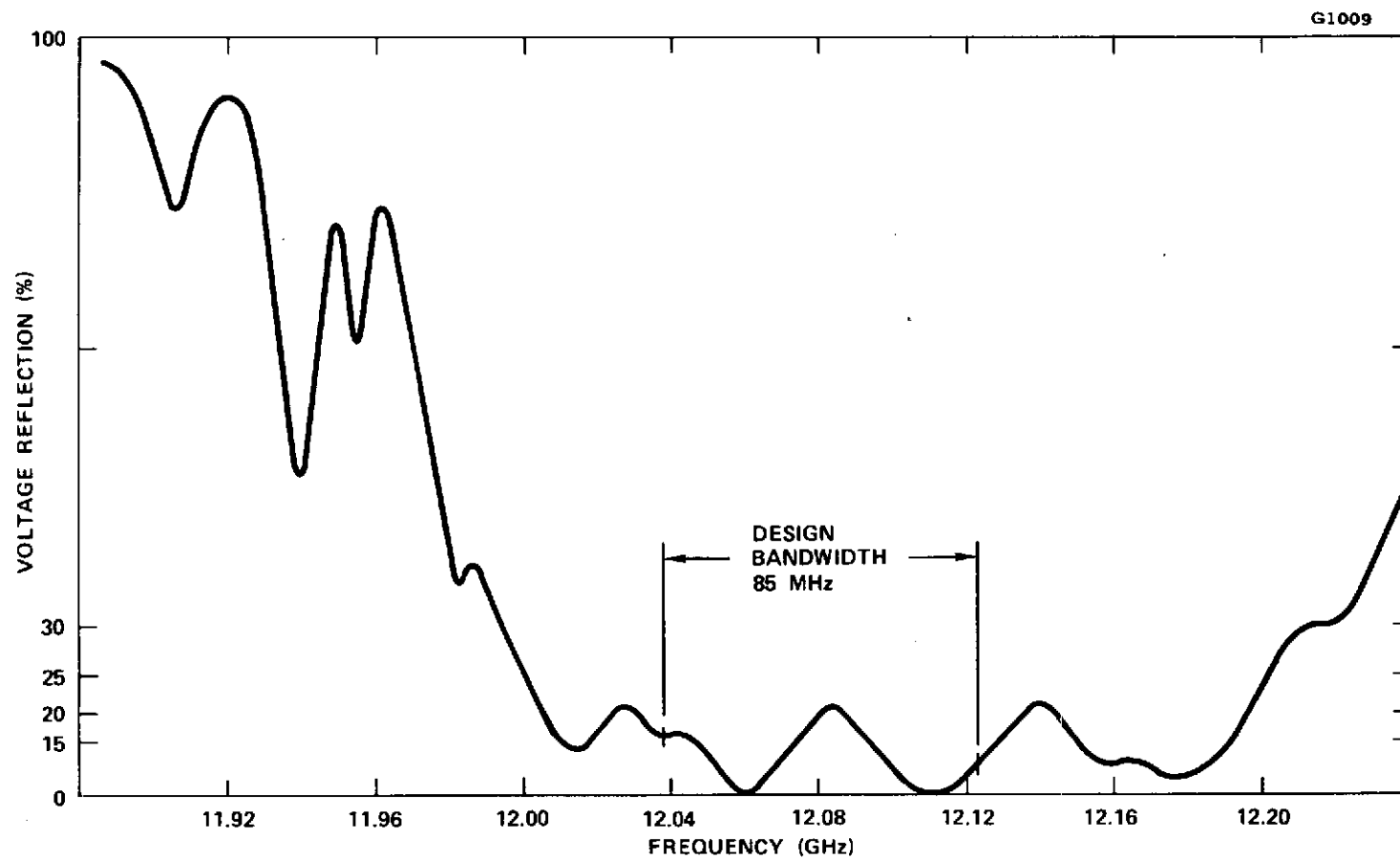


Figure 4-20 Output RF circuit match.



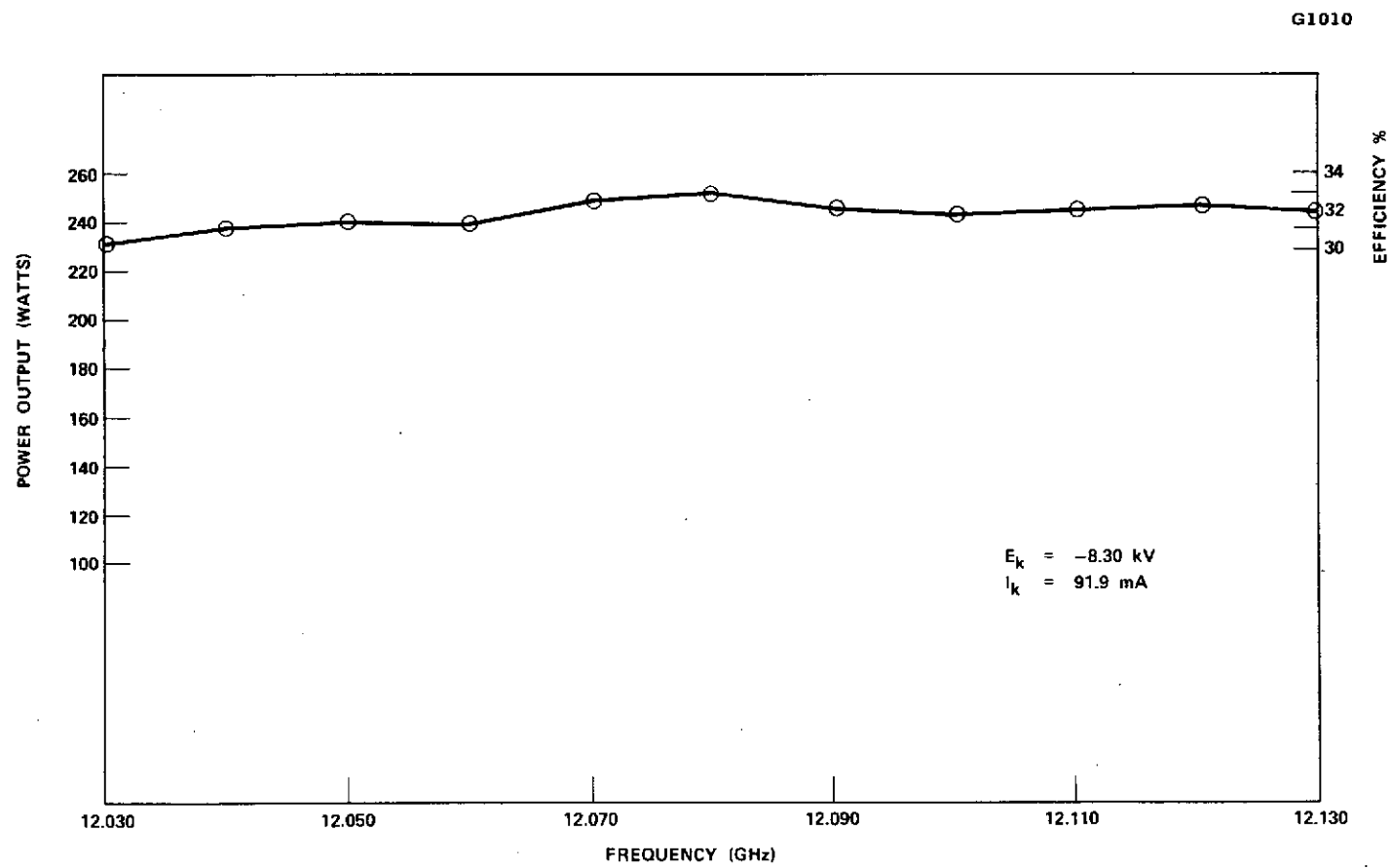


Figure 4-21 284H S/N ETM-2 saturated power output.

The OST operating voltages and currents for saturation at 12.080 GHz are given in Table 4-5. At the cathode voltage of -8.3 kV; the basic and overall efficiencies were 33 percent and 51 percent respectively. The collector voltages were equally spaced in increments of one tenth of the cathode voltage, except between the first two stages where the increment was twice as large. The negative current to the tenth element was due to positively charged ions attracted to the spike.

Figure 4-22 shows the basic, depressed and overall OST efficiencies. The basic efficiency across the design bandwidth varied between 31 and 33 percent, and the depressed efficiency was close to 53 percent. With the heater and refocusing solenoid power included, the overall efficiency was a constant 51 percent from 12.038 to 12.123. Also shown in Figure 4-22 are the basic efficiencies at four frequencies across the frequency band calculated with the large signal interaction computer program. The calculations used circuit cold test data and assumed a cathode voltage and current of -8.0 kV and 84 mA respectively. The agreement between calculated and measured efficiencies is good, noting that the higher actual operating voltage and current improved the low frequency performance and overall bandwidth and efficiency.

The swept output power versus frequency with constant input power over a 100 MHz band is given in Figure 4-23. For an optimum RF drive level of 16 dBm (40 mw) the output power varied from 235 watts to 250 watts, a 0.27 dB change. The maximum amplitude slope was only 0.025 dB/MHz. The tube was quite insensitive to RF drive variations of 2 dB.

Figure 4-24 shows constant drive performance over an extended frequency range of 150 MHz, nearly twice the required bandwidth. With a drive level of 18 dBm (63 mW) the tube produced 200 watts of nominal output power with less than 0.3 dB amplitude variation. This data was taken

TABLE 4-5

## 284H S/N ETM-2 Operating Parameters

Power Out	250 W
Gain	38 dB
Basic Efficiency	33%
Overall Efficiency	51%
Cathode Voltage	-8.30 kV
Cathode Current	91.8 mA
Body Current	6.3 mA
Filament Power	5.7 W

Collector Element	Voltage (kV)	Current (mA)
1	0	7.5
2	-1.7	10.5
3	-2.5	26.4
4	-3.3	16.4
5	-4.1	3.5
6	-5.0	3.8
7	-5.8	4.8
8	-6.6	7.4
9	-7.5	5.7
10	-8.3	-0.5

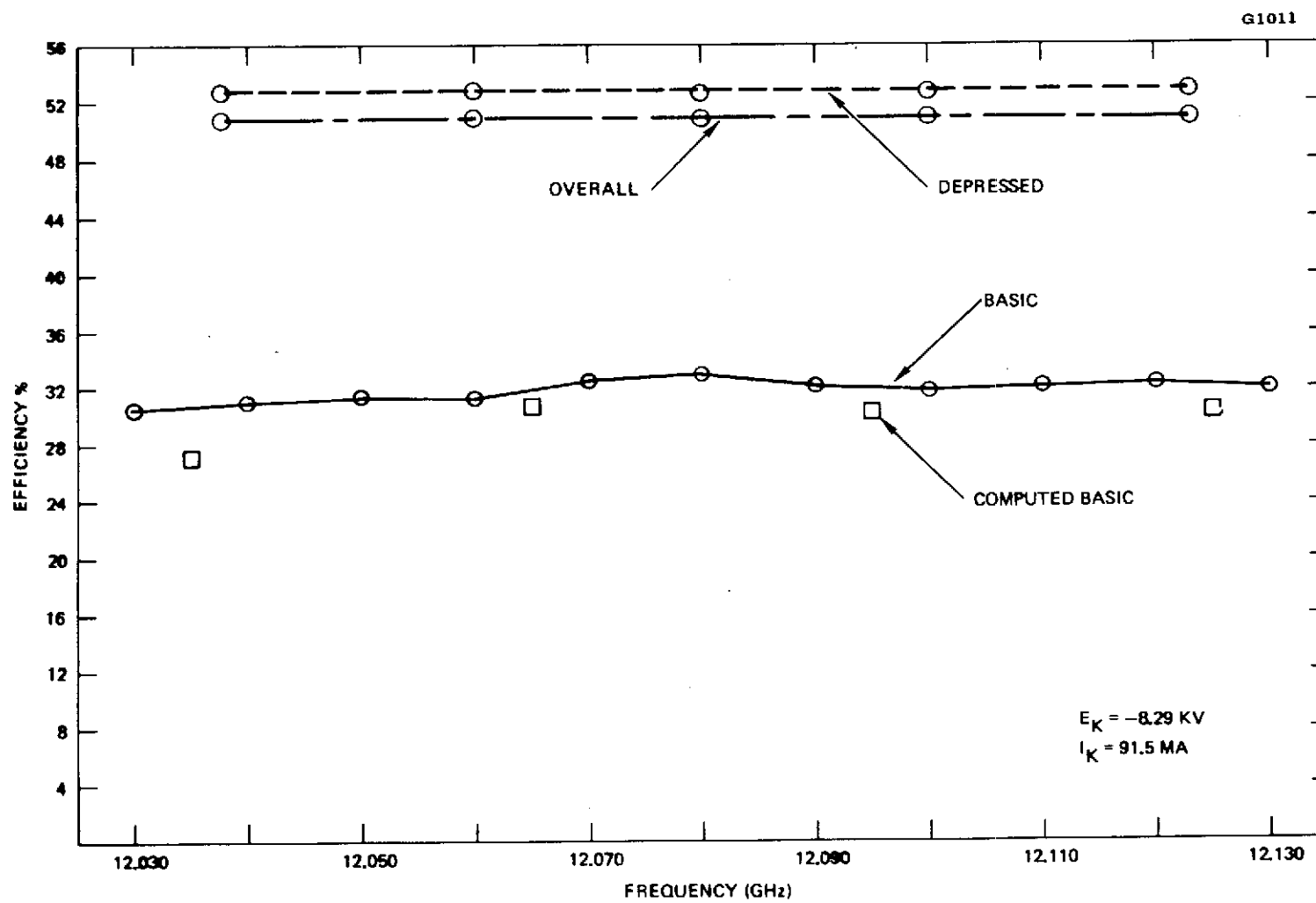


Figure 4-22 284H S/N ETM-2 saturated efficiencies.

# SWEPT POWER OUTPUT

G614

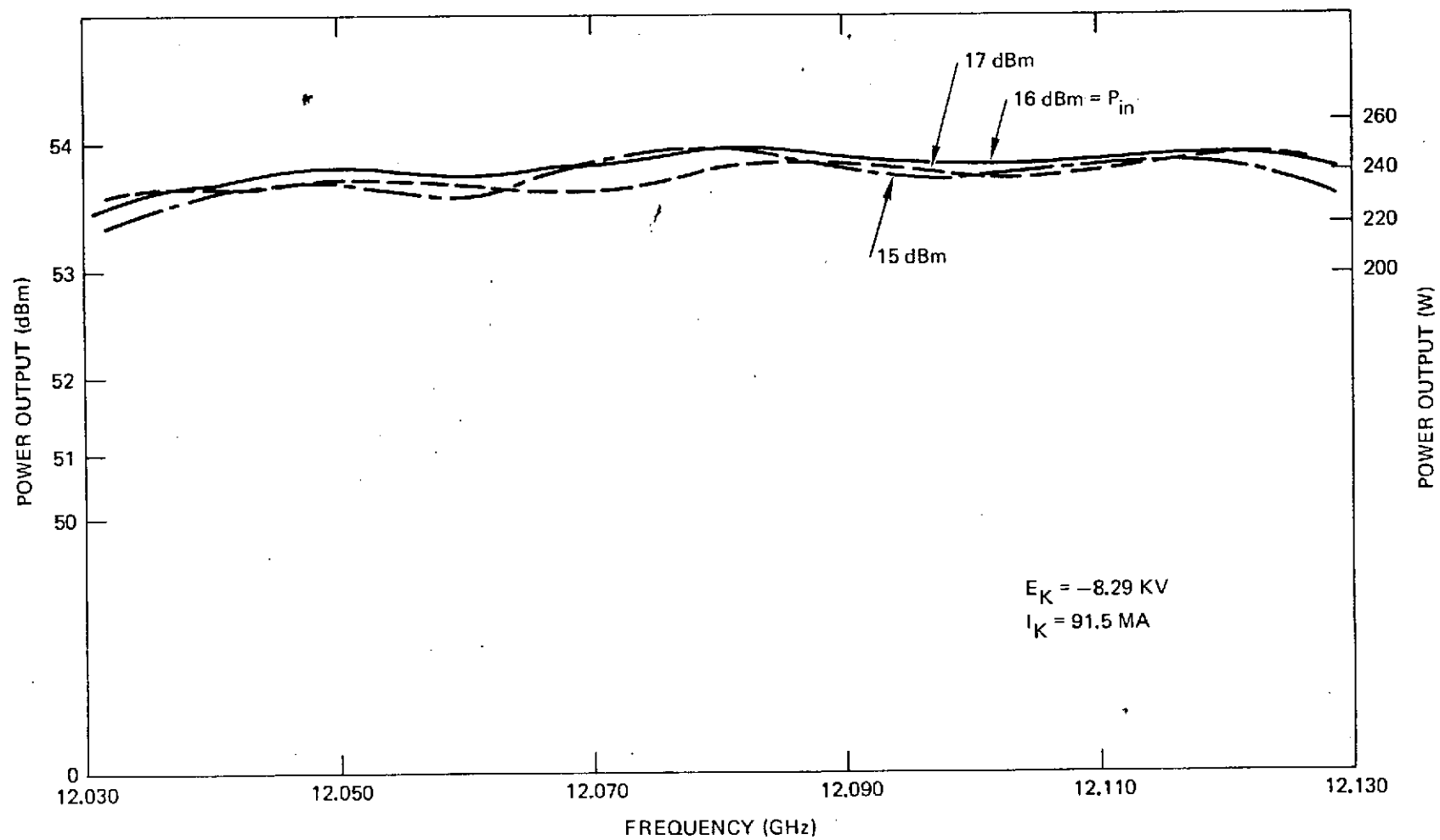


Figure 4-23 284H ETM-2 swept power output.

# SWEPT P<sub>OUT</sub> OVER 150 MHz BANDWIDTH

G668

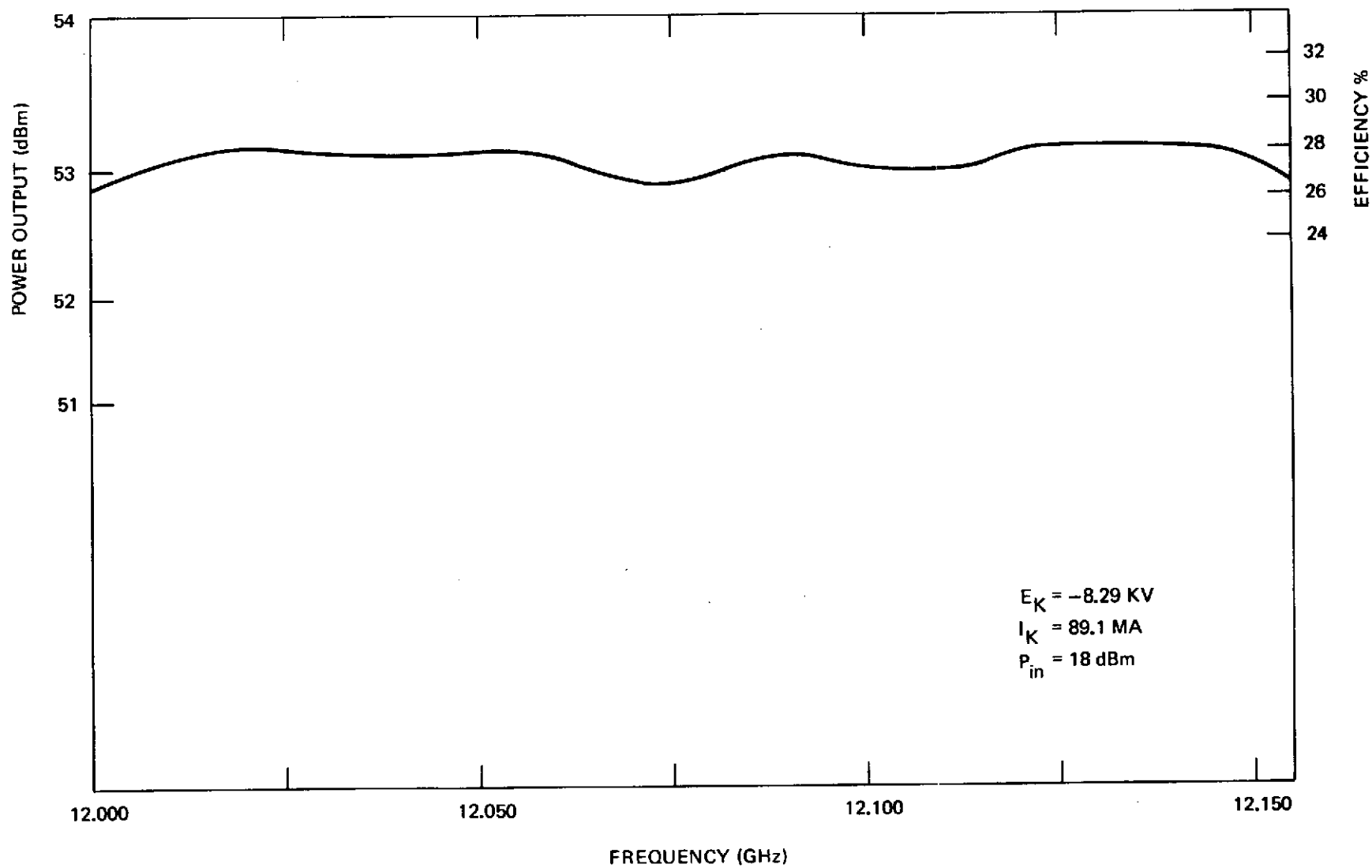


Figure 4-24 284H S/N ETM-2 swept P<sub>out</sub> over 150 MHz bandwidth.

before the final optimization of the magnetic field. As a result, the power shown is approximately 30 watts below that ultimately produced.

The larger operating bandwidth of the 284H S/N ETM-2 was due primarily to the increased beam perveance and the relatively high design value of  $\beta l c / \pi$  at midband frequency. As a result this tube had sufficient gain to produce an out-of-band, low level oscillation at 11.92 GHz with no RF drive. This oscillation was driven out well below saturation, causing no performance degradation above 50 watts output.

To eliminate this oscillation required an improvement in the circuit match near the lower cutoff of the passband. A voltage reflection below 50 percent in the frequency range of 11.90 to 11.99 was sufficient to stop the oscillation entirely. Preliminary matching of 284H S/N ETM-3 indicated that the new match criteria could be readily achieved by adjustment of the cavity gaps at the ends of the circuit sections.

The 284H OST S/N ETM-2 energy balance and power dissipations are given in Table 4-6. The computed total RF loss of 97.3 watts includes the coupler and window ohmic losses at a baseplate temperature of 60°C. The calculation is based on a circuit ohmic loss of 78 watts at 25°C and is corrected for the increased circuit temperature due to RF dissipation and beam interception. The collector to tube heat transfer is calculated using the temperatures obtained in the MDC thermal analysis discussed in an earlier section of this report.

The collector efficiency (defined as recovered power divided by spent beam power) was 74 percent. A typically higher result of 75 percent was obtained at other frequencies in the operating band. With reduced drive the collector efficiency approached 78 percent.

TABLE 4-6

## 284H ETM-2 Energy Balance at Saturation

Beam Power	Recovered Power	Overall Efficiency	RF Power Output	Baseplate Dissipation	Spent Beam Power	Collector Radiation	Collector Efficiency
762 W	287 W	51%	250 W	147 W	388 W	93 W	74%

## TWT Baseplate Dissipation at 60°C

Filament	5.7 W
Refocusing Solenoid	10.4 W
Intercepted Beam	26.4 W
RF Losses	97.3 W
Collector to TWT Transfer	<u>7.0 W</u>
Total	147.0 W



The  $P_{out}$  (RF) versus  $P_{in}$  (RF) characteristic for this OST is shown in Figure 4-25. The somewhat unconventional shape of the curve results from the strong velocity taper used in the RF circuit.

Figure 4-26 shows the phase deviation from a linear characteristic versus frequency. This data was taken at OST saturation. The total variation is less than plus or minus 7.5 degrees. This deviation is equivalent to a plus or minus 2.7 nanosecond group delay distortion. The excellent phase linearity of 284H ETM-2 is due to the broad bandwidth and the low mismatches of the circuit.

284H OST S/N ETM-2 was delivered to NASA Lewis Research Center in May, 1973. In June, 1974 the tube development portion of the contract was terminated and no additional OST's were fabricated or tested.

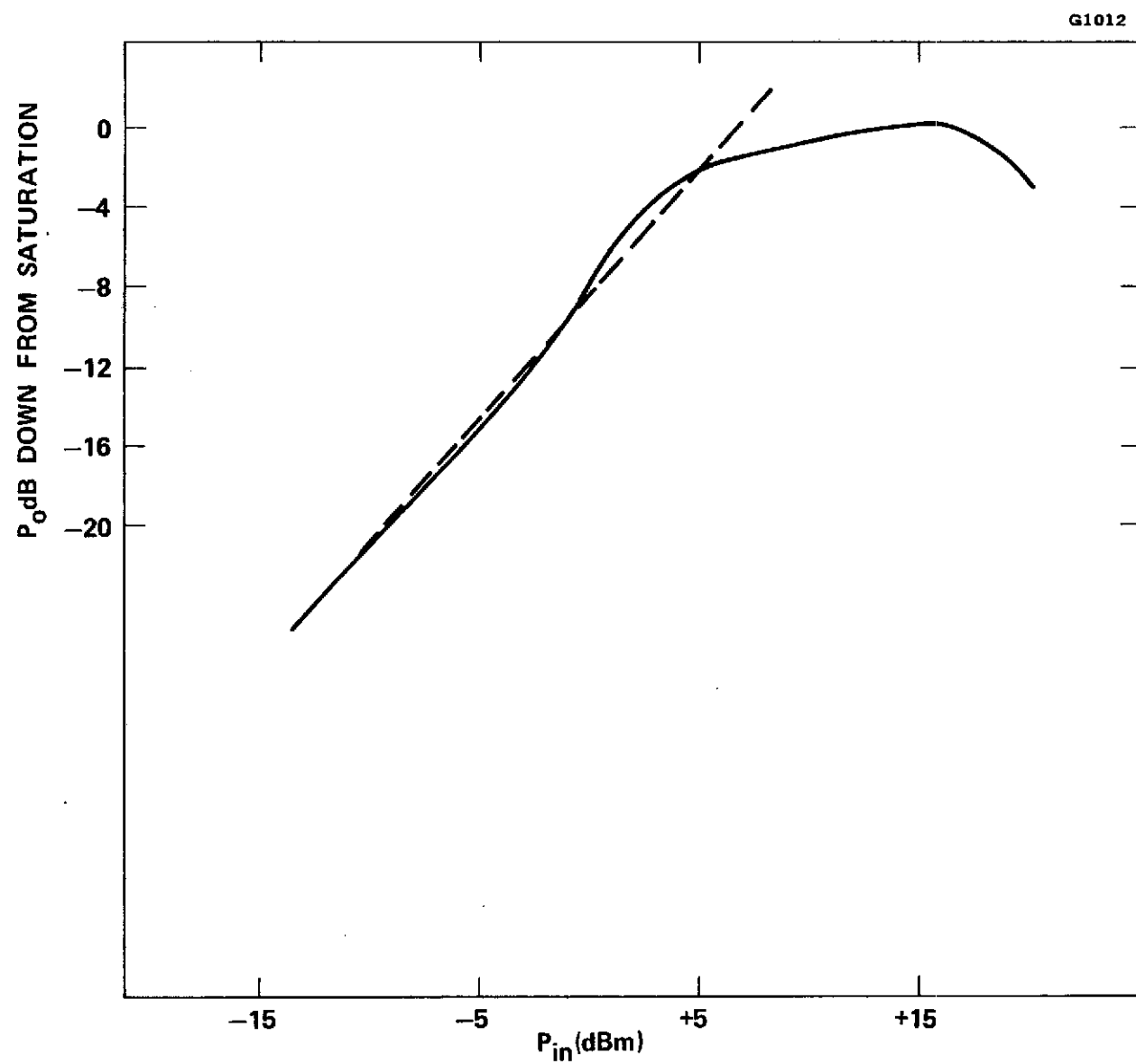


Figure 4-25 284H ETM-2 power out versus power in.

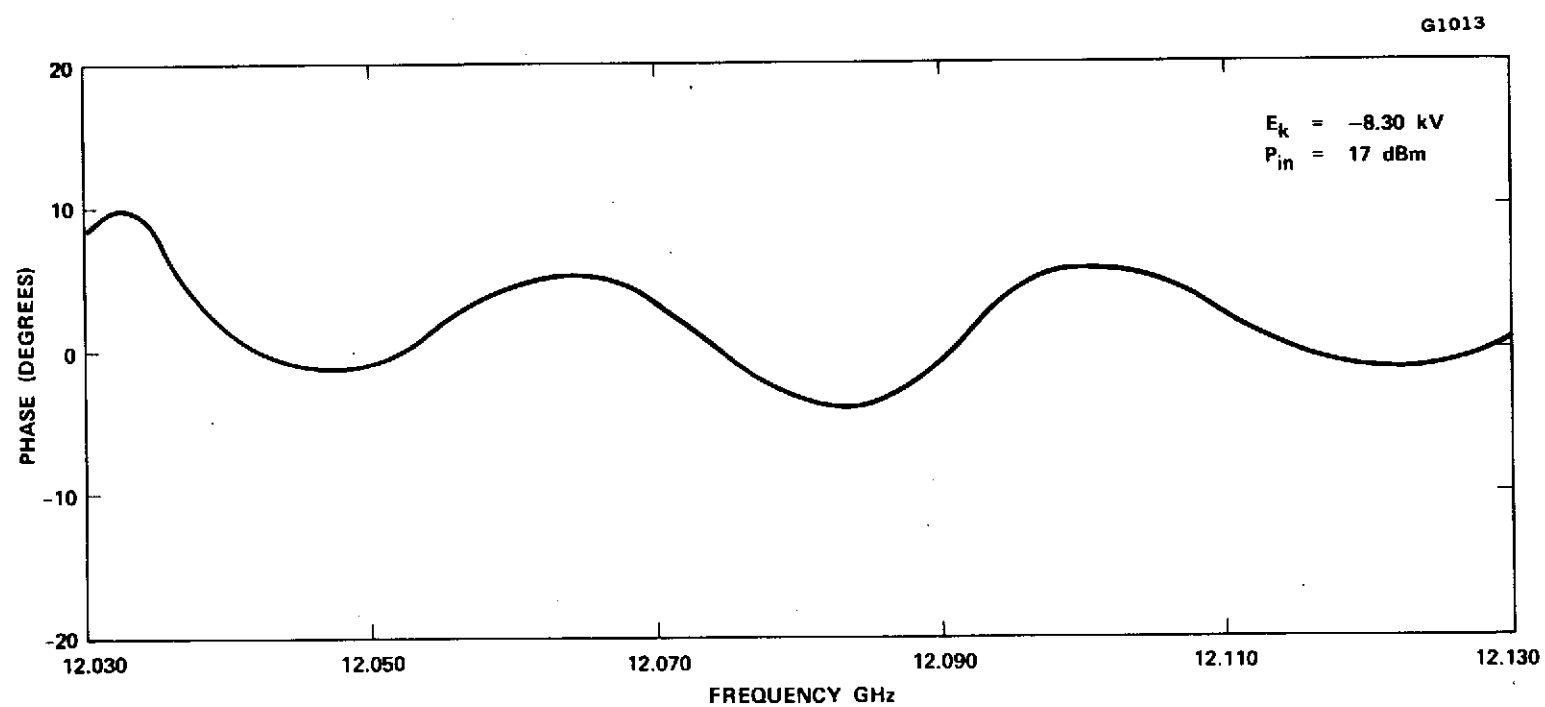


Figure 4-26 Phase linearity at saturation.

## 5.0 CONCLUSIONS

The objective of this development effort was to design, develop, and produce traveling-wave tubes providing greater than 200 watts of RF output power over an 85 MHz frequency band centered at 12.080 GHz. Other TWT characteristics were 33 dB of saturation gain and 30 percent minimum basic interaction efficiency. An overall efficiency of greater than 50 percent was required using a nine depressed stage collector designed by Dr. H. G. Kosmahl of NASA Lewis Research Center. In order to minimize the power transferred to the satellite from the tube, the collector was cooled entirely by radiation to deep space.

The analyses and experimental test data presented in the main text of this report have demonstrated that all the performance objectives of the program could be achieved.

The performance of 284H OST serial number ETM-2 at saturation met all of the specification requirements, producing greater than 235 watts of RF output power over the 85 MHz frequency band with 30 to 33 percent basic efficiency and 51 percent overall efficiency. Based on the results of this development program the following specific conclusions are drawn:

1. A coupled-cavity circuit can be designed for greater than 30 percent basic efficiency over the full 85 MHz band at 12 GHz using a two-step velocity taper.
2. The RF losses in the coupled-cavity circuit can be minimized by proper selection of the frequency passband and midband operating value of the propagation constant. A larger design passband in the 284H would have resulted in higher overall efficiency.
3. Excellent focusing is achieved at a beam voltage of 8 kV using Alnico magnets in the standard circuit and Samarium Cobalt magnets in the velocity taper.

**PRECEDING PAGE BLANK NOT FILMED**

4. The nine depressed stages collector designed by NASA improves the overall efficiency to greater than 50 percent with collector efficiencies in the range of 75 to 80 percent.
5. The depressed collector operates with no significant electron back-streaming.
6. The depressed collector for the 200 watt tube operates at acceptable temperatures using radiation cooling within a metal vacuum envelope.
7. The performance of the collector is strongly dependent upon the length of the refocusing section. A longer refocusing section on the 284H would probably have improved the overall efficiency to greater than 55 percent.
8. The 284H, 200 watt tube with a radiation cooled nine stage depressed collector will withstand the launch environment.
9. Low amplitude and phase variations at saturation can be achieved in a coupled-cavity tube with a velocity taper by careful control of the cold circuit matches.
10. The performance of high efficiency coupled-cavity traveling-wave tubes with low pervenace designs can be accurately predicted using large signal computer analysis.
11. Due to the problems experienced on the 284H tubes S/N P-1 through ETM-1 (which prevented any meaningful MDC performance evaluation) only the 6 degree aperature collector design of ETM-2 was tested. Thus no experimental comparison was obtained between the 4 degree and 6 degree aperature designs.